SPACE, TELECOMMUNICATIONS AND RADIOSCIENCE LABORATORY

STARLAB
DEPARTMENT OF ELECTRICAL ENGINEERING / SEL
STANFORD UNIVERSITY • STANFORD, CA 94305

12

THE MAGNETIC FIELD GRADIOMETER

by

A.C. Fraser-Smith

Final Technical Report E723-1

February 1983

Sponsored by
The Office of Naval Technology
The Naval Postgraduate School
and
The Office of Naval Research

The views and conclusions contained in this document are those of the author and should not be interpreted as necessarily representing the official policies, either expressed or implied, of the Naval Postgraduate School, the Office of Naval Research, or the U.S. Government.

UNCLASSIFIED

SECURITY CLASSIFICATION OF THIS PAGE (When Data Entered)

REPORT DOCUMENTATION PAGE		READ INSTRUCTIONS BEFORE COMPLETING FORM
1. REPORT NUMBER Final Technical Report No. E723-1	2. GOVT ACCESSION NO. AD-A-131477	3. RECIPIENT'S CATALOG NUMBER --
4. TITLE (and Subtitle) The Magnetic Field Gradiometer		5. TYPE OF REPORT & PERIOD COVERED Final Technical Report No. E723-1
		6. PERFORMING ORG. REPORT NUMBER E723-1
7. AUTHOR(s) A. C. Fraser-Smith		8. CONTRACT OR GRANT NUMBER(s) N00228-81-C-AB56
9. PERFORMING ORGANIZATION NAME AND ADDRESS Radioscience Laboratory Stanford Electronics Laboratories, Stanford Univ. Stanford, CA 94305		10. PROGRAM ELEMENT, PROJECT, TASK AREA & WORK UNIT NUMBERS --
11. CONTROLLING OFFICE NAME AND ADDRESS Department of Physics & Chemistry Naval Postgraduate School Monterey, CA 93940 ATTN: Professor John N. Dyer, Code 61 DY		12. REPORT DATE February 1983 13. NO. OF PAGES 98
14. MONITORING AGENCY NAME & ADDRESS (if diff. from Controlling Office) --		15. SECURITY CLASS. (of this report) Unclassified 15a. DECLASSIFICATION/DOWNGRADING SCHEDULE

16. DISTRIBUTION STATEMENT (of this report)

Approved for public release; distribution unlimited.

17. DISTRIBUTION STATEMENT (of the abstract entered in Block 20, if different from report)

18. SUPPLEMENTARY NOTES

Additional support for this work was provided by the Office of Naval Research through Contracts No.N00014-75-C-1095 and N00014-77-C-0292.

19. KEY WORDS (Continue on reverse side if necessary and identify by block number)

Gradiometers
Magnetic Field Gradiometers
Magnetometers
Differential Magnetometers
MAD

20. ABSTRACT (Continue on reverse side if necessary and identify by block number)

This report has two principal goals: First, to present a general review of magnetic field gradiometers and, second, to provide new data concerning these gradiometers, including new information about their response to magnetic dipole fields. A system of nomenclature is introduced that is consistent with the mathematical concept of gradient and which provides a basis for discussions of the different functions of magnetic field gradiometers and differential magnetometers. The distinction between component gradiometers and total field gradiometers is also stressed. An historical review provides an opportunity to

DD FORM 1 JAN 73 1473

EDITION OF 1 NOV 65 IS OBSOLETE

UNCLASSIFIED

SECURITY CLASSIFICATION OF THIS PAGE (When Data Entered)

19. KEY WORDS (Continued)

20 ABSTRACT (Continued)

describe the different characteristics of the many kinds of magnetic field gradiometers that have been developed since the first report of such a gradiometer in 1925: rotating induction loop, fixed induction loop, fluxgate, proton precession, optically pumped, and superconducting gradiometers are discussed. It is pointed out how the great sensitivity of superconducting gradiometers, and possibly other varieties of modern magnetic field gradiometers, may invalidate the popular 'source-free' assumption under particular circumstances. Further, because these high sensitivities will make the gradiometers more susceptible to the geomagnetic field gradient, expressions are derived for the components of this gradient and some representative numerical values are calculated. The response of both component and total field gradiometers to dipole sources is considered for a number of different source-gradiometer configurations. On a more speculative note, two varieties of rotating component gradiometers are discussed, with particular attention being given to their possibly unique characteristics. The report ends by recapitulating the many applications of magnetic field gradiometers, particularly in such important areas as medicine, energy production, and defense, and by stressing the need for gradiometer-related basic research.

The Magnetic Field Gradiometer

A.C. Fraser-Smith

Technical Report No. E723-1

February 1983

STAR Laboratory
Department of Electrical Engineering
Stanford University
Stanford, California 94305

Abstract

This report has two principal goals: First, to present a general review of magnetic field gradiometers and, second, to provide new data concerning these gradiometers, including new information about their response to magnetic dipole fields. A system of nomenclature is introduced that is consistent with the mathematical concept of gradient and which provides a basis for discussions of the different functions of magnetic field gradiometers and differential magnetometers. The distinction between component gradiometers and total field gradiometers is also stressed. An historical review provides an opportunity to describe the different characteristics of the many kinds of magnetic field gradiometers that have been developed since the first report of such a gradiometer in 1925: rotating induction loop, fixed induction loop, fluxgate, proton precession, optically pumped, and superconducting gradiometers are discussed. It is pointed out how the great sensitivity of superconducting gradiometers, and possibly other varieties of modern magnetic field gradiometers, may invalidate the popular 'source-free' assumption under particular circumstances. Further, because these high sensitivities will make the gradiometers more susceptible to the geomagnetic field gradient, expressions are derived for the components of this gradient and some representative numerical values are calculated. The response of both component and total field gradiometers to dipole sources is considered for a number of different source-gradiometer configurations. On a more speculative note, two varieties of rotating component gradiometers are discussed, with particular attention being given to their possibly unique characteristics. The report ends by recapitulating the many applications of magnetic field gradiometers, particularly in such important areas as medicine, energy production, and defense, and by stressing the need for gradiometer-related basic research.

Acknowledgement

This report was made possible by my appointment to the Research Chair in Applied Physics at the Naval Postgraduate School in Monterey, California, during March–June, 1980. My occupancy of the Chair, which was sponsored by the Office of Naval Technology, gave me the opportunity to prepare a first version of the report. Later support from the Postgraduate School enabled me to complete most of the writing of the report at Stanford University. Some of the research at Stanford that is included in the report was sponsored by the Office of Naval Research through Contracts No. N00014-75-C-1095 and N00014-77-C-0292 (Contract Monitor: R. Gracen Joiner, Code 414); I would particularly like to thank Dr. David M. Bubenik for his assistance during this phase of the work.

I am grateful to many of the faculty at the Naval Postgraduate School for their help and encouragement. The Dean of Research, Professor William M. Tolles, and Professors Otto Heinz and John N. Dyer of the Department of Physics and Chemistry deserve particular thanks for their kindness before, during, and after my occupancy of the Chair. Finally, I wish to thank the graduate students—Navy officers—who attended my course on electromagnetic fields in the sea.

Contents

Chapter 1

Introduction

You boil it in sawdust: you salt it in glue:
You condense it with locusts and tape:
Still keeping one principal object in view —
To preserve its symmetrical shape.

The Hunting of the Snark
LEWIS CARROLL

§1.1 Preamble

For many years magnetic field gradiometers have had potential application in a surprisingly wide variety of activities: medical research and diagnosis, prospecting for oil and other minerals, ship and submarine detection, the detection of small arms (hijack prevention), archeology (detection of artifacts), studies of electric current flow in the ionosphere, and studies of ocean waves and currents. These applications follow from the magnetic field gradiometer's primary function, which is to measure the space rate of change, or gradient, of a magnetic field. The measurements can be used in two rather different ways. First, given a magnetic field from a single time-varying source, a magnetic field gradiometer can give information about the source that would be unobtainable with a single magnetometer. Thus the gradiometer application to studies of ionospheric electric currents and to studies of ocean waves. Second, when two or more magnetic fields are present, any or all of which may be time-varying (and time-varying magnetic fields are ubiquitous, even though they are usually of small amplitude), a magnetic field gradiometer can sometimes be used to measure the characteristics of one of the fields, even a very weak field, while ignoring the others. Thus the application to medicine and to source detection. Unfortunately, until recently magnetic field gradiometers have been either too bulky or too insensitive (or, in some cases, both too bulky and too insensitive) to receive

wide use in any of their areas of application. However, remarkable advances in the technology of magnetometers over the last two decades have now made possible the construction of magnetic field gradiometers of truly unprecedented sensitivity that are also reasonably compact even portable. These new gradiometers are not yet widely available, but it is likely that they will find increasing use over the next few years, particularly in the areas I have listed above. It is even possible, in my view, that the gradiometers will finally begin to achieve some of the promise they have offered for so long and that their use will lead to substantial new capabilities and increases of knowledge not only in their obvious areas of application but in other unexpected areas as well. The purpose of this report is to provide a convenient reference for their use, and to provide some extra insight into their possible applications and the problems that might arise in these applications.

Magnetic field gradiometers are not necessarily complicated devices, as I will show in the next section. Complications can arise in their use, however, due to several different factors. In my experience the most important of these factors are intrinsic practical limitations of the equipment, ambiguous gradiometer nomenclature, and the wide variety of different gradiometer responses to the fields produced by typical sources. I will discuss each of these factors in the following chapters. I will also discuss a particular kind of magnetic field gradiometer that is not well known but which has a most desirable characteristic: its sensitivity is continuously variable over a very wide range, at least in principle. The references I give do not comprise a complete list, but they should provide a good start to any thorough search of the magnetic field gradiometer literature, which is not extensive.

§1.2 A Simple Magnetic Field Gradiometer

My acquaintance with magnetic field gradiometers began in 1967, when I was working with Lee R. Tepley at the Lockheed Palo Alto Research Laboratory. We were studying the properties of geomagnetic pulsations small fluctuations of the earth's magnetic field with frequencies less than about 5 Hz (these are called *ultra-low frequencies*, or ULF) and for this purpose Lee had designed and built a number of steel-cored multi-turn solenoids to sense the geomagnetic field changes. Since it was these solenoids that provided the basis for the simple gradiometer that I am about to describe, the following practical details of the solenoids' construction and electromagnetic properties may be of interest.

For portability, the solenoids were each made in three separable parts: the central steel core (a special high-permeability steel), and two identical coil sections. The core had a length of 1.84 m, a diameter of 3.7 cm, and a mass of about 16.6 kgm; the coil sections each contained a nominal 9200 turns of aluminum wire and they were 0.80 m long, with internal and external diameters of 4.5 cm and 7.1 cm, respectively, and their masses were about 10.9 kgm. Remembering that a kilogram is 2.2 pounds, it can be seen that the complete solenoid units were quite heavy (I learned about gradiometer portability t[illegible] hard way). The coil sections were

slipped over the steel core, without being fastened to it, and they were connected together in series to form the assembled solenoid unit. As might be expected, the inductance of the solenoids was high: on the order of 10 H at 1 Hz. Their resistance, on the other hand, was comparatively low (about 100 Ω) due to the use of heavy gauge wire.

The electrical signals from the solenoids were first amplified using low-noise galvanometer phototube amplifiers (voltage gain approximately 500,000) after which they were filtered and further amplified before being recorded on paper charts and magnetic tape. In general, two solenoids and their associated equipment were installed at each ULF geomagnetic pulsation observatory. Both solenoids were horizontal, with one oriented in a geomagnetic East-West direction and the other in a geomagnetic North-South direction. When fully adjusted and calibrated, each solenoid system had an approximately flat frequency response over the range 0.3 7.2 Hz, with a rapid decline of response outside this range; their internal noise was such that a 2 pT (peak-peak) sinusoidal magnetic field variation with a frequency in the indicated pass band could just be distinguished on the chart records (in more conventional noise terms, the measured system noise was about 0.4 $pT/Hz^{\frac{1}{2}}$ throughout the frequency range 0.3 7.2 Hz.)

Because of their high sensitivity to magnetic field changes, the solenoid systems were always installed at locations that were a large distance away from roads railroads, and any other sources of man-made magnetic fields that could be identified. However, even with the greatest care, spurious magnetic field fluctuations would be detected on occasion. For example, during heavy winds the wire fences near one pulsation observatory would vibrate and produce weak high-frequency (5 7 Hz) magnetic field changes at the solenoids. Although we ourselves were not affected, we also learned that cattle can create surprisingly strong magnetic field disturbances in their vicinity on occasion: some ranchers deliberately feed small magnets to their cattle, which lodge harmlessly in their stomachs and prevent any small pieces of wire they might ingest from progressing further through their digestive systems.

During the major outbreak of aircraft hijacking that took place in the latter half of the 1960's, we began a series of experiments to see if our sensitive magnetic field measurement systems could be used to help prevent hijacking by detecting the magnetic fields from concealed weapons. These experiments showed that weapons with ferromagnetic components could be detected at useful ranges on many occasions, but the sensitivity of the solenoid systems was limited by their simultaneous response to whatever natural magnetic field fluctuations were in progress. Worse, during magnetic storms or other large naturally-occurring disturbances of the earth's magnetic field, it was difficult, and sometimes impossible, to detect ferromagnetic objects at any range. Faced with this situation, and being aware of exploratory work at Varian Associates on magnetic field gradiometers constructed from their recently-developed cesium and rubidium vapor magnetometers [*e.g., Slack et al.*, 1967; *Staff Rept.*, 1967; *Grice*, 1968], we decided to combine two of our solenoids into a single gradiometer system and to test its ability to detect localized sources of magnetic fields.

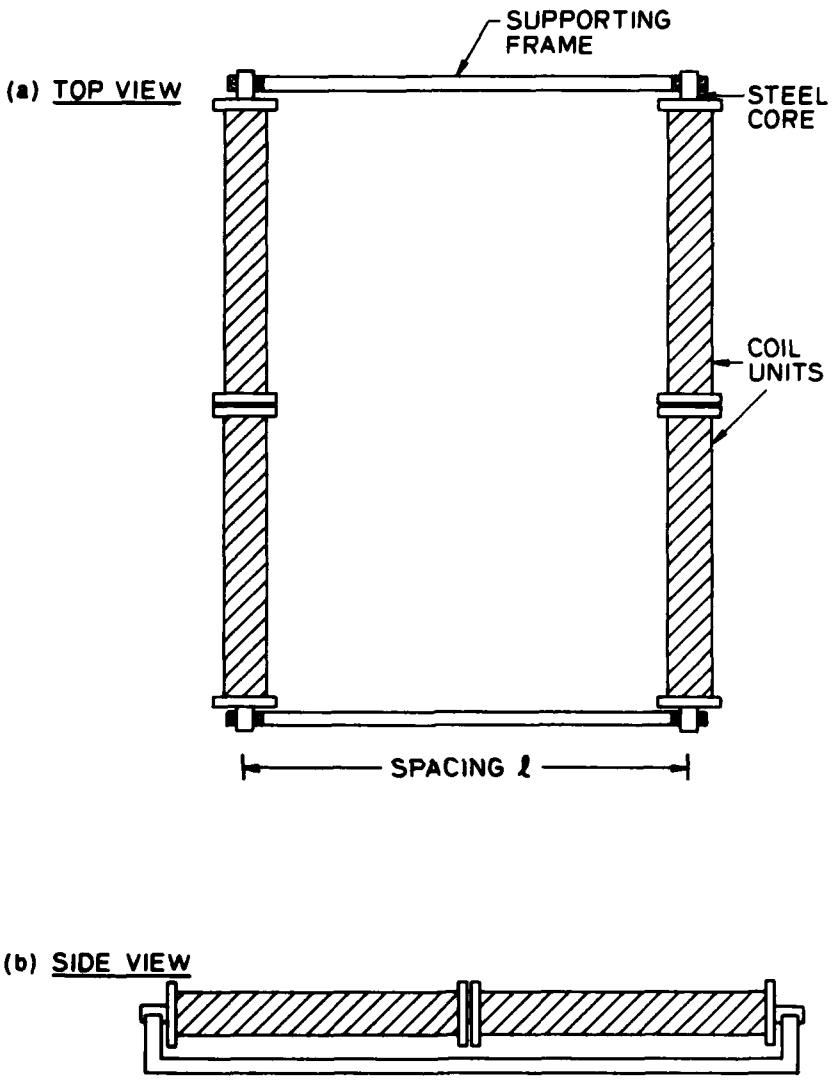

Figure 1.1. Top and side views of the two-solenoid gradient sensor used in the simple magnetic field gradiometer described in the text.

The gradiometer was constructed as follows. The two solenoids were placed 4 m apart and oriented in as close to the same horizontal direction as possible (Figure 1.1). Next, their wire leads were connected together in such a way that the electrical output of the combination was zero, or, significantly, very nearly zero, whenever the two solenoid sensors were exposed to

the same magnetic field fluctuations. A small switching unit was constructed for this purpose; it had a two-position switch that connected together the two pairs of input leads from the solenoids in their two possible combinations. Then, with the same magnetic field fluctuations applied to each solenoid, one switch setting would give an output signal that was twice the signal produced by one solenoid alone (switch in the 'aiding' position) and the other switch setting would give the minimum output (switch in the 'bucking' position). The signals produced by this solenoid combination were amplified and displayed using the same equipment as was used with the individual solenoids.

Figure 1.2 (bottom panel) shows three examples of the response of the solenoid magnetometer-gradiometer system. The first of these examples, 1, is part of a typical chart recorder trace taken during an interval of weak geomagnetic pulsation activity. Both solenoids were connected in the aiding, or magnetometer, mode for this record. The next example, 2, shows the system response when the solenoids were connected in the bucking, or gradiometer, mode. The pulsations shown in trace 1 were still occurring, but the electrical output of the two-solenoid combination was reduced almost to zero. The final example, 3, shows the response of the gradiometer when a small stool constructed largely of steel was carried past the two solenoids at a distance of 6 m from the nearest solenoid. The experimental configuration for this last experiment is detailed in the top panel of the figure. Two large-amplitude impulsive signals were recorded, one during the outward passage and the other during the return, and if the recorder trace is examined carefully it can be seen that there is an interesting difference in the form of the signals: a positive excursion occurs first on the outward passage, and a negative excursion occurs first on the return. (The amplitude difference is not significant; it was caused most probably by a small decrease in the pace at which the stool was carried past the solenoids on the return path.) The impulsive signals occurred during comparatively short time intervals centered on the times of closest approach to the near solenoid, which suggests that the response of the two-solenoid gradiometer system is highly directional. This high directionality is confirmed by theory, as will be shown in Chapter 5. In fact, the solenoid gradiometer has very little response to the changing magnetic field of a dipole source whenever the angle ϕ shown in the figure (top panel) has a magnitude greater than 20°. When account is taken of the fact that the response of the gradiometer also varies roughly with distance r as r^{-4}, where r is measured from the center of the gradiometer to the source of magnetic field, the directionality becomes obvious.

None of the data I have shown give any indication of the maximum range for detection of the steel object. However, it can be seen that this range will depend primarily on two factors: (1) the amplitude of the impulsive signals produced in the output of the gradiometer (*e.g.*, trace 3), and (2) the amplitude of the noise background (*e.g.*, trace 2). In other words, it is a signal-to-noise ratio that determines the maximum range for detection. Let us now consider how this signal-to-noise ratio can be increased.

The amplitude of the signal will depend in general on the sensitivity of the solenoid sensors and on the distance between the source and the solenoids, *i.e.*, the gradiometer sensor. The

distance between the source and this gradiometer sensor can be easily controlled under the conditions I have described, but in general, under realistic conditions, it is not a variable that the operator of the gradiometer can regulate. An effort can be made to locate the gradiometer sensor as close as possible to the location of potential sources, but there is little else that can be done to control the distance, particularly if the sources are being moved to avoid detection. This leaves the sensitivity of the solenoid sensors under the control of the gradiometer designer, and it is plain that the sensitivity should be as high as possible if the gradiometer is to be used to detect sources at large distances. The noise in the gradiometer consists of a combination of the internal noise in the solenoids (basically thermal noise) and the residual geomagnetic noise. There is not a lot that can be done about the internal noise. It can be minimized by keeping the resistance of the solenoids low, but this means that the length of the wire in the solenoids must be kept as small as possible, and this can only be done by reducing the number of turns and the sensitivity of the solenoids. Thick wire can be used, but it increases the size, weight, and cost of the solenoids. In practice, the resistance of the solenoids involves many compromises and it can only be varied within strict limits. This leaves reduction of the residual geomagnetic noise as a means of controlling the gradiometer noise background, and it is here that considerable progress is possible.

It was never anticipated that the solenoids I have been describing would be paired up to form a gradiometer sensor, and no attempt was made during their construction to make them absolutely identical. As a result, it is unlikely that the number of turns on each solenoid was the same. Further, the construction of the solenoids was not designed with accurate alignment in mind. One particular weakness in this regard was the lack of a rigid connection between the individual coils and the steel cores, which made exact alignment of the coils relative to the cores and to each other almost impossible to obtain. These two weaknesses are representative of two of the three major difficulties encountered in the design and construction of any magnetic field gradiometer, which, following *Morris and Pedersen* [1961], I will refer to as (1) electrical or magnetic mismatch , and (2) physical misalignment. It is essential, if the greatest possible gradiometer sensitivity is to be achieved, that there be complete symmetry between the constituent sensors; they should be identical electrically and magnetically, and, if component sensors, they should be capable of being aligned in the exactly the same direction with the greatest possible accuracy. The third major difficulty that is encountered hardly needs separate listing, but it is the most basic one in gradiometer design; it is (3) obtaining magnetometers with sufficient sensitivity to give a gradiometer with adequate range. The history of magnetic field gradiometer development is essentially a history of how increasingly more advanced technology has been brought to bear on the problems caused by the above difficulties. I will review this history in the following chapter, but first, in the following section, I will provide some background information on the magnetometers that are presently being used, or which might be used, in modern gradiometer construction.

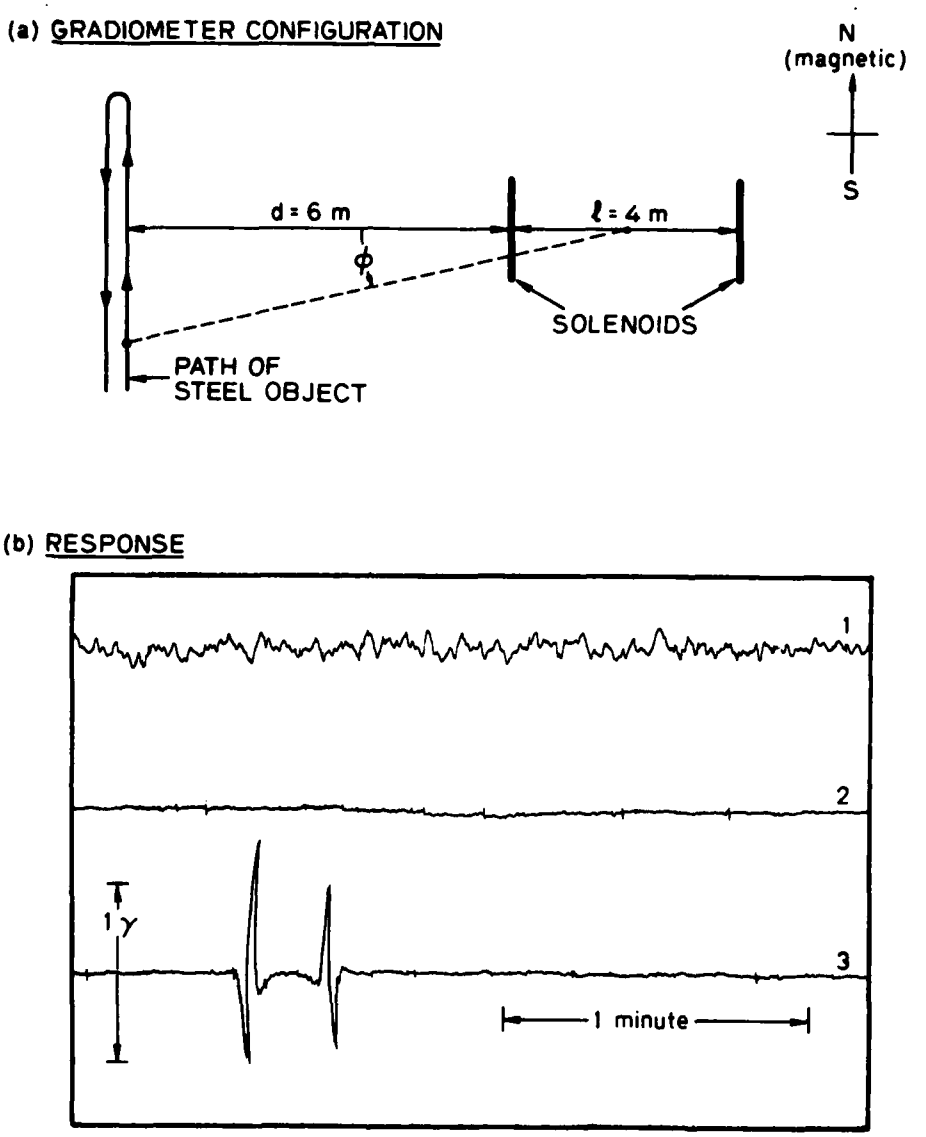

Figure 1.2. Examples of the magnetic field data recorded with the two-solenoid gradiometer sensor shown in Figure 1.1. The first two traces in the bottom panel show the magnetometer and gradiometer responses of the sensor, and the bottom trace shows what happens to the gradiometer trace when a small steel object is carried by the solenoids, as depicted in the upper panel.

§1.3 Technology and Modern Gradiometers

If the gradiometer technology described in the previous section were representative of its ultimate possible development, it would be safe to say that magnetic field gradiometers would be limited to a few specialized applications. However, as I have indicated in Section 1.1, recent technological developments have created new opportunities for these gradiometers, since it is now possible to construct magnetic field gradiometers that combine remarkable compactness with extraordinary sensitivity. The technological developments under discussion involve magnetometers the basis for any magnetic field gradiometer.

This century has established an unprecedented record for technological development, and the changes in technology have been so many, and in some cases so remarkable for their impact on the public, that a few of the changes have gone largely unrecognized except among comparatively small groups of specialists. The changes in the technology of magnetometers provide one good example. These instruments have been the subject of scientific research for some hundreds of years, and by the end of the last century they had reached a high level of refinement, particularly those that were used in magnetic observatories (see Chapter XXVI of *Chapman and Bartels* [1940], for an authoritative discussion of the early history of these observatories). Considering this long history of development, it may be difficult to believe that there are now two to three more different **kinds** of magnetometers in use than there were at the end of last century. Nevertheless, it is a fact that magnetometers based on the Hall effect [*Rubin and Sample*, 1980], fiber optics [*Yariv and Windsor*, 1980; *Lewis*, 1980], proton precession [*Packard and Varian*, 1954; *Waters and Francis*, 1958; *Hartmann*, 1972], thin films [*West et.al.*, 1963; *Irons and Schwee*, 1972], optical pumping [*Grivet and Malnar*, 1967; *Hartmann*, 1972, *Aleksandrov*, 1978], fluxgates [*Fromm*, 1952; *Serson*, 1957; *Gordon and Brown*, 1972], and the the Josephson effect in superconductivity [*Josephson*, 1962; *Webb*, 1972; *Clarke*, 1974] are all new, most of them having been developed only over the last three decades. Any pair of these magnetometers can be combined in a spaced configuration to give a particular kind of magnetic field gradiometer, with its own individual characteristics. This is one reason for the new opportunities that have arisen in gradiometer research.

The new magnetometers differ in many respects, but in general they provide new accuracy, sensitivity, reliability, and convenience of use for magnetic field measurements. However, it is the increase of sensitivity that is their most remarkable feature. To illustrate the magnitude of this increase, consider the change that has taken place in studies of the earth's magnetic field. As pointed out by *Grivet and Malnar* [1967], the traditional magnetic field unit in these studies for many years was the *gamma* (γ), which was essentially the smallest measurable variation of the field. In present MKS/SI units, the gamma is equivalent to 10^{-9} Tesla, *i.e.*, 1 nanoTesla (nT). Practically all of the newly-developed magnetometers used for geomagnetic measurements have sensitivies exceeding 1 nT, and the sensitivities of some of them exceed this limit by many orders of magnitude. The magnetometers based on the Josephson effect, which

are commonly referred to as *superconducting magnetometers* (even though only a very small part of them is superconducting), are the most sensitive of all at the present time: the first commercial models could easily measure magnetic field variations with amplitudes in the range 0.1–1 picoTesla (pT; 1 pT = 10^{-3} nT) [*Fraser-Smith and Buxton*, 1975] and recent models can measure variations as small as 10^{-3} pT if required. In other words, there has been an improvement by a factor of approximately a million in the sensitivity that can be achieved with magnetometers over the last few decades.

Magnetometers based on proton precession and optical pumping measure the total field, whereas the others I have listed measure components of the field. It is of course always possible in principle to assemble an array of the component magnetometers, measure three orthogonal components of the magnetic field, and compute the total field. However, difficulties arise with this procedure in practice and it appears likely as a result that gradiometers constructed from total field magnetometers will form a special class of gradiometer for a long time to come, with their own special applications. Of the component magnetometers, superconducting magnetometers are the most sensitive, as I have already pointed out. They have an additional advantage in that their sensing elements are small plane superconducting loops [*e.g., Goodman et al.*, 1973; *Clarke*, 1974], which can be constructed with considerable precision; they can also be assembled in pairs on a single compact supporting structure, balanced magnetically (with great accuracy), and connected in opposition to produce a gradiometer sensing element. These elements are so exceptionally compact and integrated that superconducting gradiometers could well appear to provide an exception to the rule that magnetometers are the basis for any magnetic field gradiometer. However, as noted, the individual small plane superconducting loops can also be used as magnetometer sensing elements—once this fact is recognized, there can be no doubt that superconducting gradiometers conform to the rule. Because sensitivity and symmetry are the two most desirable characteristics for the pair (or pairs) of sensors comprising a gradiometer, and superconducting gradiometers are distinguished by the sensitivity and symmetry of their sensing elements, it seems likely that superconducting gradiometers will provide the most innovative gradient measurements for some years to come.

Chapter 2

The Gradient Concept

§2.1 Introduction

Suppose we wish to measure a simple scalar quantity, temperature T for example, which varies over a known region of space but which is not varying with time. We can start with a single measuring instrument, in this case a thermometer, and measure the temperature at representative points throughout the region, thus obtaining a plot of temperature with position. Figure 2.1 shows the kind of result that might be obtained for a two-dimensional distribution of temperature. If the representative points are closely spaced, the picture obtained of the temperature variation throughout the region will be comparatively complete and the contours that are drawn, as in Figure 2.1, or other representations of the temperature distribution, will be comparatively accurate. On the other hand, if the points where measurements are made are widely spaced, the picture obtained of the temperature distribution will be comparatively incomplete and the contours or other representations of the field will be inaccurate.

A difficulty arises if the temperature distribution is varying with time and only a single thermometer is available for measurement. If the time variation is harmonic, a plot similar to that shown in Figure 2.1 can be prepared by measuring the maximum value of the temperature at each point and then using these maximum values as original data for the plot. However, if the time variation is not harmonic, or contains a non-harmonic component (or, in practice, if it is harmonic over too long a time scale), arrays of thermometers must be used to make simultaneous measurements of the temperature. Plots similar to those in Figure 2.1 can then be prepared showing the temperature distribution at particular instants of time.

The temperatures shown in the figure comprise a *scalar* field: there is a value of temperature at each point (either indicated specifically or implied), but no direction is associated with the values. We will mostly be concerned with *vector* fields in this work, where each point in the region of interest has associated with it both the magnitude and direction of some quantity, but scalar fields can always be constructed from these vector fields either by neglecting the direction

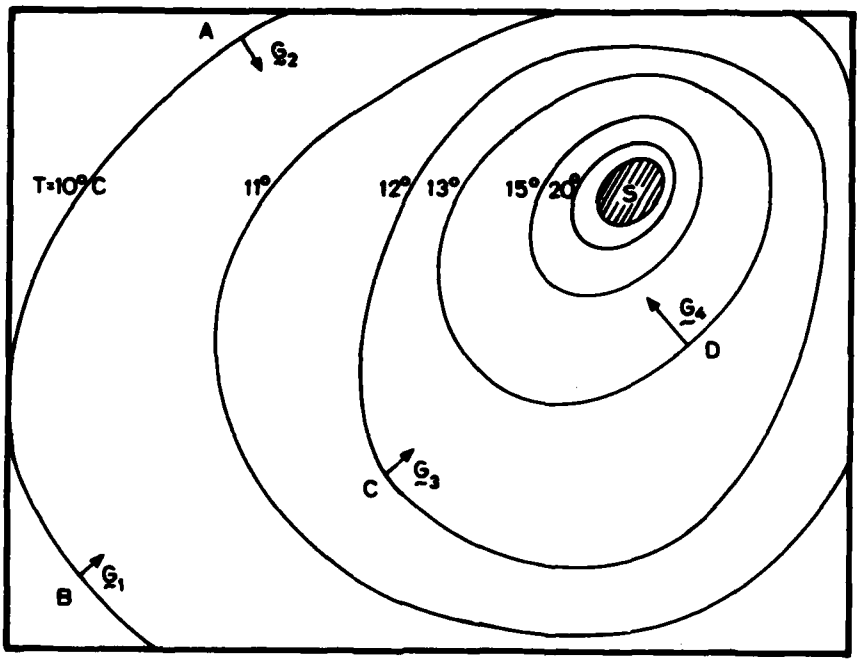

Figure 2.1. Two-dimensional temperature distribution surrounding a source of heat, S. Four temperature gradient vectors $\mathbf{G}_1, \ldots, \mathbf{G}_4$ are shown in the figure and discussed in the text.

and considering only the magnitude of the quantity or by taking and using these components either singly or in various combinations. Similarly, vector fields can be constructed from scalar fields by a variety of techniques. One of these techniques is to compute the *gradient* of the scalar quantity at each point.

Without going into great detail, an initial non-mathematical picture of the meaning of the gradient operation and of the significance of the vector quantities that are obtained by this operation can be obtained by considering the temperature contours in Figure 2.1. Suppose arrows are drawn in the direction of increasing temperature and perpendicular to the contours at points A, B, C, and D. It is immediately apparent that the arrows tend to point toward the source of heat S that is producing the temperature distribution. We obviously should not expect this directivity at all times, particularly when many different sources and sinks of heat are present, but it is an interesting feature of the arrows that suggests they may have some physical significance.

To see this physical significance, consider the flow of heat in our hypothetical example. We know from the laws of thermodynamics that heat will not flow spontaneously between two points at the same temperature. It follows that the direction of heat flow in the figure must everywhere be perpendicular to the constant temperature contours, just as water on the ground tends to flow (when it is moving slowly) in directions perpendicular to the altitude contours. Thus the arrows in Figure 2.1 and the direction of heat flow share the property of being perpendicular to the constant temperature contours; they differ in that their actual directions are antiparallel, since heat flows toward lower temperatures and the arrows are directed toward higher temperatures.

Suppose we now consider other constant temperature contours close to those drawn in the figure and necessarily differing from the original contours only slightly in temperature. It is readily seen that the maximum rate of change of temperature with distance occurs along the perpendiculars to the contours. This circumstance suggests that we should quantify our arrows by making their magnitudes (i.e., their lengths) equal to the maximum rate of change of temperature with distance at the points where they are located. The final result linking heat flow with the arrows in the figure is then provided by experiment: it is found that the rate of heat flow between two points at different temperatures in a conducting medium is directly proportional to the difference in temperature and inversely proportional to the distance between the two points. This means that the heat flow at points A, B, C, and D in Figure 2.1 takes place in directions antiparallel to the arrows and that the rate of heat flow is proportional to the magnitude of the arrows. The physical significance of the arrows is now clear: they relate heat flow in the figure to the temperature distribution.

The vector quantities represented by the arrows are referred to as the gradient of the temperature at the applicable points. More generally, given a scalar field such as T, a vector field denoted by **grad** T (or, equivalently, by ∇T) can be constructed from the scalar field by determining the direction and magnitude of the maximum spatial rate of increase of the scalar quantity at each point and using these directions and magnitudes to define the vector field.

§2.2 Mathematical Definition of Gradient

Given a three dimensional scalar field $f(x, y, z)$, the gradient of f is a vector field defined by

$$\mathbf{grad}\, f = \frac{\partial f}{\partial x}\mathbf{i} + \frac{\partial f}{\partial y}\mathbf{j} + \frac{\partial f}{\partial z}\mathbf{k}, \tag{2.1}$$

where $\mathbf{i}, \mathbf{j}$, and $\mathbf{k}$ are unit vectors directed along the positive x, y, and z axes of the Cartesian coordinate system. It is not immediately apparent that this gradient quantity is identical to the gradient discussed in the preceding paragraphs. However, the following argument used by *Skilling* [1974], shows that the two gradients are identical.

Suppose we have an infinitesimal length **dl** given by

$$\mathbf{dl} = dx\,\mathbf{i} + dy\,\mathbf{j} + dz\,\mathbf{k}, \tag{2.2}$$

which lies in the scalar field f. Taking the scalar product of **grad** f and **dl**, we obtain

$$\mathbf{grad}\, f \cdot \mathbf{dl} = \frac{\partial f}{\partial x}dx + \frac{\partial f}{\partial y}dy + \frac{\partial f}{\partial z}dz = df, \tag{2.3}$$

where df is the total differential of f, i.e., the change in f over the distance **dl**. Now consider the scalar product in greater detail. First, **grad** $f \cdot$ **dl** $= 0$ generally only when **dl** and **grad** f are at right angles. This condition also implies that $df = 0$, i.e., there is no change in f over the distance **dl**, which will only occur in general when **dl** lies in a surface of constant f. It follows that **grad** f must always be normal to surfaces of constant f. This result also implies that **grad** $f \cdot$ **dl** $= df$ is a maximum when **dl** is similarly oriented in a direction perpendicular to the surfaces of constant f. Clearly, the direction of the gradient is also the direction of the greatest spatial rate of change of the scalar function f and its magnitude is actually equal to this greatest rate of change. This magnitude will be written $|\mathbf{grad}\, f|$ and it follows from Equation 2.1 that

$$|\mathbf{grad}\, f| = \left[\left(\frac{\partial f}{\partial x}\right)^2 + \left(\frac{\partial f}{\partial y}\right)^2 + \left(\frac{\partial f}{\partial z}\right)^2\right]^{\frac{1}{2}}. \tag{2.4}$$

It is interesting to note the growth in complexity that occurs when the gradient operation is used to convert a scalar field to the corresponding gradient vector field. The initial scalar field $f(x, y, z)$ is completely defined by a single value of the scalar quantity at each point, whereas the corresponding gradient field requires knowledge of three quantities at each point if it is to be completely defined. If measurements are made at a single point, the scalar field requires just one measurement, while at least three measurements and perhaps as many as six measurements must be made to obtain the gradient. The larger number arises because the variations of f with distance in each of the x, y, and z directions can only be determined, at least in principle, by measurements made at two or more locations spaced a small distance apart. It is possible, of course, to construct a single sensor containing two or more measuring units that will automatically provide measurements of the spatial rate of change of f in a particular direction. A combination of three such sensors oriented at right angles to each other, and three measurements (one by each sensor), would then suffice to determine the gradient. Such an instrument is very naturally called a *gradiometer*. The somewhat confusing and inconsistent nomenclature used for gradiometers at the present time will be described in the following chapter and a consistent nomenclature introduced, but an inconsistency immediately becomes apparent in the title to this report. If a gradiometer measures the gradient of a scalar quantity, how can there exist such an instrument as a magnetic field gradiometer?

§2.3 Gradient of Vector Quantities

The gradient of a vector quantity, such as the magnetic field, can be defined by a simple extension of the basic definition given above for a scalar field. Suppose the vector quantity is **A**, with components (A_x, A_y, A_z). Each of the three components designates a scalar field, and the following three gradients can be defined:

$$\begin{aligned}
\mathbf{grad}\, A_x &= \frac{\partial A_x}{\partial x}\mathbf{i} + \frac{\partial A_x}{\partial y}\mathbf{j} + \frac{\partial A_x}{\partial z}\mathbf{k}, \\
\mathbf{grad}\, A_y &= \frac{\partial A_y}{\partial x}\mathbf{i} + \frac{\partial A_y}{\partial y}\mathbf{j} + \frac{\partial A_y}{\partial z}\mathbf{k}, \\
\mathbf{grad}\, A_z &= \frac{\partial A_z}{\partial x}\mathbf{i} + \frac{\partial A_z}{\partial y}\mathbf{j} + \frac{\partial A_z}{\partial z}\mathbf{k}.
\end{aligned} \tag{2.5}$$

We can then speak of the gradient of the vector **A** on the understanding that this gradient consists of the three independent parts **grad** A_x, **grad** A_y, and **grad** A_z. In matrix notation, **grad A** can be written

$$\mathbf{grad}\,\mathbf{A} = [\mathbf{grad}\, A_x \;\; \mathbf{grad}\, A_y \;\; \mathbf{grad}\, A_z\,],$$

where

$$[\mathbf{grad}\, A_x \;\; \mathbf{grad}\, A_y \;\; \mathbf{grad}\, A_z\,] = [\mathbf{i} \;\; \mathbf{j} \;\; \mathbf{k}] \begin{bmatrix} \frac{\partial A_x}{\partial x} & \frac{\partial A_y}{\partial x} & \frac{\partial A_z}{\partial x} \\ \frac{\partial A_x}{\partial y} & \frac{\partial A_y}{\partial y} & \frac{\partial A_z}{\partial y} \\ \frac{\partial A_x}{\partial z} & \frac{\partial A_y}{\partial z} & \frac{\partial A_z}{\partial z} \end{bmatrix}. \tag{2.6}$$

The 3×3 square matrix will be referred to as the gradient matrix [G]. In general, this matrix contains 9 independently varying quantities, each of which must be measured if a complete measure of the gradient of the vector quantity is to be obtained.

In the special case of the magnetic field **B**, not all of the 9 terms in the gradient matrix are independent. The restrictions on the terms are of a fundamental nature and they may be derived directly from two of Maxwell's equations. The first restriction arises because of the requirement that div $\mathbf{B} = 0$, which may be written

$$\frac{\partial B_x}{\partial x} + \frac{\partial B_y}{\partial y} + \frac{\partial B_z}{\partial z} = 0. \tag{2.7}$$

Thus the sum of the three diagonal terms in the gradient matrix for the magnetic field must be zero, or, given any two of the terms, the third is restricted to the negative sum of the other two.

The second restriction of the terms in the gradient matrix only applies in a 'source-free' region, where another of Maxwell's equations can be written **curl B** = 0. (A source-free region here implies that both the impressed current density **J** and the displacement current density $\partial \mathbf{D}/\partial t$ are zero). Equating the individual components of **curl B** to zero, we obtain

$$\frac{\partial B_z}{\partial y} = \frac{\partial B_y}{\partial z}; \quad \frac{\partial B_z}{\partial x} = \frac{\partial B_x}{\partial z}; \quad \frac{\partial B_y}{\partial x} = \frac{\partial B_x}{\partial y}. \tag{2.8}$$

These three relations imply that the gradient matrix in a source-free region is symmetric. Combining Equations 2.7 and 2.8, it can be seen that only 5 of the 9 terms in the gradient matrix for the magnetic field can be truly independent in such a region. Although there is no difficulty visualizing source-free regions in theory, there may be considerable practical difficulty obtaining such regions for gradient measurements, particularly if measurements of high sensitivity are involved. The validity of the source-free assumption is examined in Appendix A.

§2.4 Gradient of the Total Field

As was noted in Section 2.1, it is possible to construct a scalar field from a vector field by neglecting the direction and considering only the magnitude of the quantity. For example, given the vector field $\mathbf{A} = (A_x, A_y, A_z)$ considered in the previous section, we have at each point a magnitude $|\mathbf{A}|$ given by

$$|\mathbf{A}| = [A_x^2 + A_y^2 + A_z^2]^{\frac{1}{2}}. \tag{2.9}$$

In many contexts this scalar quantity $|\mathbf{A}|$ is referred to as the *total field* in distinction to the components A_x, A_y, and A_z of the field.

Given the scalar field represented by $|\mathbf{A}|$, we can obtain the gradient by using

$$\mathbf{grad}\,|\mathbf{A}| = \frac{\partial |\mathbf{A}|}{\partial x}\,\mathbf{i} + \frac{\partial |\mathbf{A}|}{\partial y}\,\mathbf{j} + \frac{\partial |\mathbf{A}|}{\partial z}\,\mathbf{k}. \tag{2.10}$$

Then, since

$$|\mathbf{A}|\frac{\partial |\mathbf{A}|}{\partial x} = A_x\frac{\partial A_x}{\partial x} + A_y\frac{\partial A_y}{\partial x} + A_z\frac{\partial A_z}{\partial x},$$

$$|\mathbf{A}|\frac{\partial |\mathbf{A}|}{\partial y} = A_x\frac{\partial A_x}{\partial y} + A_y\frac{\partial A_y}{\partial y} + A_z\frac{\partial A_z}{\partial y},$$

$$|\mathbf{A}|\frac{\partial |\mathbf{A}|}{\partial z} = A_x\frac{\partial A_x}{\partial z} + A_y\frac{\partial A_y}{\partial z} + A_z\frac{\partial A_z}{\partial z},$$

we have

$$\begin{aligned}|\mathbf{A}|\,\mathbf{grad}\,|\mathbf{A}| =&(A_x\frac{\partial A_x}{\partial x}+A_y\frac{\partial A_y}{\partial x}+A_z\frac{\partial A_z}{\partial x})\,\mathbf{i}\\ &+(A_x\frac{\partial A_x}{\partial y}+A_y\frac{\partial A_y}{\partial y}+A_z\frac{\partial A_z}{\partial y})\,\mathbf{j}\\ &+(A_x\frac{\partial A_x}{\partial z}+A_y\frac{\partial A_y}{\partial z}+A_z\frac{\partial A_z}{\partial z})\,\mathbf{k},\end{aligned}$$

or

$$\mathbf{grad}\,|\mathbf{A}| = |\mathbf{A}|^{-1}\,(A_x\,\mathbf{grad}\,A_x + A_y\,\mathbf{grad}\,A_y + A_z\,\mathbf{grad}\,A_z). \tag{2.11}$$

In matrix form, this expression can be written

$$\mathbf{grad}\,|\mathbf{A}| = |\mathbf{A}|^{-1}\,[\mathbf{i}\quad\mathbf{j}\quad\mathbf{k}]\,[\mathrm{G}]\begin{bmatrix}A_x\\A_y\\A_z\end{bmatrix}, \tag{2.12}$$

where [G] indicates the 3×3 gradient matrix defined in the previous section.

It is easily seen that the gradient of the magnitude of a vector (*i.e.*, the gradient of the total field) is not a simple quantity. In practice, measurement of the gradient of the total field can be quite involved if only component sensors are available, or relatively simple if sensors are available that provide a measure of the total field. Let us suppose that only component sensors are available. In this case a single measurement of the gradient of the total field involves, in general, nine separate, simultaneous measurements of the nine spatial rates of change of the three field components as well as three separate, simultaneous measurements of the actual components themselves, *i.e.*, 12 simultaneous measurements in all. On the other hand, if total field sensors are available, only three measurements of the spatial rates of change $\partial|\mathbf{A}|/\partial x$, $\partial|\mathbf{A}|/\partial y$, $\partial|\mathbf{A}|/\partial z$ need be made and the gradient can then by calculated directly using Equation 2.10. For measurements of the magnetic field, it turns out that both component and total field magnetometers are available and it would appear, at least on the surface, as if the gradient of the total field could be measured most easily with total field sensors, even though there would be some simplification in the component measurements due to the relationships between some of the terms involved (as discussed in the previous section). Unfortunately, total field magnetometers are relatively insensitive. There is no ambiguity for electric fields: all electric field sensors in common use measure components of the electric field.

Chapter 3

The Magnetic Field Gradiometer Nomenclature

The present nomenclature for magnetic field gradient measurements has developed largely on an *ad hoc* basis and it contains terms that are not standard and which are sometimes used differently by different investigators. In addition, there is at least one term coming into informal use, namely 'long-baseline gradiometer,' which does not in fact usually describe a gradiometer; the related term, 'short-baseline gradiometer' is not quite as undesirable, but it contains a redundancy. In this section a system of standardized nomenclature is introduced, which is then used throughout the remainder of the report. This might all sound very dry and pedantic, but it is a necessary step for us to take if we are to avoid a lot of unnecessary confusion while discussing gradiometers, and it gives us an opportunity to consider the essential characteristics of a magnetic field gradiometer.

§3.1 Gradient and Gradiometers

One of the first difficulties that arises in gradiometer nomenclature is the use of the term 'gradient' for different quantities. On the one hand we have the well-established gradient of vector analysis, which is intrinsically a vector quantity with both magnitude and direction (Section 2.2). On the other hand, we have the everyday concept of gradient as a slope, or spatial rate of change, with direction undefined or at best specified only in vague, general terms. In between these two concepts of gradient we have the gradient defined in the dictionary as the change in value of a quantity per unit distance in a specified direction. This definition is close to the one used in vector analysis, but it differs in one important feature: the vector analysis gradient has a direction that is completely determined, whereas the dictionary definition appears to leave open the possibility of choice of direction. The vector analysis and dictionary definitions can be made to correspond by simple additions to the latter to give the following:

> The gradient is the change in value of a scalar quantity per unit distance in a specified direction, i.e., the direction in which the increase in value of the quantity per unit distance is a maximum.

In this work the term 'gradient' will be used in its strict vector analysis sense, as described in the previous chapter. The gradient is therefore a vector quantity derived basically from a scalar function of position according to Equation 2.1. The gradient of a vector quantity is also meaningful, provided it is derived according to the procedure described in Section 2.3. Total field gradients are potentially troublesome to measure unless total field sensors are available, but there is no inconsistency in the concept of a total field gradient in the sense discussed in Section 2.4. We can therefore use the term 'gradiometer' without misgiving provided it is used solely to describe an instrument for the measurement of the gradient of scalar or vector fields, with gradient being used in its strict vector sense. Simple descriptive terms can then be added to indicate the type of gradiometer. For example, we can speak of temperature gradiometers, magnetic field gradiometers, and so on.

§3.2 Number of Axes

A second difficulty that arises with nomenclature is a moderately simple one involving the number of measurements of the components of the gradient that a given gradiometer can make simultaneously. The simplest gradiometers, such as the one described in Chapter 1, consist basically of two sensors spaced a small distance apart and they only have the capability of measuring one spatial rate of change at any one time. If it is the gradient of a scalar field that is being measured, the gradiometer must in general be reoriented two more times along orthogonal directions in order for all three components of the gradient to be obtained. This procedure may not be a problem if the scalar field is stationary, but if it is varying with time it may be impossible to obtain a meaningful gradient measurement. The difficulty with vector fields is even more acute, since at least five and possibly as many as eight measurements have to be made to obtain the gradient of a magnetic field, and nine measurements are required in general. It is possible of course to argue that the gradient measurements only have to be made along the direction of **maximum** spatial rate of change of the scalar quantity or vector component that is of interest, and that this will cut down on the measurements required. However, this is not a valid argument, because the direction of maximum spatial rate of change can only be detected with a simple two-sensor gradiometer by varying its orientation until a maximum measurement is obtained. If the fields are time varying the gradient measurement obtained by this means will once again probably not be meaningful.

It is important therefore to be able to specify the capability of a gradiometer to measure simultaneously a given number of orthogonal spatial variations. The necessary nomenclature is already partly in use: a gradiometer that can measure just one spatial variation at a time is sometimes referred to as a *single-axis gradiometer* and gradiometers intended for magnetic field measurements are occasionally described as *five-axis gradiometers*. I suggest that the descriptive term 'n-axis,' where n is the number of spatial variations that can be measured simultaneously, be appended to any gradiometer reference, at least initially, so that the capability of the gradiometer is immediately apparent. In summary, the general gradiometer nomenclature I would recommend for use at the present time has the form

n-axis (optional: mode of operation) (kind of field) gradiometer

with typical examples being single-axis temperature gradiometer, five-axis magnetic field gradiometer, and five-axis superconducting magnetic field gradiometer.

§3.3 Gradiometers or Differential Magnetometers?

Let us now consider a third difficulty with terminology, namely the appropriateness of the term 'long-baseline' in the description of a gradiometer. (Notice that I have left a place for this term in my nomenclature designation above!) As should be obvious by now, I have been recommending terminology that is faithful to the mathematical basis of vector analysis, and this is the first instance of a description that is frequently used in a manner that is inconsistent with this mathematical basis. Before passing any possibly arbitrary judgement on the term, I will briefly outline how it arises.

Suppose the solenoid sensors in my simple single-axis magnetic field gradiometer (Section 1.2) were to be moved further apart than the 4 m that was specified for the gradiometer, but with no change made in their orientation. It would soon be found that the spacing, or *baseline*, could be made very large indeed before the natural magnetic field fluctuations measured by each solenoid became so different that the signals from each solenoid would no longer cancel. The measurements that have been made so far of the spatial rates of change of fluctuations with frequencies in the range 0.3 7.2 Hz are not yet adequate enough for me to quote distances for cancellation with confidence, but I am reasonably sure that substantial cancellation would be observed in the solenoid system for spacings of up to 1 10 km. Now, suppose we wished to count the number of cars driven along a particular stretch of road by placing one of the solenoid sensors beside the road and using the large output signals produced every time a car went by [*Johnston and Stacey*, 1968] to operate an automatic counter. If we were to set up such a system we would soon find that it was quite unreliable, because every time there was a magnetic storm, or other large natural magnetic disturbance, the signal produced by a car would either (1) be lost in the noise produced by the natural disturbance or (2) it could not be distinguished from other comparable signals produced by the disturbance. The solution to this noise problem is to place another similarly-oriented solenoid sensor some distance away from the road sensor, at a location where the signals produced by the cars have become too small to be measured, and to use its output to cancel the natural noise component in the output of the monitoring solenoid. Then, ideally, the only output of the two-solenoid system would be the signals produced by the cars on the road, and they could be processed automatically without concern for the effects of natural magnetic field fluctuations.

Monitoring systems analogous to the one I have just described have been studied for a number of years [*e.g., Boger and Bostick*, 1968; *Smith et al.*, 1969; *Fowler et al.*, 1973; *Ko et al.*, 1976; *Goubau et al.*, 1978; *Cornwell and Hart*, 1979; *Ware*, 1979] and they provide valuable information. It is systems such as these that are now being informally referred to as long-baseline gradiometers. However, as I will now show, they are not really gradiometers at all.

As pointed out in the previous chapter, an essential feature of gradient measurements is the determination of spatial rates of variation of the form $\partial f/\partial x$, where f is the scalar field quantity whose gradient is required and x is a measure of distance. In practice, the gradient measurement involves a determination of ratios of the form $\Delta f/\Delta x$, where Δf is the change

in f over the small distance Δx. Strictly, the gradient term under consideration is obtained in the limit, since

$$\frac{\partial f}{\partial x} = \lim_{\Delta x \to 0} \frac{\Delta f}{\Delta x}, \tag{3.1}$$

where I assume the other independent variables are kept constant as Δx is varied. An extraordinarily conscientious experimenter would therefore choose a small distance over which to measure the change in f; he (or she) would then halve the distance and measure the change in f again. If the limit is being approached, the ratio $\Delta f/\Delta x$ will be very closely the same in the two cases. Such a procedure would be impossibly time-consuming if many gradient measurements were required, and it is not a regular procedure in any event. However, it does provide us with a useful practical criterion for determining when a pair of magnetometers is spaced correctly for gradiometer operation. The basic criterion of course is that the spacing between the magnetometers must be 'small,' but the question arises small relative to what? We can now answer this question by stating the following two **practical criteria for gradiometer operation**:

The spacing between two magnetometers is suitable for the pair to be used as a gradiometer if (1) the spacing is small relative to the applicable gradiometer-to-source distance. If this criterion leaves any doubt, we can further specify that (2) the spacing is small when the response of the magnetometer pair (when connected in opposition) to the magnetic field of the source varies linearly with the spacing. The latter criterion follows from Equation 3.1.

Having developed criteria for gradiometer spacing, we can now establish whether a particular magnetometer pair is capable of functioning as a gradiometer under a specified set of experimental conditions. It follows from the criteria that the use of magnetometer pairs for monitoring under the specific conditions I have described above for the two-solenoid system is not a legitimate gradiometer application: the spacing between the magnetometers is comparable to the distance from the source to the center of the line joining the magnetometers. Note, however, that the magnetometer pair could function as a gradiometer if the source that was being monitored was moved far enough away from the magnetometers for the gradiometer criteria to apply.

The nomenclature I would suggest for monitoring systems based on pairs of widely-spaced magnetometers is once again derived from descriptions used by some authors (*e.g., Chapman and Nelson* [1957], and *Breiner* [1973]). Instead of long-baseline gradiometer, I recommend use of the term *differential magnetometer*. Thus a magnetic field gradiometer can be considered to be a particular kind of differential magnetometer, *i.e.*, one distinguished by the fact that the spacing between its sensors is small with respect to the distance to the sources whose gradients are to be measured [*Breiner*, 1973]. Short-baseline gradiometers, of course, are best referred to simply as gradiometers under most circumstances because of the redundancy in terminology, but there may be special situations, such as the one mentioned at the end of this section, where 'short-baseline' is a meaningful gradiometer description.

The reader is now asked to refer back to the description of the simple gradiometer given in Section 1.2, and in particular to the top panel of Figure 1.2, and to question whether the two-solenoid system is being used strictly as a gradiometer when it detects the magnetic field of the steel object. Correct! The system is being used as a differential magnetometer, and not as a gradiometer, because the distance from the source of magnetic field to the center of the line joining the solenoids (8 m) is comparable to the length of the baseline (4 m).

Before concluding this discussion of pairs of widely-spaced magnetometers and their transition into gradiometers as their spacing is reduced, or as the distance to the source of magnetic fields is increased, I would like to draw attention to an important feature of a magnetic field gradiometer's response. When the spacing between the two magnetometers is small according to the criteria I have listed, it is still possible to vary the spacing between zero and some maximum value that will depend on the particular source-gradiometer configuration, and there is an advantage to having the spacing close to the maximum value. Since we are still in the linear regime, by definition, the difference signal produced by the pair of magnetometers is largest when their spacing is at its maximum value. Assuming that the noise in the magnetometers (or in the system as a whole) is independent of the spacing, which is likely to be a good assumption for most systems, it can be seen that the largest signal-to-noise ratio is obtained for the largest spacing. There is therefore considerable incentive to have the spacing between the magnetometers as large as possible while still operating in the gradiometer mode. For this last situation, and for others where the spacing is smaller but still comparatively large, use of the term 'long-baseline gradiometer' may well be appropriate to distinguish the gradiometer from one with a comparatively small baseline ('short-baseline gradiometer').

§3.4 The Order of a Gradiometer

The fourth and final difficulty with nomenclature that I wish to consider here arises in the design and application of superconducting gradiometers. These gradiometers are being used increasingly for biomedical research and as clinical instruments. For these applications, the gradiometers are operated in what *Goodman et al.* [1973] call the 'near-to-source field measurement' mode: because of the extreme weakness of the fields, the gradiometer must be located very close to their sources (*e.g.*, the heart, lungs, or brain of a living person). Unfortunately, the gradiometers must also be operated in laboratories or clinics, where sources of electromagnetic noise are abundant and located close to the gradiometers. It is usually impractical to construct a completely shielded enclosure for the gradiometer measurements, although at least one such enclosure has been built for research purposes [*Cohen et al.*, 1970; *Cohen*, 1975]. A particularly effective solution to this problem is to construct more complicated coil configurations for the gradiometer sensor, which make the gradiometer less sensitive to the magnetic fields from nearby noise sources while retaining high sensitivity to the fields from sources close to the gradiometer. I have not yet described the sensors used in superconducting magnetometers and gradiometers; they consist of small superconducting coils, usually of a single turn, that are connected to the input coil of a Superconducting QUantum Interference

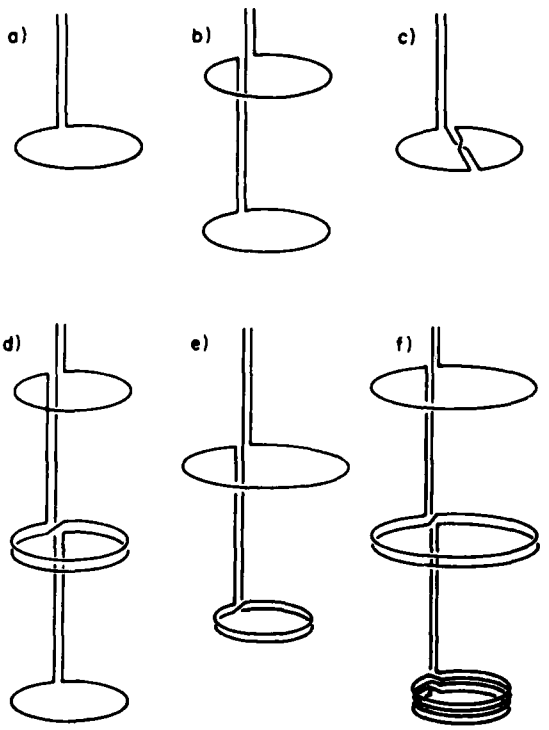

Figure 3.1. Sensing coils used in superconducting magnetometers and gradiometers. The following configurations are shown: a) magnetometer, b) simple, or first-order, gradiometer, c) off-diagonal gradiometer, d) second-order gradiometer, e) asymmetrical first-order gradiometer, f) asymmetrical second-order gradiometer [*Williamson and Kaufman*, 1981]. All of the gradiometer configurations are single-axis, *i.e.*, they only make measurements on a single magnetic field component.

Device, or *SQUID* [*Clarke* 1974] - a Josephson junction device that is the electronic heart of any superconducting magnetometer and gradiometer. Although the sensing coils are small and superconducting, their configurations are conventional: a single coil is used as the basic sensing element in superconducting magnetometers, two coils connected in series opposition are used as the sensing element in superconducting gradiometers. Figure 3.1, taken from a review by *Williamson and Kaufman* [1981], shows these two coil configurations labelled a) and b). The other coil configurations in the figure represent most of the varieties of the more complicated configurations that are used in practice.

The configuration of immediate interest to us is the one labelled d) and referred to as a *second-order* gradiometer. It will also be noted that the basic (single-axis) gradiometer is referred to by Williamson and Kaufman as a *first-order* gradiometer. We have not so far encountered these descriptive terms for gradiometers in this report, nor has the term *asymmetric* been used. In fact, this new terminology is presently confined largely to those

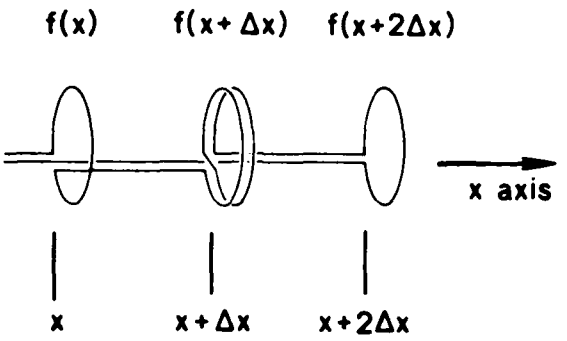

Figure 3.2. The second-order gradiometer shown in Figure 3.1 d), with an x-axis added and labelling to denote the positions of the coils on the axis. The quantities f shown above the coils indicate what the coils are measuring.

superconducting gradiometers used for biomedical research and as clinical instruments. I discuss it here not merely for completeness but for the more positive reason that it is useful terminology and the instrumentation that is being developed could have application in other areas.

The two examples of asymmetrical gradiometers shown in Figure 3.1 adequately illustrate the meaning of the term and we need not be concerned further with it here. The origin of the descriptions first- and second-order may not be so obvious, unless it is recognized that the second-order gradiometer sensor shown in the figure is simply two of the first-order, or standard, gradiometer sensors moved a small distance apart along their common axis (in the example shown this distance is equal to the spacing of the coils) and connected in series opposition. The procedure used to construct a second-order gradiometer is therefore wholly analogous in principle to the procedure used to construct a (first-order) gradiometer from a magnetometer. It should be no surprise to learn that the second-order gradiometer measures the second spatial derivative of the magnetic field component directed along the gradiometer axis. The following derivation shows how the second-derivative response can be obtained from first principles using only our basic knowledge of gradiometers.

Let us assume that we have two single-axis double-loop gradiometers of the kind illustrated in Figure 3.1 a), both sharing the same axis and identical in every way. Take this common axis to be the x-axis, and suppose one of the gradiometers is moved along the axis relative to the other gradiometer until two of the coils coincide, thus giving the configuration shown in Figure 3.1 d) once the gradiometers are connected in series opposition. The spacing between the coils in the gradiometers is Δx, which is assumed to be small relative to the distance to the source of the magnetic field component that they are measuring. For generality, and to maintain a notation consistent with the one used in Section 3.3, I will use f to denote the quantity being measured. Looking more closely at these measurements, the coils in the 4-coil system (which I am not referring to as a gradiometer at this stage) make three simultaneous measurements of f, as indicated in Figure 3.2. With the notation shown in the figure, the gradiometer on the

left measures the quantity

$$\frac{f(x) - f(x + \Delta x)}{\Delta x},$$

and the gradiometer on the right measures the quantity

$$\frac{f(x + \Delta x) - f(x + 2\Delta x)}{\Delta x}.$$

The 4-coil system measures the difference between the measurements made by the individual gradiometers. Assuming that the coil spacing Δx is included in this measurement in the same way as it is in the measurements made by the gradiometers, the output of the 4-coil system can be written

$$\frac{1}{\Delta x}\left(\frac{f(x) - f(x + \Delta x)}{\Delta x} - \frac{f(x + \Delta x) - f(x + 2\Delta x)}{\Delta x}\right).$$

We now use Taylor series expansions to convert the functions $f(x + \Delta x)$ and $f(x + 2\Delta x)$ into the following approximate forms

$$\begin{aligned} f(x + \Delta x) &= f(x) + \frac{\partial f}{\partial x}\Delta x + \frac{1}{2}\frac{\partial^2 f}{\partial x^2}(\Delta x)^2, \\ f(x + 2\Delta x) &= f(x) + \frac{\partial f}{\partial x}2\Delta x + \frac{1}{2}\frac{\partial^2 f}{\partial x^2}(2\Delta x)^2. \end{aligned} \tag{3.2}$$

The approximation involved in these expansions is the neglect of higher-order terms, and as Δx tends to zero the expansions become increasingly accurate. Inserting the expanded forms of $f(x + \Delta x)$ and $f(x + 2\Delta x)$ into the expression for the output of the 4-coil system and taking the limit, we obtain

$$\lim_{\Delta x \to 0}\left(\frac{f(x) - f(x + \Delta x)}{\Delta x} - \frac{f(x + \Delta x) - f(x + 2\Delta x)}{\Delta x}\right) = \frac{\partial^2 f}{\partial x^2}. \tag{3.3}$$

This shows that the 4-coil system does indeed measure the second spatial derivative of the variable of interest. It is therefore appropriate to refer to it as a second-order (single axis) magnetic field gradiometer—an instrument that measures the second spatial derivative of the magnetic field component directed along its axis.

The advantage of the second-order single-axis gradiometer is its increased discrimination against noise from nearby sources. If even greater discrimination is needed, it is possible to repeat the gradiometer generation process with two second-order single-axis gradiometers and thus produce a third-order single-axis gradiometer that measures $\partial^3 f/\partial x^3$ [*Vrba et al.* 1982]. The procedure could be repeated *ad infinitum*, but probably with a rapidly diminishing return.

Chapter 4

The Magnetic Field Gradiometer Historical Development

§4.1 Early Gradiometers

The first published article describing a magnetic field gradiometer appears to be one authored by *Haalck* [1925], who based his gradiometer on what was then a well-known measuring instrument in Physics laboratories- the earth inductor. Haalck's article is written in German, but an English summary is given by C. A. Heiland in a later article by *Roman and Sermon* [1934] describing a similar form of gradiometer. Both of the gradiometers described by these authors consist of two identical coils spaced a small distance (1-2 m) apart and rotated together at the same speed, either on parallel shafts [*Roman and Sermon*, 1934] or on a single common shaft [*Haalck*, 1925]. Haalck's gradiometer was more typical in that his coils were connected in series and in opposition, with the pair producing no output signal when the two coils were rotated in the same magnetic field. When the two coils were not located in the same magnetic field, the output signal consisted of the difference of the emf's induced in the coils. It is worth noting that this output signal was proportional to the speed of rotation of the coils. Roman and Sermon measured the ratio of the emf's produced in their coils, which is independent of the speed of rotation of the coils and which, in addition, is not a direct measure of the gradient of the geomagnetic field. (However, Roman and Sermon point out that the ratio measures a relative gradient that is nearly proportional to the actual gradient.)

The work of *Haalck* [1925] and *Roman and Sermon* [1934] broke new ground, but it was never followed up, as one would expect, by further publications describing improvements to their rotating coil gradiometers. The reason for this apparent dead-end to their line of research is not completely clear. However, the development of fluxgate magnetometers and research during World War II on *magnetic anomaly detection* (MAD; the description is commonly used synonymously with submarine detection) that led to more sensitive gradiometers based on

fluxgate sensors appear to have played a major role, as indicated by the following comments taken from an article by *Fromm*[1952]:

> British MAD developments were such that by early 1941 a two-coil gradiometer was being tested operationally. This gradiometer consisted of coils about 1 ft in diameter, mounted coaxially in a supporting framework and separated by about 8 ft. Because this gradiometer system measured the space rate of change of the magnetic gradient, which varies inversely as the fifth power of the distance from the submarine, its performance was poor and its possibilities very limited. However, its development was continued in the United States until late in 1941, at which time it became apparent that the saturable-core magnetometer was more promising. Development of other magnetometers, including the gradiometer, was therefore terminated.

According to Fromm, the coils in these gradiometers were not rotated. It was intended that they would be flown in aircraft and that signals would be induced in them because of their translational motion through the geomagnetic and any other magnetic fields that might be present. The lack of rotation of the coils may have been a convenience, but it meant that the amplitudes of the signals induced in the coils were proportional to the speed of the aircraft, which was not very great in the early 1940's (and which probably can never be very great in any case during a search for submarines). The combination of slow aircraft speed, giving small induced signals in the coils, and the inverse fifth power decline with distance of the response of the gradiometer to submarine fields, was a severe handicap to overcome, and in retrospect it is no surprise that the performance of the gradiometer was poor.

§4.2 The Fluxgate Gradiometer

Fromm [1952] indicates that gradiometer development for MAD, and presumably for other uses as well, was abandoned during World War II in favor of work on the fluxgate, or saturable-core, magnetometer. Although research on the fluxgate principle had been undertaken during the 1930's, it appears that V.V. Vacquier of the Gulf Research and Development Company was the first to suggest its application in sensitive magnetic field detectors and the development of fluxgate magnetometers for prospecting purposes was begun by Gulf in 1940. *Hood* [1965] reports that Vacquier applied for a (fluxgate) gradiometer patent in 1941, at the same time as he applied for a patent on the fluxgate sensor: both patents were awarded in 1946. As might be expected, application of fluxgate magnetometers to submarine detection followed rapidly on their initial development for geophysical prospecting, and Fromm describes the resulting instrumentation in considerable detail. It appears that Vacquier's fluxgate gradiometer concept was not pursued further during the war. Following the war, an article by *Wurm* [1950] appeared describing wartime research in Germany on both a fluxgate instrument (Feldstärkemesser) and a gradiometer based on it (Feldstärkedifferenzmesser). However, as pointed out by Fromm, the instrumentation that was developed does not seem to have been put into operational use, and the lack of later publications concerning it suggests that the idea of a fluxgate gradiometer was not pursued further in Germany. In fact, by the early 1950's, when Wurm and Fromm

published their articles, the brief life of fluxgate gradiometers was rapidly drawing to a close. An attempt by Gulf to use one for airborne prospecting was a failure [*Wickerham*, 1954], although the fluxgate magnetometer continued to be actively developed for 'aeromagnetics' [*Reford and Sumner*, 1964]. A final paper describing a fluxgate gradiometer constructed for laboratory measurements was published by *Morris and Pedersen* [1961]. This latter instrument had a base length of 4.6 m and a noise level of about 5 nT/m peak-to-peak for a bandwidth that was unspecified but which was probably of the order of 0 1 Hz (*i.e.*, the bandwidth mentioned by *Serson* [1957] for his fluxgates, on which the gradiometer was based).

One of the driving forces behind the development of magnetic field sensors after the war was the interest in using the sensors for geophysical prospecting, and fluxgate gradiometers did not prove to be useful la gely because of the difficulty ensuring that the sensor elements were accurately aligned at all times. As pointed out at the end of Section 1.2, the alignment problem is one of the crucial problems that must be faced when using gradiometers based on component magnetometers (in distinction to total field magnetometers), and it is particularly difficult to ensure alignment when the gradiometer is subject to considerable handling and substantial vibration, which can hardly be avoided on an aircraft. Wickerham's comments on this problem are still pertinent today:

> The requirements for alignment of one element with respect to the other are impossibly high. If operated in the most favorable position, namely, parallel to the total vector, the total ambient field observed by each element may be of the order of 50,000 gamma. Then, from an orientation standpoint, a misalignment of 1 gamma represents $\cos^{-1}\theta = 0.99998$, or $\theta = 1/3^{\circ}$. Hence a transient misorientation of one element axis with respect to the other of $1/3^{\circ}$ would be recorded as a very significant apparent anomaly.

Partly because of this alignment problem, there was interest among the geophysical prospecting community in what was called 'time-derivative gradiometers' [*Wickerham*, 1954; *Glicken*, 1955].

§4.3 The Time-Derivative Gradiometer Technique

The time-derivative gradiometer technique is best illustrated by reference to Figure 4.1, which is taken from the article by Wickerham [1954]. Shown in the bottom portion of the figure, beneath the line designating the earth's surface, is an idealized intrusion of igneous rock, which is comparatively highly magnetic. In this idealized example the igneous rock has a typical narrow zone of mineralization at its interface with the surrounding weakly magnetic or non-magnetic rock. Locating this mineralization is the primary goal of the aeromagnetic search. The upper part of the figure shows an example of the kind of record of the total field that might be obtained by an aircraft equipped with a total field magnetometer as it flies over the intrusion at constant speed in a horizontal straight line. The variation of the total field that is shown is a variation with distance, but it could as well be considered a variation with time since the distance travelled by the aircraft is proportional to the time measured from the start of the pass over the intrusion. The dashed line in the figure shows the spatial rate of

change of the total field along the line travelled by the aircraft; it is obtained by differentiating the upper curve with respect to distance. With the exception of one feature that I will shortly discuss, the dashed curve is essentially the response that would be obtained from a single-axis total field gradiometer if it was flown along the path of the aircraft with its axis aligned along the path. It is for this reason, and because the differentiation with respect to distance is equivalent to differentiation with respect to time insofar as the shape of the gradient curve is concerned, that the system is referred to as a time-derivative gradiometer. I prefer not to call it a gradiometer, since its sensor is a single total field magnetometer, but 'time-derivative gradiometer technique' is descriptive and not inaccurate. The defect of this technique is not discussed either by Wickerham or Glicken, but the reader will surely be aware of it by now: the total field variation recorded by the magnetometer includes time variations of the geomagnetic field that occur during the flight. As a result of these time variations, the small oscillations of the gradient curve that are supposed to identify the mineralization could as well be caused by a magnetic storm or other strong disturbance of the geomagnetic field.

The time derivative gradiometer technique was effectively rendered obsolete by one of the two major advances that have taken place in gradiometer technology since World War II. In this case the major advance was the invention and development of compact and reasonably rugged total field magnetometers—not fluxgate sensors oriented and stabilized by mechanical means along the direction of the magnetic field (as were used by Wickerham and Glicken), but magnetometers with an intrinsic response to the total field. These magnetometers could easily be flown in pairs and their output signals combined in opposition to produce a true single-axis total field gradiometer, thus avoiding the ambiguity caused by natural geomagnetic field fluctuations in the time-derivative technique.

§4.4 Total Field Magnetometers and Gradiometers

The first of the new total field magnetometers appeared in 1953 [*Packard and Varian*, 1954] and they are now generally referred to either as proton precession magnetometers or, more generally, as one variety of a class of *resonance magnetometers* [*Grivet and Malnar*, 1967; *Hartmann*, 1972] Their construction is simple and rugged and they are therefore much used for geophysical measurements [*Breiner*, 1973], where these characteristics and their easy portability are particular advantages. They usually do not have a continuous output and readings are provided every few seconds; the actual rate depends to some extent on the sensitivity and higher reading rates generally imply lower sensitivity. Gradiometers have been constructed using these magnetometers [*Waters and Francis*, 1958; *Aitken and Tite*, 1962] and commercial units are available. *Aitken and Tite* [1962] used a 3.05 m (10 ft) baseline and achieved a sensitivity of about 600 pT/m, *i.e.*, the smallest gradient that could be distinguished above the system's internal noise (and possibly also external noise) was about 600 pT/m. Assuming linearity of response (as did Aitken and Tite), this sensitivity transforms into a value of 2000

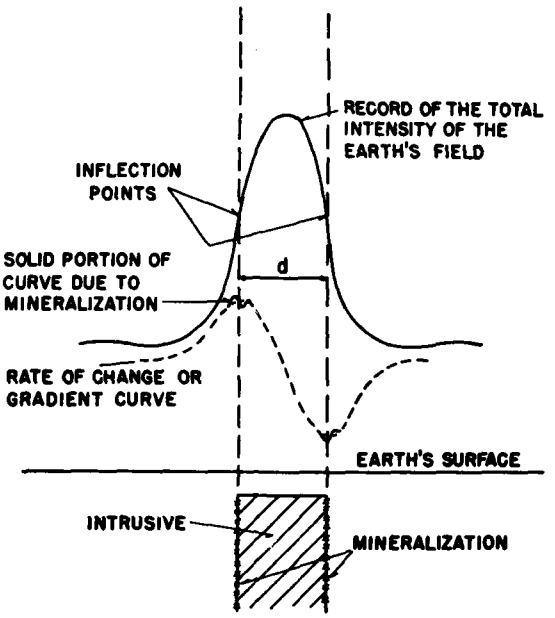

Figure 4.1. Illustrative profiles showing the variation with horizontal distance of the total magnetic field (solid line) and of the horizontal component of the gradient of the total magnetic field (dashed line) associated with an idealized intrusion of igneous rock [*Wickerham*, 1954].

pT/m for a 1 m baseline. The sensitivity of one recent commercial unit is advertised as being 0.82 pT/m, but the magnetometer spacing required to achieve this sensitivity is a high 152 m. Once again assuming linearity of response, the sensitivity transforms into 125 pT/m for a 1 m baseline—a greatly improved sensitivity compared with that of Aitken and Tite's pioneering instrument.

The second variety of the new total field magnetometers made its first appearance in 1957. Operation of these magnetometers is based on the principle of optical pumping of electrons in a gas or vapor; the principle was well known in the 1950's, but the feasibility of the magnetometers only became apparent following the work of *Dehmelt* [1957]. Alkali metal vapors (usually rubidium or cesium vapors) or helium gas are now most commonly used as the active medium in a small absorption cell, and the magnetometers are referred to variously as rubidium-vapor, cesium-vapor, and helium magnetometers depending on the active medium. Because the same general resonance theory applies to the processes involved in these magnetometers, the optically-pumped magnetometers are sometimes included with the proton precession magnetometers under the general title of resonance magnetometers [*Grivet and Malnar*, 1967; *Hartmann*, 1972]. However, considering the very substantial differences in their construction and operation, it seems more appropriate to separate them, and other systems based on them, into two classes as I have done here.

Optically-pumped magnetometers have a continuous output, a high signal-to-noise level, and high sensitivity, but they are complicated instruments particularly when compared with proton precession magnetometers. The complication depends very much on the intended use of the instrument. If it is to be used in a geomagnetic observatory, for example, where no motion is involved, a single sensing cell may be used and the magnetometer will be comparatively simple [*Usher and Stuart*, 1970]. For most field operations, however, and for aeromagnetic surveys and airborne ASW in particular, additional sensing cells are required and the complexity of the instrument is increased. There are two reasons for having the additional cells, both relating to the dependence of the output signal of an optically-pumped cell on its orientation relative to the earth's magnetic field [*Reford and Sumner*, 1964; *Slack et al.*, 1967]. The first reason for adding cells is to avoid a comparatively minor error in the measured value of the field that occurs when an individual cell is rotated through 180°: a dual cell, single axis sensor solves this problem. The other reason for adding cells is to avoid dead zones in the response of the cells. These zones result from the changes that occur in the amplitude of the output signal of an individual cell as its orientation changes with respect to the earth's field. No error is involved, but the signal amplitude can drop below a level required for operation of the signal processing electronics. The solution to this problem is to triple the number of cells and arrange for their axes to be mutually perpendicular. The net result of these two solutions is a sensor assembly containing six cells. Despite the need for a number of cells, the resulting optically pumped magnetometers can be made rugged enough for airborne operation, and the large number of articles in the scientific literature describing measurements made by airborne instruments attests to their reliability and sensitivity. It might also be added that the standard airborne magnetometer for ASW in the U.S. is the Model ASQ-81 helium magnetometer, containing six helium cells.

Considerable use has been made of optically pumped magnetometers in gradiometers, usually for airborne use. In most cases the two magnetometers comprising the gradiometer are flown one above the other in a predominantly vertical configuration, thus measuring the vertical component of the gradient of the total field (more precisely, because the gradiometer is being flown, it will measure the variation along some horizontal line of the vertical component of the gradient) [*Slack et al.*, 1965]. To assist in the interpretation of the gradient data, theoretical studies have been made of the variation of the vertical component over various representative magnetic anomalies [*e.g., Hood and McClure*, 1965; *Hood*, 1965]. Marine application of the magnetometers appears to have been minimal. However, a cesium-vapor gradiometer for marine use was constructed and tested in 1966. Incorporated into a catamaran, and intended to be towed behind another vessel, the gradiometer consisted of two magnetometers about 4 m (12 ft) apart and its noise level in the absence of swell was quoted as being about 4 pT/m [*Staff Rept.*, 1967].

The sensitivities of gradiometers constructed from optically pumped magnetometers are reasonably high. The sensitivity of the gradiometer described by *Slack et al.* [1965], for example, was about 0.7 pT/m for a 30.5 m (100 ft) baseline; the corresponding value for our reference 1 m baseline is 20 pT/m. The catamaran gradiometer had a similar sensitivity in the absence of wave noise. It is very likely that the sensitivities have been improved in recent years.

§4.5 Superconducting Magnetometers and Gradiometers

We come now to the most recent major magnetometer development: superconducting magnetometers. The development of these magnetometers followed the discovery of the Josephson effect [*Josephson*, 1962; *Anderson*, 1970] – a discovery in basic science that has since had a major impact on applied science and engineering. The remarkably sensitive new instruments, including magnetometers, that utilize the Josephson effect are well documented [*e.g., Webb*, 1972; *Goodman et al.*, 1973; *Clarke*, 1974], so I will not review the development of the magnetometers here. Instead, I will list the following properties of the magnetometers that are relevant to their gradiometer applications: (1) their sensitivities are high compared with all other magnetometers, and may be several orders of magnitude better than the sensitivities of fluxgate or optically-pumped magnetometers, (2) they measure components of the magnetic field, not the total field (they are therefore more closely comparable with fluxgate magnetometers than with proton precession or optically pumped magnetometers), (3) they have a flat frequency response from dc to frequencies in the kilohertz range, (4) their sensing elements are small superconducting loops, as described in the previous section, (5) their sensing loops can be completely isolated from the natural magnetic noise background by means of superconducting shields, thus making possible direct measurement of their internal noise, and (6), a disadvantage, their sensing assembly must be maintained at liquid helium temperatures while they are in operation, which means that a liquid helium dewar and a regular supply of liquid helium are required.

The first superconducting gradiometer of which I have any record is one discussed by *Ottala* [1969], but it is unclear whether it was ever put into operation. It appears therefore that the first superconducting gradiometer to be built and tested is the one described by *Zimmerman and Frederick* [1971]. This gradiometer was extraordinarily small by conventional gradiometer standards: the spacing between the two sensing elements (single-turn superconducting loops with a radius of 1.25 cm) was only 10 cm. Despite its small size, Zimmerman and Frederick inferred that its sensitivity was of the order of 1 pT/m (0.1 pT/m for a standard 1 m baseline). There has since been much improvement both in the internal noise characteristics of SQUID systems and in the alignment and balancing procedures used in the construction of multi-loop gradiometer elements [*e.g., Overweg and Walter-Peters*, 1978; *Jaworski and Crum*, 1980] and it is probable that sensitivities much greater than 0.01 pT/m (for a 1 m baseline) will be achieved in the near future. Indeed, recent instruments have already demonstrated substantially improved sensitivities. For example, *Goodman et al.* [1973] measured a peak-to-peak magnetic field gradient noise of less than 10^{-3} pT/m (bandwidth 0–40 Hz) with a 20 cm baseline single-axis gradiometer at a remote test site. *Wynn et al.* [1975] reported a sensitivity of 3×10^{-2} pT/m for a single-axis gradiometer having sensing loops of 2.5 cm radius and a 30 cm baseline (equivalent to a sensitivity of 9×10^{-3} pT/m for a 1 m baseline) and, more recently, *Ketchen et al.* [1977] obtained a sensitivity of about 2 pT/m (at frequencies near 1 Hz, in a 1 Hz bandwidth) with an innovative thin-film superconducting gradiometer having a baselength of the order of 2.4 cm (equivalent to a sensitivity of 5×10^{-2} pT/m for a 1 m

baseline). These sensitivities appear to be close to the value of 3×10^{-3} pT/m described as 'today's target' in 1971 by *Nicol* [1971]. A caution is needed, however, in interpreting the sensitivities too literally. As pointed out by *Gillespie et al.* [1977], the sensitivites reported by *Zimmerman and Frederick* [1971] and by *Wynn et al.* [1975] do not take adequate account of the variation of the gradiometer noise with frequency. *Gillespie et al.* [1977] carried out a careful investigation of the noise characteristics of their gradiometer, which was ultimately used to measure the magnetic field gradients associated with internal waves in the sea [*Podney and Sager*, 1979], and they found that intrinsic noise of its SQUID dominated the measured noise spectrum on quiet days for frequencies less than 0.1 Hz. At frequencies above 0.1 Hz the predominant source of noise appeared to be thermal noise from non-superconducting metal components located near the SQUID. Gillespie et al.'s gradiometer had sensor coils 2.225 cm in radius and a baseline of 25 cm and its measured sensitivity near 1 Hz was about 0.2 pT/m in a 1Hz bandwidth, or about 0.05 pT/m for a standard 1 m baseline. It appears therefore that further development work is required before Nicol's 1971 target can be met. Nevertheless, the sensitivities currently available with superconducting gradiometers are remarkable compared with those that were typical just a decade previously.

Superconducting gradiometers differ from all other gradiometers through their combination of high sensitivity and short baseline. This means that they can not only perform the gradiometer's traditional task of detecting and measuring the magnetic fields from distant sources in the presence of natural or man-made magnetic noise but in addition they can detect and measure the fields from sources close at hand while rejecting the fields from distant sources. To the best of my knowledge, this dual capability was first explicitly pointed out by *Goodman et al.* [1973], who divided gradient measurements into two categories: (1) away-from-source gradient measurements, which are directed at characterizing the source, and (2) near-to-source measurements, which require the high common mode noise immunity of the gradiometer. In each of these categories, superconducting gradiometers are now being developed that will provide their users with new capabilities.

Because they are so compact, a number n of single-axis superconducting gradiometers can be combined in a single instrument to produce an n-axis gradiometer that is still moderately portable. If the number n is five or more, indicating that at least five independent simultaneous measurements can be made on orthogonal spatial variations of a magnetic field, and if provision is made to measure the actual components of the magnetic field as well (which is easy to do in a superconducting instrument), a new kind of magnetic field instrument is obtained. As was pointed out in increasing detail by *Nicol* [1971], *Goodman et al.* [1973], and *Wynn et al.* [1975], such an instrument

> can provide from a single location and a single set of measurements: 1) direction to the source; 2) distance to the source; 3) magnitude of the source equivalent dipole; and 4) orientation of the source equivalent dipole [*Goodman et al.*, 1973].

The combination of single-axis gradiometers and magnetometers can therefore track a moving magnetic dipole source while obtaining information about the size and orientation of its moment. This new kind of instrument is sometimes referred to as a *tracker and classifier* (R. J. Dinger, personal communication, 1981). I discuss some possible problems with the use of these instruments in Appendix A, but there is no doubt that their development forms a unique new chapter in the history of magnetic source detection.

The close-to-source capability of superconducting gradiometers has introduced an entirely new application for gradiometers: biomedical and clinical monitoring of the various magnetic fields associated with some of the body's important organs (primarily the heart, lungs, and brain). These biomedical and clinical applications are discussed in an excellent review by *Williamson and Kaufman* [1981], to which the reader is referred for further details.

§4.6 Total Field versus Component Gradiometers

A number of different magnetometers and gradiometers are described in the foregoing sections and it might well be asked why so much effort has been given to developing new instrumentation when the same effort devoted to the improvement of some of the existing magnetometers and gradiometers could have led to a substantially enhanced capability. It is important to recognize, however, that the apparently large number of magnetometers, and the gradiometers based on them, can be divided into two groups depending on whether it is the total field that is being measured (proton precession and optically pumped magnetometers and gradiometers) or a component of the field (stationary and rotating induction loop gradiometers, fluxgate and superconducting magnetometers and gradiometers). Once this division has been made, it is apparent that the number of instruments in each group is not large, but the question still remains of why there should be two groups. Why, in other words, has so much effort gone into developing both total field and component magnetometers and gradiometers?

The reason for the division is an important practical one. Total field magnetometers are comparatively immune to the effects of motion in the earth's magnetic field, whereas component magnetometers are comparatively strongly affected. No sophisticated effects are involved. A total field magnetometer measures a quantity that does not vary with the orientation of the instrument (at least to the first order; as I have described above, the measurements obtained with a single-cell optically pumped magnetometer may vary to some extent with orientation. However, this effect is eliminated in the multi-cell models intended for use while in motion); a component magnetometer, on the other hand, measures a quantity that varies substantially with orientation. For example, suppose a single-axis component magnetometer is used to measure the horizontal component of the earth's field at a location where the component is 0.2×10^{-4} T (0.2 Gauss). If for some reason the magnetometer is displaced through a small angle of 0.1°, the measurement will change by $0.2 \times 10^{-4} \cos(0.1^\circ)$ T, or by 30.5 pT. This change is easily measured by a sensitive component magnetometer. Obviously, it would be impossible

to interpret the measurements of a component magnetometer in motion, since the data would consist almost entirely of motion-induced noise. This difference in motional sensitivity is the basic reason for the effort to develop both total field and component magnetometers.

The same motional problems associated with component magnetometers carry over to the gradiometers based on them. If the two magnetometers comprising single-axis gradiometer could be completely fixed in position relative to each other there would be no problem, but there is inevitably some elastic yielding in the supports and motional noise results. This is the reason for the failure of the airborne fluxgate gradiometer described by *Wickerham* [1954]. Because of these problems with motionally-induced noise, component gradiometers have been largely confined to uses where they can be kept at rest, and total field gradiometers used for measurements where motion is involved. This situation may change in the future as superconducting gradiometers come into more widespread use. Because their coils can be made of thin films deposited on a compact and rigid substrate [*e.g., Goodman et al.*, 1973; *Ketchen et al.*, 1977], the superconducting magnetometer sensor elements may prove resistant to motion-induced noise. Unfortunately, there are likely to be other motion-induced noises, which will have to be strictly controlled if the gradiometer is to produce useful data. Motion of the liquid helium in the dewar, or of any of the other components of the gradiometer, including in particular the superconducting plates or other devices used to balance the gradiometer, could all lead to an unacceptable level of motion-induced noise.

§4.7 The Future

To end this record of the historical development of magnetic field gradiometers, the following news item points to a possible new application of gradiometers:

> Use of magnetic gradiometry technology for cruise missile terminal guidance is being evaluated by Sperry Corp. for Defense Advanced Research Projects Agency (DARPA). The study is focused on the types of fixed and mobile military targets that could be detected by this passive sensing technique which is embodied in the magnetic anomaly detectors used in antisubmarine warfare [*Staff Rept.*, 1982].

There seems little doubt that further new applications will be forthcoming in the near future. However, even if these new applications do not eventuate, the present applications of magnetic field gradiometers would be sufficient to keep the field active for many years to come.

Chapter 5

The Magnetic Field Gradiometer Response to Magnetic Dipole Fields

§5.1 Relevance of Dipole Fields

Most magnetic field gradiometers are used to detect and then to measure the characteristics of magnetic dipole fields. This concentration of effort is the result of two factors. First, gradiometers are used most frequently to detect and measure the fields from distant sources: ships, submarines, ore bodies, buried archeological artifacts, and so on. Second, the magnetic fields outside an arbitrary, bounded source approximate more and more closely to magnetic dipole fields as the distance from the source is increased. It is the combination of these two unrelated factors that makes dipole fields of particular importance in magnetic field gradiometer studies.

I will not include a mathematical proof of the tendency for magnetic fields to resemble dipole fields with increasing distance, since a complete proof is given by *Stratton* [1940]. However, I will point out that the key to the proof is the demonstration that the field from the arbitrary source can be broken up into a series of terms that vary with distance r as r^{-n}, where n takes values $n = 3, 4, 5, \ldots$. The first of these terms ($n = 3$) is the dipole term, the next term ($n = 4$) is a quadrupole term, the following term ($n = 5$) is an octupole term, and so on to higher multipole terms. Thus, at distances that are moderately large compared with the dimensions of the source, but not very large, one might expect to see a predominant dipole field together with some admixture of a quadrupole field. Closer to the source, further higher-order terms will appear, but it can be anticipated that these higher-order terms will generally be weak in comparison with the dipole and, to a lesser extent, the quadrupole terms. The appearance of the higher-order non-dipole terms as the source-receiver distance is reduced may be important under some circumstances, particularly if the field measurements are being processed to derive information about the source and it is assumed that the field is purely

dipolar. However, it appears that the dipole approximation holds up very well in practice, as illustrated by the following additional quote from *Fromm* [1952]:

> The modern sea-going submarine is large enough so that its various sections may have individual magnetic characteristics. However, at distances greater than approximately the length of the submarine, the effect of each individual magnetized portion is small relative to that of the overall magnetic moment so that for all normal considerations of its magnetic field the submarine may be considered as a single magnetic dipole.

The submarines referred to by Fromm are no longer modern, of course, and the distance criterion given in the quote may no longer be wholly appropriate for the larger and more complex submarines now entering service. Further, the increase in the sensitivity of magnetometers over the last two decades is likely to have made the distance approximation less appropriate now than it was in 1952. However, once the distance criterion has been changed suitably (distances greater than approximately twice the length of the submarine?), Fromm's quote is necessarily as applicable today as it was in 1952, since it is firmly based on physical principle. Having ascertained the relevance of magnetic dipole fields, let us now consider how magnetic field gradiometers respond to these fields.

§5.2 Response of Single-axis Component Gradiometers

In this section we will consider the various responses of the two major types of single-axis component gradiometers to the field of a magnetic dipole. There are a wide variety of possible dipole/gradiometer configurations and thus a large number of different responses so many different responses that I will not be able to consider them all in detail. Fortunately, there is a basic method for deriving the response for a given configuration that I will cover in several worked examples. Thereafter, I will merely quote results and present curves showing particular responses. This is the first time this material has appeared in a report and there are few other published results with which it may be compared. The only other similar derivation appears in an article by *Karp and Duret* [1980], but the approach is different from mine and the response data that are presented are much more limited. However, *Karp and Duret* [1980] provide some data on the response of second- and higher-order gradiometers, which I will not consider here, and the reader is referred to their article for a useful general account of gradiometer response.

The two major types of single-axis gradiometers are distinguished by the configuration of the two component magnetometers comprising their gradient sensor assembly. These magnetometers may be arranged in either a parallel or a series configuration: in the parallel, or *paraxial*, configuration the baseline of the gradiometer is perpendicular to the axes of the magnetometers, *i.e.*, perpendicular to the common direction along which the magnetometers are measuring the magnetic field, whereas in the series, or *coaxial*, configuration the baseline is aligned along the shared axis of the magnetometers. The simple gradiometer described in the first chapter is an example of paraxial gradiometer; it could be converted to a coaxial

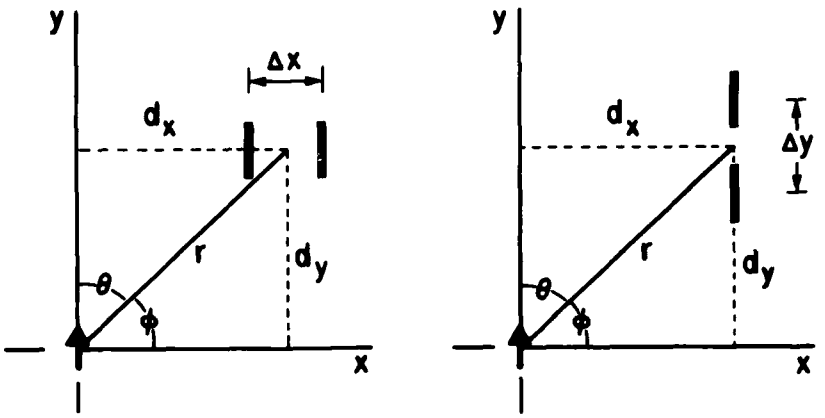

Figure 5.1. Diagrams showing the coordinate systems used to derive the dipole magnetic field responses of (a), left panel, the simple magnetic field gradiometer described in Section 1.2 (an example of a *paraxial* gradiometer), and (b), right panel, a *coaxial* gradiometer. The arrow at the origin of each system represents the dipole source.

gradiometer by locating the two solenoids a short distance apart on the same axis (or, putting it another way, in the parallel configuration the solenoids are located side-by-side, whereas in the series configuration they are located one behind the other).

I will use a short solid line to represent the component magnetometers, as in Figure 1.2 or thus: ▬. The axis defined by the line is the axis of the magnetometer. When seen 'end-on,' as will occur in several of the configurations, the magnetometer will be represented by a small solid circle, thus: ● . Every gradiometer configuration will necessarily involve two component magnetometers. However, a few of the configurations will be shown with what appears to be only one magnetometer. In these cases the magnetometers comprising the gradiometer are displaced in the z-direction, *i.e.*, in and out of the page, and the magnetometer in front obscures the one behind.

5.2.1 Simple Magnetic Field Gradiometer

Let us now begin our analysis of the response of magnetic field gradiometers by taking the simple gradiometer discussed in Chapter 1.2 as a first example. Figure 5.1 (a) shows the dipole/gradiometer geometry that will be used; the dipole is represented by an arrow at the origin, pointing in the y-direction, and the gradiometer in this case is also shown oriented in the y-direction. A z axis perpendicular to the x, y plane in the figure is not displayed.

but its presence is assumed. Because the magnetometers are spaced apart in the x-direction, while measuring the magnetic field components in the y-direction, the gradiometer is paraxial and it measures $\Delta B_y/\Delta x$, where ΔB_y is the difference in the B_y measurements made by the two magnetometers and $\ell = \Delta x$ is the gradiometer spacing. Assuming, as I will throughout this chapter, that the spacing is small compared with the distance r from the dipole to the gradiometer, the gradiometer also measures $\partial B_y/\partial x$.

The dipole magnetic field components B_r and B_θ can be written

$$B_r = \frac{2\mu_0 M \cos\theta}{4\pi r^3}, \qquad B_\theta = \frac{\mu_0 M \sin\theta}{4\pi r^3}, \tag{5.1}$$

where M is the dipole moment. Starting with these basic equations, we now need to derive an expression for the y component of the magnetic field, since it is B_y that is measured by the gradiometer's sensors. Following some algebra, we obtain

$$B_y = \frac{K}{r^3}(2\cos^2\theta - \sin^2\theta), \tag{5.2}$$

where $K = \mu_0 M/4\pi$ is a constant. In cartesian coordinates, Equation 5.2 becomes

$$B_y = K\,\frac{2y^2 - x^2}{(x^2+y^2)^{\frac{5}{2}}}. \tag{5.3}$$

Now, to obtain the response of the gradiometer to the dipole field, we need to derive $\partial B_y/\partial x$ from Equation 5.3. Carrying out the differentiation, we obtain

$$\frac{\partial B_y}{\partial x} = K\,\frac{3x(x^2 - 4y^2)}{(x^2+y^2)^{\frac{7}{2}}}. \tag{5.4}$$

Since $y/x = \tan\phi$, this equation can also be written

$$\frac{\partial B_y}{\partial x} = K\,\frac{3\cos^7\phi}{x^4}(1 - 4\tan^2\phi). \tag{5.5}$$

Finally, writing d_x for x and assuming that $d_x \gg \ell$, we have

$$\Delta B_y = \frac{3\mu_0 M \ell}{4\pi d_x^4} f(\phi), \tag{5.6}$$

where

$$f(\phi) = \cos^7\phi(1 - 4\tan^2\phi). \tag{5.7}$$

Equations 5.6 and 5.7 are the ones I will use to obtain a graphical display of the *gradiometer response*, which I can now define to be the difference in the magnetic field measurements made by the two magnetometers comprising the gradiometer. In the present case, the quantity ΔB_y is the response. Other quantities could just as well be defined as the response, but in practice it is the difference in the magnetic field measurements that is most likely to be displayed and understood to be the instrument's response by the gradiometer operator.

To investigate the variation of gradiometer response with distance to the source, let us consider Equation 5.4 in its polar coordinate form:

$$\frac{\partial B_y}{\partial x} = K \frac{3\sin^3\theta}{r^4}(1 - 4\cot^4\theta). \tag{5.8}$$

This equation shows that the gradiometer response varies with distance r to the source as r^{-4}. This should be compared with the equivalent r^{-3} distance factor in the response of a magnetometer. Thus, in the absence of a background of natural magnetic noise (and therefore limited only by magnetometer internal noise), a gradiometer is intrinsically much more limited in range than a magnetometer. When natural noise is present the situation changes, as discussed in the previous chapters, and depending on the level of the natural background the range of the gradiometer can exceed that of a magnetometer despite its r^{-4} decline of response with distance.

Returning to Equations 5.6 and 5.7, let us suppose that the dipole shown in Figure 5.1 (a) begins to move in the positive y direction. The only quantity in Equation 5.6 that varies during this motion is the angular function $f(\phi)$, so we need only consider the variation of $f(\phi)$ with position of the dipole along the y-axis to determine the corresponding variation in the response of the gradiometer. Before looking at this variation, however, we should consider the actual physical situation that is being analyzed. Comparing the dipole/gradiometer configuration in Figure 5.1 (a) with the experimental arrangement shown in the top panel of Figure 1.2, an exact equivalence can be seen. Note the direction of the magnetic field in the experimental configuration: it will magnetize steel bodies to give a dipole moment in the correct direction (the positive y direction) for the theory derived above to apply.

The angular function $f(\phi)$, or *response function*, is plotted in Figure 5.2. There is a moderately sharp peak of response centered on $\phi = 0^\circ$: it has a half-amplitude width of 32.4° and zeros at $\phi = \pm 26.6^\circ$. Outside of the angular range $-20^\circ < \phi < 20^\circ$ the response is always less than a third of the maximum value for $\phi = 0^\circ$, which, as shown by Figure 5.1 (a), defines the point of closest approach of the dipole to the gradiometer.

The simple gradiometer does not have conventional component magnetometers as sensors, and its response is a modified version of what I have just described. Since induction loops are used as sensors, the rate of change of the dipole field at the sensors must also be taken into account. The change from an increasing to a decreasing field at the time of closest approach introduces a sign change into the output of the gradiometer, which then consists of a positive

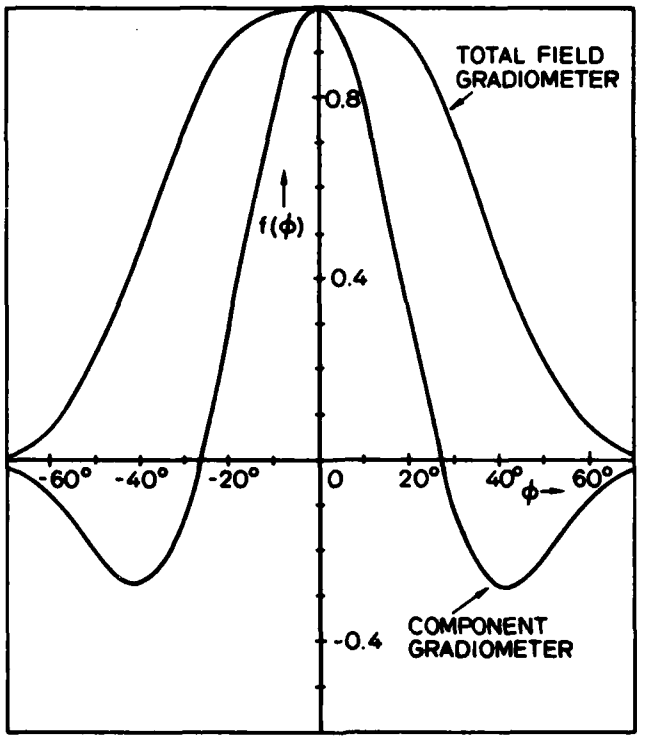

Figure 5.2. Plots of the response function $f(\phi)$ for the simple magnetic field gradiometer ('component gradiometer') and for an equivalent total magnetic field gradiometer.

or negative pulse while the dipole moves moves from $\phi = 20^\circ$ to $\phi = 0^\circ$, zero output at the moment of closest approach, and then a pulse of opposite sign to the initial one as the dipole moves from $\phi = 0^\circ$ to $\phi = -20^\circ$, as was seen in Figure 1.2. Motion of the dipole in the positive y-direction is equivalent to motion of the gradiometer in the negative y-direction. Once the gradiometer moves below the x-axis, which is the same as the dipole moving above the d_x line in Figure 5.1 (a), ϕ becomes negative).

Suppose the dipole were to be moved in the positive x-direction instead of in the positive y-direction while maintaining its moment in the y-direction, *i.e.*, it is moved sideways in Figure 5.1 (a) and not upwards. There is a simple technique for deriving the response of the gradiometer for this new situation. All that is necessary is to substitute $d_y \cot \phi$ for d_x in Equation 5.6 for the response and then to incorporate the resulting $\tan^4 \phi$ factor into the angular function. Since d_y remains constant during the motion of the dipole along the x-axis, the substitution once again places all the variables into the angular function. When the substitution is made,

we obtain

$$\Delta B_y = \frac{3\mu_0 M \ell}{4\pi d_y^4} f(\phi), \tag{5.9}$$

where

$$f(\phi) = \cos^7\phi \tan^4\phi (1 - 4\tan^2\phi). \tag{5.10}$$

This last expression does not look very different from the one in Equation 5.7, but the extra $\tan^4\phi$ factor and the different range of ϕ (now 0° 180°) ensure that the variation of the response function is quite different from the previous one. The new variation is shown in Figure 5.3(c), (top scale).

Figure 5.2 also shows the variation of the angular function for a total magnetic field gradiometer operating under exactly the same conditions as the simple induction loop gradiometer. The angular function is derived in a later subsection, but its variation is shown here to provide a contrast with the component gradiometer curve. It can be seen that the total field gradiometer is much less directive than the component gradiometer.

5.2.2 Coaxial Gradiometer

The analysis in the previous subsection dealt solely with a paraxial gradiometer. We will now derive the response of the coaxial gradiometer shown in Figure 5.1 (b). Because of their orientation, the component magnetometers in this new gradiometer measure the same magnetic field component B_y as did the gradiometer we have just analyzed. However, because the magnetometers are now spaced apart in the y-direction, the gradiometer measures $\Delta B_y/\Delta y$, where ΔB_y is the difference in the B_y measurements made by the two magnetometers and $\ell = \Delta y$ is the gradiometer spacing. Since Δx is assumed to be small, the gradiometer also measures $\partial B_y/\partial y$.

Using the same cartesian coordinate expression for B_y that was derived in the previous subsection (Equation 5.3), it is easy to show that

$$\frac{\partial B_y}{\partial y} = K \frac{3y(3x^2 - 2y^2)}{(x^2 + y^2)^{\frac{7}{2}}}, \tag{5.11}$$

where $K = \mu_0 M/4\pi$ as before. Introducing ϕ, we obtain

$$\frac{\partial B_y}{\partial y} = K \frac{3\cos^7\phi \tan\phi}{x^4} (3 - 2\tan^2\phi). \tag{5.12}$$

Once again writing d_x for x and assuming that $d_x \gg \ell$, we have

$$\Delta B_y = \frac{3\mu_0 M \ell}{4\pi d_x^4} f(\phi),$$

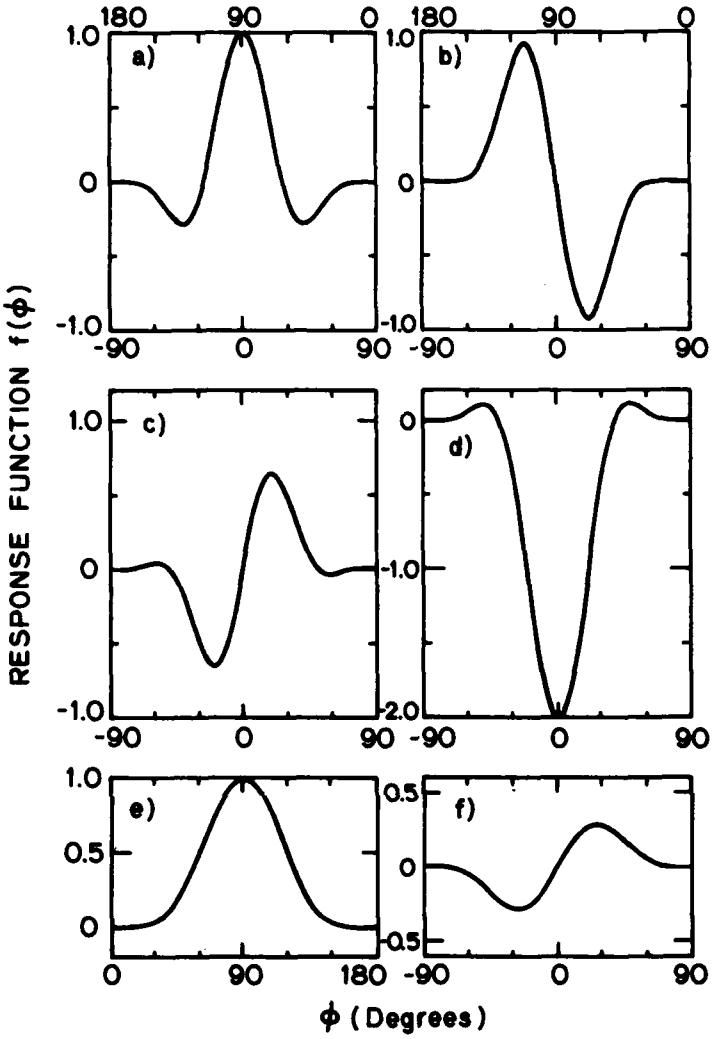

Figure 5.3. Further plots of the response function $f(\phi)$ for single-axis component gradiometers. Note the additional ϕ scales at the tops of the upper two plots.

which is formally the same as Equation 5.6, but where we now have

$$f(\phi) = \cos^7 \phi \tan \phi (3 - 2\tan^2 \phi). \tag{5.13}$$

If the dipole is now moved in the positive y-direction, the only quantity in the response equation that varies is the angular function given by Equation 5.13. This angular function is plotted in Figure 5.3 (c).

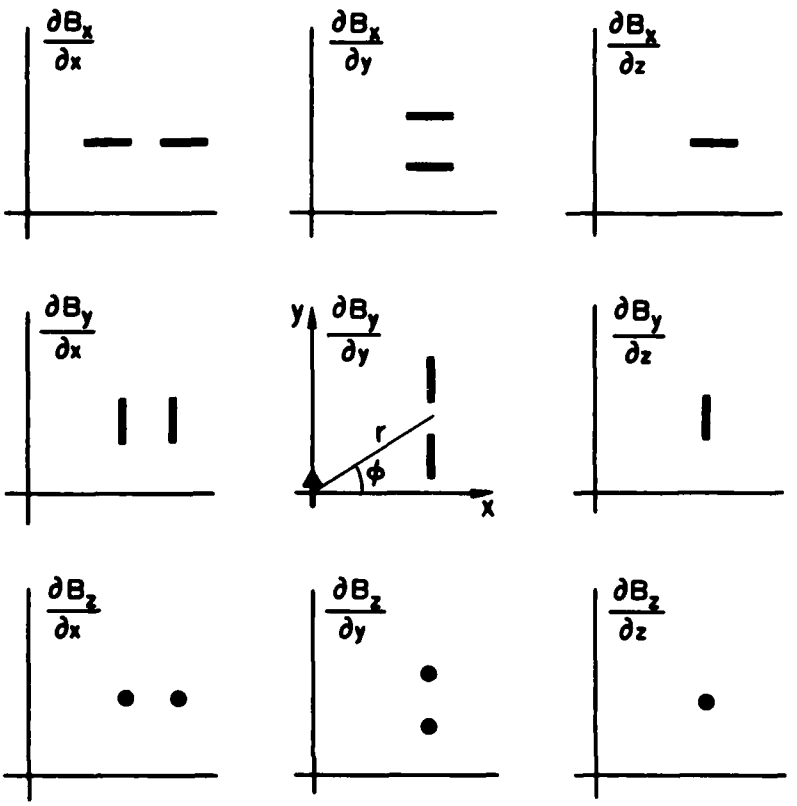

Figure 5.4. Single-axis gradiometer configurations for the measurement of each of the indicated nine spatial variations of the magnetic field components B_x, B_y, and B_z.

Let the dipole now be moved in the positive x-direction. Using the same technique as was used for the simple gradiometer, the following equations for the response are obtained:

$$\Delta B_y = \frac{3\mu_0 M \ell}{4\pi d_y^4} f(\phi),$$

where

$$f(\phi) = \cos^7\phi \tan^5\phi (3 - 2\tan^2\phi). \tag{5.14}$$

This last response function is plotted in Figure 5.3 (d); it has a comparatively large minimum when $\phi = 90°$, *i.e.*, when the dipole source is closest to the gradiometer. A minimum may be unexpected in this case, but it is consistent with the fact that B_y is positively directed at the gradiometer sensors and that it is decreasing as y increases: $\partial B_y/\partial y$ is negative at the gradiometer.

5.2.3 Generalized Two-Dimensional Approach

We have now considered two different dipole/component gradiometer configurations and obtained four different response curves. All of these curves are shown in Figure 5.3, where the curve in panel (a) will now be recognized as being a redrawn version of the component gradiometer curve in Figure 5.2. I will now generalize the approach I have been using through one step to include the nine gradiometer configurations shown in Figure 5.4. These configurations include the two previous ones and like them they are still basically two-dimensional, since the centers of the gradiometer sensor assemblies all lie in the x, y plane. Notice, however, that the magnetometer axes are perpendicular to the x, y plane for three of the configurations and in another group of three the magnetometers are located a very small distance $\Delta z/2$ above and below the x, y plane. (One of the configurations belongs to both of these groups).

The reason for the choice of these nine configurations is indicated by the partial derivatives adjacent to each of the gradiometers shown in the figure. Each of the single-axis gradiometers measures one of the spatial variations in the gradient matrix. If all nine of the gradiometers were present together and centered on the one point, they would provide a complete measure of the gradient of the magnetic field at the central point. We know, of course, that one of the three spatial variations $\partial B_x/\partial x$, $\partial B_y/\partial y$, and $\partial B_z/\partial z$ will be dependent on the other two, or zero, because of the requirement that div $\mathbf{B} = 0$, and and in a source-free region three of the other variations will also cease to be independent.

To see how the various single-axis gradiometers respond to a magnetic dipole field, I will once again assume that there is a dipole located at the origin of their coordinate systems and directed in the positive y-direction. The responses and angular functions can then be derived as in the two preceding subsections. I will not consider dipole motion out of the x, y plane at this stage, since it requires a three-dimensional approach.

For a dipole directed along the y-axis there is no z-component of magnetic field; the B_y component was derived in Section 5.2.1 (Equation 5.3) and the B_x component can be derived similarly. When collected together, the components have the following cartesian coordinate forms

$$B_x = K\frac{3xy}{(x^2+y^2)^{\frac{5}{2}}},$$

$$B_y = K\frac{2y^2-x^2}{(x^2+y^2)^{\frac{5}{2}}}, \tag{5.15}$$

$$B_z = 0,$$

from which the following six partial derivatives can be derived

$$\begin{aligned}
\frac{\partial B_x}{\partial x} &= \frac{3\mu_0 M}{4\pi x^4}\cos^7\phi\,\tan\phi(\tan^2\phi - 4),\\
\frac{\partial B_x}{\partial y} &= \frac{3\mu_0 M}{4\pi x^4}\cos^7\phi(1 - 4\tan^2\phi),\\
\frac{\partial B_y}{\partial x} &= \frac{\partial B_x}{\partial y},\\
\frac{\partial B_y}{\partial y} &= \frac{3\mu_0 M}{4\pi x^4}\cos^7\phi\,\tan\phi(3 - 2\tan^2\phi),\\
\frac{\partial B_z}{\partial x} &= \frac{\partial B_z}{\partial y} = 0.
\end{aligned} \tag{5.16a}$$

The remaining three partial derivatives in the gradient matrix, $\partial B_x/\partial z$, $\partial B_y/\partial z$, and $\partial B_z/\partial z$, cannot be derived from Equations 5.15, since the equations provide no information about the field values out of the x, y plane. It would be expected that $\partial B_x/\partial z = \partial B_y/\partial z = 0$, because of the rotational symmetry of the dipole field about its axis, and for the same reason it would be expected that $\partial B_z/\partial z$ would have some non-zero value, but this is as far as we can go with the present two-dimensional approach. I derive the actual partial derivatives in the following section, using a three dimensional approach, and they have the form

$$\begin{aligned}
\frac{\partial B_x}{\partial z} &= \frac{\partial B_y}{\partial z} = 0,\\
\frac{\partial B_z}{\partial z} &= \frac{3\mu_0 M}{4\pi x^4}\cos^5\phi\,\tan\phi.
\end{aligned} \tag{5.16b}$$

Equations 5.16 show that there are only four independent spatial variations under the restrictive two-dimensional conditions that have been assumed. Four of the spatial variations are zero, and when they are matched up with their corresponding configurations in Figure 5.4 it is found that the only configuration among the five in the bottom row and right column that has any gradiometer response to the dipole magnetic field is the one measuring $\partial B_z/\partial z$. The remaining configurations include the simple (paraxial) gradiometer and the coaxial gradiometer that we have already studied. To help in the description of the responses, I will begin specifying the configurations in Figure 5.4 by means of the coordinate axes involved in the partial derivatives. Thus the configuration giving $\partial E_{\cdot}\ '\partial y$, for example, will be referred to as the x,y configuration, and so on. Collecting the results from the previous subsections, and adding new results where needed, the responses of the five configurations with a gradiometer response to motions of the dipole source along the x- and y-axes are as follows:

(1) *X,X* Configuration. For dipole motion along the x-axis the response is given by

$$\Delta B_x = K_y f(\phi) = K_y \cos^7\phi\,\tan^5\phi(\tan^2\phi - 4), \tag{5.17a}$$

and for dipole motion along the y-axis the response is given by

$$\Delta B_x = K_x f(\phi) = K_x \cos^7\phi \tan\phi(\tan^2\phi - 4). \tag{5.17b}$$

For the x-axis motion $f(\phi)$ is plotted in Figure 5.3 (a) (top scale), and for the y-axis motion $f(\phi)$ is plotted in Figure 5.3 (b) (bottom scale).

(2) X,Y Configuration. For dipole motion along the x-axis the response is given by

$$\Delta B_x = K_y f(\phi) = K_y \cos^7\phi \tan^4\phi(1 - 4\tan^2\phi), \tag{5.17c}$$

and for dipole motion along the y-axis the response is given by

$$\Delta B_x = K_x f(\phi) = K_x \cos^7\phi(1 - 4\tan^2\phi). \tag{5.17d}$$

For the x-axis motion $f(\phi)$ is plotted in Figure 5.3 (b) (top scale), and for the y-axis motion $f(\phi)$ is plotted in Figure 5.3 (a) (bottom scale).

(3) Y,X Configuration. Same response as for the x,y configuration. For dipole motion along the x-axis the response ΔB_y is the same as the response ΔB_x for the x,y configuration (Equation 5.17c), and for dipole motion along the y-axis the response ΔB_y is the same as the response ΔB_y for the x,y configuration (Equation 5.17d).

(4) Y,Y Configuration. For dipole motion along the x-axis the response is given by

$$\Delta B_y = K_y f(\phi) = K_y \cos^7\phi \tan^5\phi(3 - 2\tan^2\phi), \tag{5.17e}$$

and for dipole motion along the y-axis the response is given by

$$\Delta B_y = K_x f(\phi) = K_x \cos^7\phi \tan\phi(3 - 2\tan^2\phi). \tag{5.17f}$$

For the x-axis motion $f(\phi)$ is plotted in Figure 5.3 (d), and for the y-axis motion $f(\phi)$ is plotted in Figure 5.3 (c).

(5) Z,Z Configuration. For dipole motion along the x-axis the response is given by

$$\Delta B_z = K_y f(\phi) = K_y \sin^5\phi, \tag{5.17g}$$

and for dipole motion along the y-axis the response is given by

$$\Delta B_z = K_x f(\phi) = K_x \cos^5\phi \tan\phi. \tag{5.17h}$$

The angular function $f(\phi)$ for the x-axis motion is plotted in Figure 5.3 (e), and for the y-axis motion $f(\phi)$ is plotted in Figure 5.3 (f).

The K_x and K_y in the above equations are constants given by $K_x = 3\mu_0 M\ell/4\pi d_x^4$ and $K_y = 3\mu_0 M\ell/4\pi d_y^4$, where d_x and d_y are the perpendicular distances of the centers of the gradiometer sensor assemblies from the x- and y-axes. It can be seen that the six angular variations in Figure 5.3 provide all the information we need to describe the angular responses of the configurations shown in Figure 5.4 provided the dipole motions are restricted to the x- and y-axes.

5.2.4 Total Field Gradiometer

The response of a total magnetic field gradiometer under the same two-dimensional conditions I have been assuming can be derived using the same techniques that were used for the component gradiometers. To illustrate, I will now derive the response of a total field gradiometer under the same conditions as those assumed for the simple paraxial gradiometer (Subsection 5.2.1); the configuration will be identical to the one shown in Figure 5.1 (a), but the two magnetic field sensors will now be understood to be total field magnetometers.

The first step in deriving the response is to obtain the total field in cartesian coordinates. Using Equations 5.15 for the x and y components, the total field B_T is obtained from

$$B_T = (B_x^2 + B_y^2)^{\frac{1}{2}},$$

giving

$$B_T = \frac{K\,(4y^4 + 5x^2y^2 + x^4)^{\frac{1}{2}}}{(x^2 + y^2)^{\frac{5}{2}}}, \tag{5.18}$$

where $K = \mu_0 M/4\pi$ as before. Differentiating, we find

$$\frac{\partial B_T}{\partial x} = \frac{-3K\,x(x^2 + 5y^2)}{(x^2 + 4y^2)^{\frac{1}{2}}(x^2 + y^2)^{\frac{6}{2}}}. \tag{5.19}$$

Again using $y = x\tan\phi$, $1 + \tan^2\phi = \cos^{-2}\phi$, we have

$$\frac{\partial B_T}{\partial x} = \frac{-3K}{x^4}\,\frac{\cos^6\phi(1 + 5\tan^2\phi)}{(1 + 4\tan^2\phi)^{\frac{1}{2}}}. \tag{5.20}$$

Thus, for dipole motion along the y-axis, the response is given by

$$\Delta B_T = -\frac{3\mu_0 M\ell}{4\pi d_x^4}\,f(\phi), \tag{5.21}$$

where

$$f(\phi) = \frac{\cos^6\phi(1 + 5\tan^2\phi)}{(1 + 4\tan^2\phi)^{\frac{1}{2}}}. \tag{5.22}$$

This last angular function is the one labelled 'Total Field Gradiometer' in Figure 5.2.

For dipole motion along the x-axis, the response of the total field magnetometer is found by substituting $d_x = \cot\phi\, d_y$ in Equation 5.21 and incorporating the resulting $\tan^4\phi$ term into the angular function. We then have

$$\Delta B_T = -\frac{3\mu_0 M\ell}{4\pi d_y^4}\,f(\phi), \tag{5.23}$$

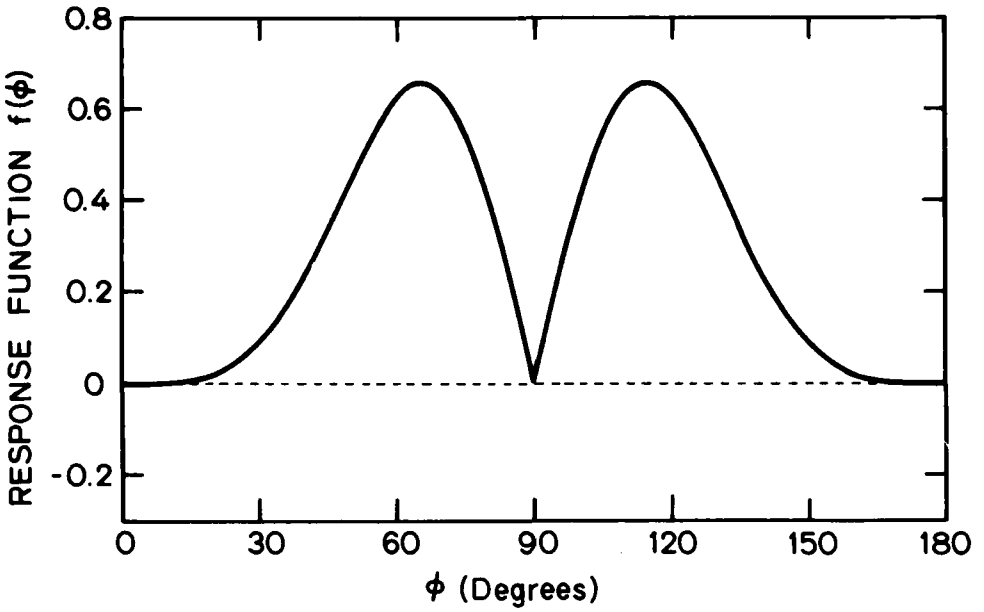

Figure 5.5. Additional plot of a response function $f(\phi)$ for a total magnetic field gradiometer.

where

$$f(\phi) = \frac{\cos^6\phi \tan^4\phi(1 + 5\tan^2\phi)}{(1 + 4\tan^2\phi)^{\frac{1}{2}}}. \tag{5.24}$$

Figure 5.5 shows the variation of this final angular function with angle ϕ. The data in this last figure, combined with the total field data in Figure 5.2, suggest strongly that the total field gradiometer is basically a less-directive instrument than a component gradiometer. It is possible, however, that use could be made of the null in the response (Figure 5.5) to obtain moderate directionality.

§5.3 Three-Dimensional Approach

Up to this point I have confined my derivation of gradiometer responses to magnetic dipole fields to moderately simple dipole/gradiometer configurations. This has enabled me to obtain some useful response data that, as I will shortly discuss, can be applied to a number of practical situations. Once the configurations are made more general, the derivation of gradiometer response becomes difficult because of the algebraic complexities involved and the response functions are complicated. I will present the results of a generalized two-dimensional analysis in the next chapter, and it will be seen that even in two dimensions the response functions can become particularly complicated. In three dimensions the difficulties involved in obtaining response information are very great, except for the most simple configurations (in their simplest

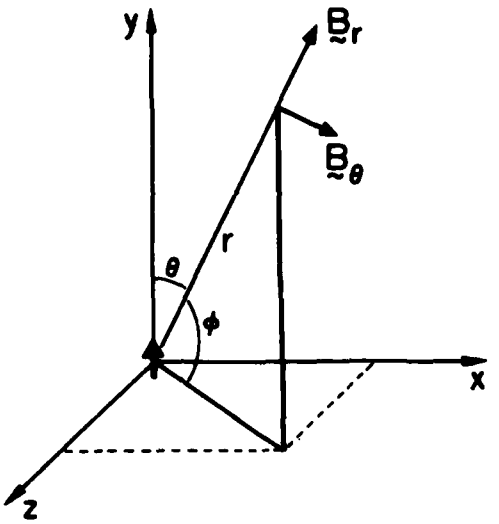

Figure 5.6. Coordinate system for the three-dimensional analysis of gradiometer response.

forms these configurations are the two-dimensional ones we have already analyzed), and the use of computers to obtain relevant numerical data is clearly indicated. As a result, I will confine myself in this section to a presentation of the basic three-dimensional component and spatial variation data, which is the essential raw material for a computer analysis.

Suppose our magnetic dipole is now located at the center of a three-dimensional cartesian coordinate system with the dipole moment directed along the z-axis, as shown in Figure 5.6. The three components of the dipole magnetic field can be derived from the two two-dimensional polar coordinate components B_r and B_θ given in Subsection 5.2.1 once account is taken of the fact that there is no azimuthal component of magnetic field in Figure 5.6. The two components are shown, in vector form, in the figure, and the three corresponding cartesian coordinate components of the field are

$$B_x = \frac{3Kxz}{r^5},$$

$$B_y = \frac{3Kyz}{r^5}, \tag{5.25}$$

$$B_z = \frac{K(3z^2 - r^2)}{r^5},$$

where the same $K = \mu_0 M/4\pi$ is used as in the previous section. Carrying out the appropriate differentiation, the gradient matrix can be written

$$\begin{bmatrix} \frac{\partial B_x}{\partial x} & \frac{\partial B_y}{\partial x} & \frac{\partial B_z}{\partial x} \\ \frac{\partial B_x}{\partial y} & \frac{\partial B_y}{\partial y} & \frac{\partial B_z}{\partial y} \\ \frac{\partial B_x}{\partial z} & \frac{\partial B_y}{\partial z} & \frac{\partial B_z}{\partial z} \end{bmatrix} = \frac{3K}{r^7} \begin{bmatrix} y(r^2-5x^2) & x(r^2-5y^2) & -5xyz \\ x(r^2-5y^2) & y(3r^2-5y^2) & z(r^2-5y^2) \\ -5xyz & z(r^2-5y^2) & y(r^2-5z^2) \end{bmatrix}. \tag{5.26}$$

The nine expressions in the evaluated gradient matrix are the raw material for any three dimensional response analysis. It will be noted that the matrix is symmetric and the sum of the three diagonal terms is zero, as is required for the gradient of a magnetic field in source-free region.

To illustrate the use of this material, suppose we have a component gradiometer with its center located at the point $(x, y, -|z|)$, with its two sensors both located in the x, y plane passing through the center, and with its sensitivity axis parallel to the y-axis. This configuration is deliberately chosen for its pertinence to the two-dimensional simple magnetic field gradiometer studied in Subsection 5.2.1: if the gradiometer is visualized as being laid flat on the ground, as it was in the original situation (Chapter 1), the dipole can now be considered to be raised in the air a distance $|z|$, with everything else unchanged. Because of its orientation, the gradiometer measures $\partial B_y/\partial x$ which, according to our evaluated gradient matrix, is given by

$$\frac{\partial B_y}{\partial x} = \frac{3Kx}{r^7}(r^2-5y^2). \tag{5.27}$$

This expression can also be put in the form

$$\frac{\partial B_y}{\partial x} = \frac{3Kx}{d^5}\cos^7\phi(1-4\tan^2\phi), \tag{5.28}$$

where ϕ is the angle shown in Figure 5.6 (it is the three-dimensional equivalent of the ϕ shown in Figure 5.1) and $d = (x^2+z^2)^{\frac{1}{2}}$ is the perpendicular distance from the center of the gradiometer to the y-axis (it is the three-dimensional equivalent of d_x in Figure 5.1).

The ϕ dependence in Equation 5.28 is the same as that encountered in the equivalent two-dimensional configuration (see Equation 5.5); there is therefore no difference between the three-dimensional and two-dimensional angular responses. There is a difference in the distance dependence, however, and the magnitude of the response is reduced in the three-dimensional case compared with its two-dimensional equivalent because of the presence of the distance term d ($d>x$). This illustrative example shows that the response curves given in Figure 5.3 are relevant not just to two-dimensional dipole/gradiometer configurations but also to three-dimensional configurations as well.

To end this section on the three-dimensional approach, let us consider what happens to the evaluated gradient matrix in Equation 5.26 when we take $z = 0$. The gradient matrix then

applies to the two-dimensional situations considered earlier in this chapter, and it has the form

$$[\mathrm{G}]_{z=0} = \frac{3K}{(x^2+y^2)^{\frac{7}{2}}} \begin{bmatrix} y(y^2-4x^2) & x(x^2-4y^2) & 0 \\ x(x^2-4y^2) & y(3x^2-2y^2) & 0 \\ 0 & 0 & y(x^2+y^2) \end{bmatrix}. \tag{5.29}$$

The last row of this evaluated gradient matrix gives us the following equations

$$\begin{aligned} \frac{\partial B_x}{\partial z} &= \frac{\partial B_y}{\partial z} = 0, \\ \frac{\partial B_z}{\partial z} &= \frac{3Ky}{(x^2+y^2)^{\frac{5}{2}}}, \end{aligned} \tag{5.30}$$

which, with appropriate modifications, are the same as those used in Subsection 5.2.3 (Generalized Two-Dimensional Approach; see Equations 5.16b).

§5.4 Applications of the Response Data

The various two-dimensional response curves and other two-dimensional response data given in this chapter may appear to be too idealistic to be of much use in practice. If so, the appearance is misleading. In fact, the two-dimensional data have immediate application to a number of practical situations in both two and three dimensions, and even when they do not have immediate application, as would be the case in a three-dimensional situation with arbitrary orientation of the gradiometer, they can often be used to give an approximate picture of the gradiometer response pending a complete computation. One application of the response data has already been discussed—it covers the response of the simple gradiometer described in the first chapter. Another possible application is suggested by the physical configuration of the coaxial gradiometer: it would be much easier to tow a coaxial gradiometer through the sea than it would be to tow one of the paraxial varieties. The response functions derived for the coaxial gradiometer could then be used to interpret the response of the gradiometer to the magnetic field from submerged sources under the following conditions: (1) The magnetic moments of the sources are induced by the geomagnetic field and are therefore predominantly North-South directed, and (2) the gradiometer is towed either in North-South or East-West directions.

The comparatively large minimum obtained with the coaxial gradiometer when the dipole motion takes place in the x-direction (Figures 5.1 (b) and 5.3 (d)) suggests use of the configuration for monitoring. An illustrative use would be the monitoring of vessels through a narrow East-West oriented strait such as the Strait of Gibraltar by means of a North-South oriented coaxial gradiometer located on one side of the strait. This configuration would provide the largest possible signals. If signal amplitude was not as important a factor as directivity, one of the configurations with a positive-negative response (Figures 5.3 (b) and (c)) could be used. Squaring of the output, or simply taking the absolute value, would give a sharp minimum at the time of closest approach.

Chapter 6

Rotating Component Gradiometers

As I pointed out in Chapter 4, the first two magnetic field gradiometers described in the scientific literature used rotating induction loops as their basic magnetic field sensors. Later gradiometers did not follow their lead, however, and no gradiometers with rotating components appear to have been constructed for many years. There are compelling engineering reasons for avoiding use of a gradiometer with moving components when gradiometers of similar or better sensitivity are available that have no moving parts, and the early gradiometers had no distinctive advantages that would encourage their further development once fluxgate gradiometers became available. Nowadays, with vastly more sensitive gradiometers available, a gradiometer with moving components would have to have some particularly distinctive properties to be considered practicable.

In this chapter I discuss two magnetic field gradiometers with rotating components that might have sufficiently distinctive properties for them to be useful. In both cases they differ from the early rotating loop gradiometers in that their sensor assemblies are rotated as a whole. In one of these gradiometers it is immaterial what kind of magnetometers are contained in the sensor assembly, provided they measure components of the magnetic field, are not induction loop magnetometers, and that they are not incapacitated by motion. Such a gradiometer may have useful directional properties. The other gradiometer requires induction loops as sensors. Its response to magnetic dipole fields falls off either as the inverse fourth- or fifth-power of distance, depending on how the loops are connected, but it also depends on the rotation frequency. Thus its sensitivity can be changed simply by varying the rotation frequency and in principle it can be made very large. Neither of these two rotating gradiometers has ever been constructed, to the best of my knowlege, and they are quite speculative.

§6.1 Rotating Component Gradiometer

Suppose we return to the two-dimensional single axis paraxial gradiometer configuration that we first considered in Section 5.2.1, and we now rotate it until its sensitivity axis is oriented

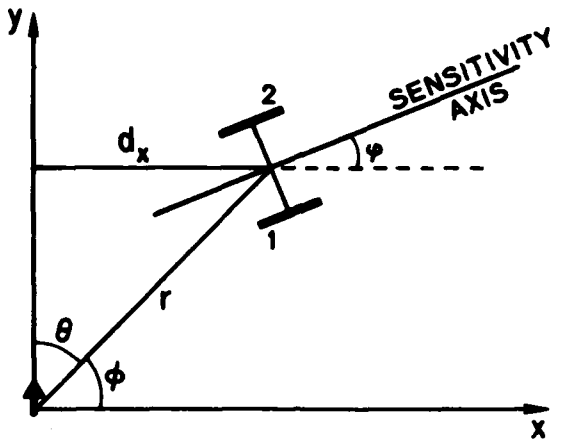

Figure 6.1. Diagram showing the coordinate system and gradiometer geometry that are used in the derivation of the response of a rotating paraxial gradiometer.

at an arbitrary angle $(90^\circ - \varphi)$ relative to the axis of the magnetic dipole, as shown in Figure 6.1. With the ultimate object of obtaining information about the variation of the response of the gradiometer as its sensor assembly is rotated about its center, let us derive the response of the gradiometer for this arbitrary orientation.

Resolving the two vector components B_r and B_θ along the sensitivity axis of the gradiometer, we find that the resolved component of the magnetic field at the center of the gradiometer, B_g, is given by

$$B_g = \frac{K}{r^3}\left(2\cos\theta\,\sin(\theta+\varphi) + \sin\theta\,\cos(\theta+\varphi)\right), \tag{6.1}$$

where $K = \mu_0 M/4\pi$ as in the previous chapter. The response of the gradiometer is given by

$$\Delta B_g = \frac{\partial B_g}{\partial r}\,\Delta r + \frac{\partial B_g}{\partial \theta}\,\Delta\theta, \tag{6.2}$$

where, from Equation 6.1, we have

$$\begin{aligned}\frac{\partial B_g}{\partial r} &= -\frac{3K}{r^4}\left(2\cos\theta\,\sin(\theta+\varphi) + \sin\theta\,\cos(\theta+\varphi)\right),\\ \frac{\partial B_g}{\partial \theta} &= \frac{3K}{r^4}\left(\cos\theta\,\cos(\theta+\varphi) - \sin\theta\,\sin(\theta+\varphi)\right).\end{aligned} \tag{6.3}$$

The incremental quantities Δr and $\Delta\theta$ are given by

$$\begin{aligned}\Delta r &= \ell\,\cos(\theta+\varphi),\\ \Delta\theta &= -\frac{\ell}{r}\,\sin(\theta+\varphi),\end{aligned} \tag{6.4}$$

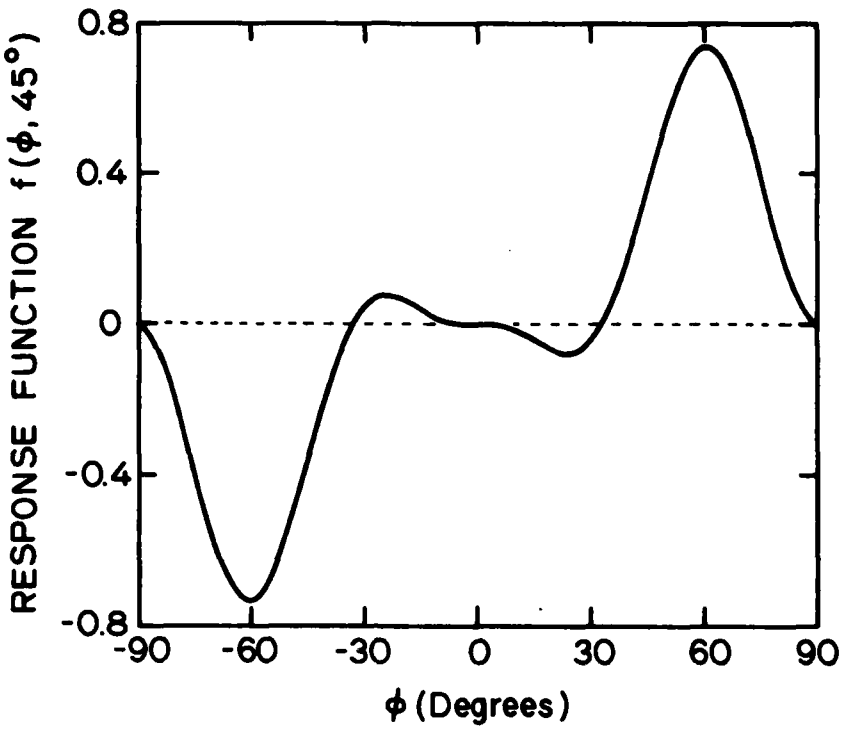

Figure 6.2. Plot of the response function $f(\phi, 45^\circ)$ for the paraxial gradiometer shown in Figure 6.1. The dipole source is assumed to move in the positive y-direction and, as indicated by the notation for the response function, the sensitivity axis of the gradiometer is taken to be at an angle $\varphi = 45^\circ$ to the x-axis.

where the incremental change is measured from sensor 1 to sensor 2 and ℓ is the gradiometer spacing, which is assumed small compared with the distance r to the dipole.

Combining Equations 6.2–6.4 and simplifying, we obtain the following expression for the response of the gradiometer

$$\Delta B_g = \frac{3K\ell}{2r^4} f(\theta, \varphi), \tag{6.5}$$

where the angular function $f(\theta, \varphi)$ has the form

$$f(\theta, \varphi) = -(3 \cos\theta \sin 2(\theta + \varphi) + 2 \sin\theta \cos 2(\theta + \varphi)). \tag{6.6}$$

which may also be written

$$f(\theta, \varphi) = \cos\theta(7 \sin^2\theta - 3\cos^2\theta) \sin 2\varphi + 2 \sin\theta(\sin^2\theta - 4\cos^2\theta) \cos 2\varphi. \tag{6.7}$$

This last expression for the angular function is somewhat more convenient for computation.

These latter equations for the response of a paraxial gradiometer reduce to previously derived equations when $\varphi = 0^\circ$, and 90°. They also provide information about the response for any other two-dimensional configuration: they represent another generalization of the two-dimensional approach I introduced in Section 5.2, and they are also relevant in a three-dimensional dipole/gradiometer context because of the applicability of the two-dimensional data to many three-dimensional problems. To illustrate the use of the new response information, I will now derive the response of the paraxial gradiometer when $\varphi = 45^\circ$ for dipole motion along the y-axis (Figure 6.1).

If $\varphi = 45^\circ$ in Equation 6.7, we have

$$f(\theta, 45^\circ) = \cos\theta\,(7\sin^2\theta - 3\cos^2\theta), \tag{6.8}$$

which, changing from θ to ϕ to conform with the work in Section 5.1, can also be written

$$f(\phi, 45^\circ) = \sin^3\phi\,(7\tan^2\phi - 3). \tag{6.9}$$

Choosing motion of the dipole in the positive y-direction, without any change in its orientation, and taking $r = d_x \cos^{-1}\phi$, we obtain

$$\Delta B_g = \frac{3K\ell}{2d_x^4} f(\phi, 45^\circ), \tag{6.10}$$

where the response function $f(\phi, 45^\circ)$ is given by

$$f(\phi, 45^\circ) = \cos^4\phi\,\sin^3\phi\,(7\tan^2\phi - 3). \tag{6.11}$$

A plot of this response function is shown in Figure 6.2.

The generalization I have introduced above can be easily extended to coaxial gradiometers and thus the two-dimensional response, or generalized two-dimensional response (as discussed in Section 5.2.3), of any arbitrarily oriented component gradiometer to a dipole magnetic field can be calculated. This is the last generalization I will make, since I have now provided all the information necessary to compute the response of gradiometers to dipole fields in any two- or three-dimensional configuration. Let us now consider what happens to the response of the paraxial gradiometer considered above when it begins to rotate about its center.

To investigate the rotational response of the gradiometer, suppose we return to Equations 6.5 and 6.7 and compute $f(\theta, \varphi)$ for $\theta = 0^\circ$, 45°, and 90°, and $\varphi = \omega t$, *i.e.*, we allow the gradiometer sensor to rotate at angular frequency ω (period T) for three different values of its position angle θ. If we assume r is kept fixed, the physical situation now being analyzed is equivalent to having a dipole source moving in a circle around the rotating gradiometer sensor while maintaining the orientation of its moment in a fixed direction. This is not a

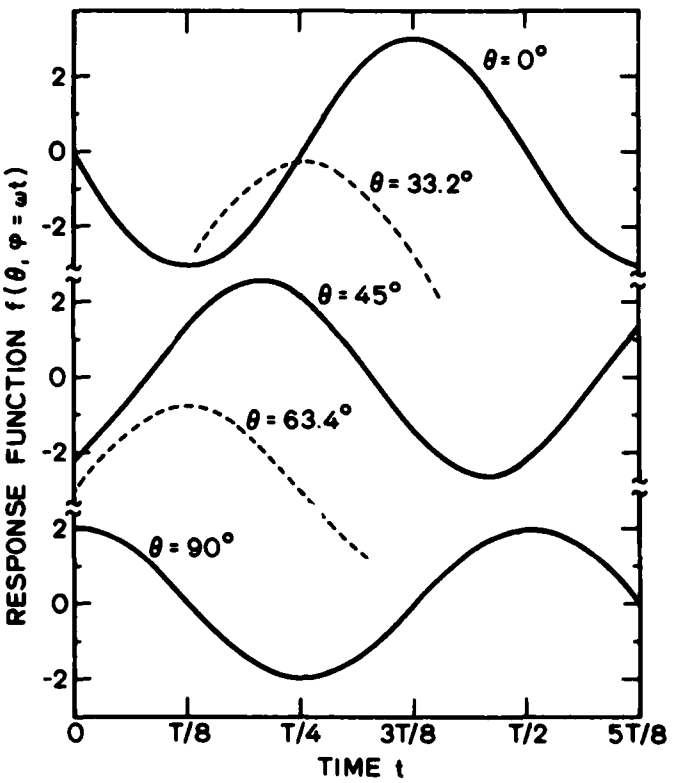

Figure 6.3. Plots of the function $f(\theta, \varphi)$ for the rotating component gradiometer, where φ is allowed to vary with time t according to the relation $\varphi = \omega t$ and θ is given the three fixed values $\theta = 0^\circ$ (top), 45° (middle), and 90° (bottom). Also shown (dashed lines) are parts of the variation of $f(\theta, \varphi)$ for $\theta = 33.2^\circ$, and 63.4°.

particularly idealistic situation and the response of the gradiometer will provide information about its possible practical applications.

Figure 6.3 shows the variation of the response function $f(\theta, \varphi)$ under the assumed conditions. It can be seen that there is some variation in the amplitude of the response functions for the various values of θ, but the change of particular relevance to us is the shift of the maximums in the response curves to smaller values of t as θ increases from 0° to 90°. For example, the peak that originally occurred at $t = 3T/8$ ($\varphi = 135^\circ$) for $\theta = 0^\circ$ has moved to $t = 0^\circ$ ($\varphi = 0^\circ$) for $\theta = 90^\circ$. Although there is not a 1:1 relationship between the changes in θ and the peak in the response curve, the data suggest that it should be possible to track the change in bearing of a moving dipole source using a rotating component gradiometer. Needless to say, the data from the rotating gradiometer ought to be processed by means of a minicomputer to take full advantage of the theoretical knowledge of the gradiometer's response, but

this processing should not involve any new techniques and need not be discussed further here. Further research on this passive technique for tracking magnetic dipole sources could lead to new MAD instrumentation.

§6.2 Rotating Induction Loop Gradiometer

To introduce the concept of a rotating induction loop gradiometer (RILG), I will once again consider a comparatively simple example and then generalize from it to more involved situations. Let us start therefore by considering the RILG configuration shown in Figure 6.4. The RILG itself consists of two physically-connected coplanar loops of N turns and area A, which are separated by a distance ℓ (measured between centers) in the plane of the loops and which rotate about an axis passing through the midpoint of the line joining their centers (the baseline). Different varieties of RILG's can be constructed depending on the orientation of the rotation axis relative to the baseline and the plane of the loops; I will assume here that the axis is perpendicular to the plane of the loops. Thus, in the figure, the two loops rotate in a circle about the center of the line joining them. The magnetic dipole source is located a distance r away from the center of the loop assembly and it will be assumed to be directed vertically upwards, *i.e.*, its moment is directed upwards out of the plane of the figure and is parallel to the axis of rotation of the RILG.

Because of the assumed geometry, the magnetic field of the dipole is everywhere directed perpendicularly downwards into the loop plane. It has no angular variation and its magnitude is given by

$$B = \frac{K}{r^3}, \tag{6.12}$$

which follows from Equations 5.1 when $\theta = 90^\circ$. The quantity K is given by $K = \mu_0 M/4\pi$ as in the previous section. The loop spacing ℓ is assumed to be very small compared with r, and the loop areas A are also taken to be so small that the magnetic field can be considered to be uniform over each area. With these assumptions the magnetic flux passing through the coils can be written

$$\Phi = \int_S \mathbf{B}.\mathbf{dS} = -NAB. \tag{6.13}$$

The emf's induced in the loops are given by $-\partial\Phi/\partial t$ and $-\partial\Phi/\partial t$, which can also be written $NA\partial B_1/\partial t$ and $NA\partial B_2/\partial t$, where the subscripts indicate which loop is involved. We now need to derive B_1 and B_2 in order to compute the emf's.

If we write r_1 and r_2 for the distances from the dipole to the centers of loop 1 and loop 2, respectively, we have, to a first approximation,

$$\begin{aligned} r_1 &= r + \frac{\ell}{2}\cos(\phi - \varphi), \\ r_2 &= r - \frac{\ell}{2}\cos(\phi - \varphi), \end{aligned} \tag{6.14}$$

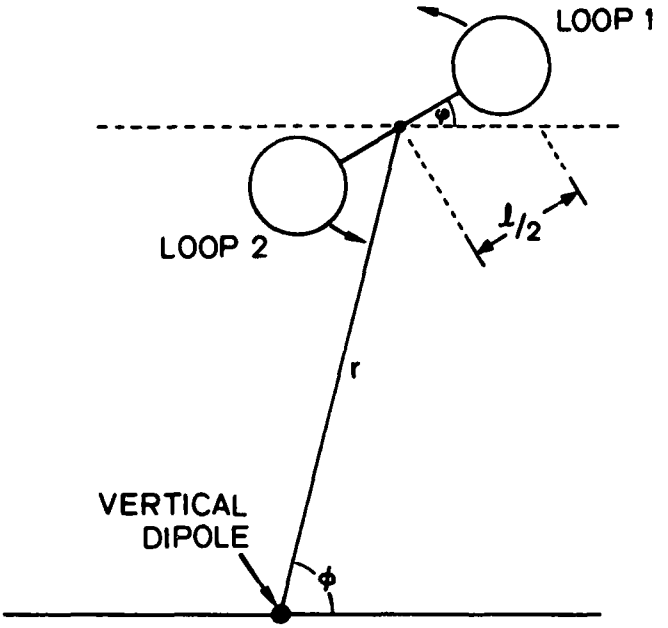

Figure 6.4. Diagram showing the geometry used in the analysis of the response of a rotating induction loop gradiometer (RILG). In the particular configuration shown the dipole source is directed vertically upwards out of the plane of the figure, which also happens to be (1) the plane containing the two loop sensors and (2) the plane of rotation of the loop assembly.

giving

$$B_1 = Kr^{-3}\left(1 + \frac{\ell}{2r}\cos(\phi - \varphi)\right)^{-3},$$
$$B_2 = Kr^{-3}\left(1 - \frac{\ell}{2r}\cos(\phi - \varphi)\right)^{-3}. \tag{6.15}$$

Using a binomial series expansion and omitting third and higher order terms, Equations 6.15 can be written

$$B_1 = Kr^{-3}\left(1 - \frac{3\ell}{2r}\cos(\phi - \varphi) + \frac{3\ell^2}{4r^2}\cos^2(\phi - \varphi)\right),$$
$$B_2 = Kr^{-3}\left(1 + \frac{3\ell}{2r}\cos(\phi - \varphi) + \frac{3\ell^2}{4r^2}\cos^2(\phi - \varphi)\right). \tag{6.16}$$

Since the loops are rotating, we can write $\varphi = \omega t$, where ω is the angular frequency and t the time, in Equations 6.16. When differentiated with respect to time, and then substituted in the

expressions for the induced emf's, B_1 and B_2 give

$$\begin{aligned} \text{emf}_1 &= \frac{3NAK\ell\omega}{2r^4}\left(-\sin(\phi-\omega t)+\frac{\ell}{2r}\sin 2(\phi-\omega t)\right), \\ \text{emf}_2 &= \frac{3NAK\ell\omega}{2r^4}\left(+\sin(\phi-\omega t)+\frac{\ell}{2r}\sin 2(\phi-\omega t)\right). \end{aligned} \tag{6.16}$$

If the two loops are now connected in series opposition, the output of the rotating loop sensor assembly will be a voltage V_{g1} given by

$$V_{g1} = \frac{3NAK\ell\omega}{r^4}\sin(\phi-\omega t), \tag{6.17}$$

or, if the are connected in series with the emf's adding, the output of the sensor assembly will be a voltage V_{g2} given by

$$V_{g2} = \frac{3NAK\ell^2\omega}{4r^5}\sin 2(\phi-\omega t). \tag{6.18}$$

The RILG can therefore respond to the magnetic field of the dipole in one or the other of two modes. The first mode can be considered to be a first-order gradiometer mode, since the coils are connected conventionally in series opposition and the output of the RILG is proportional to the inverse fourth power of the distance to the source as in other first-order gradiometers. However, the output of the gradiometer is far from orthodox in other ways, and most particularly in the way it consists of a sinusoidal variation with an amplitude that can be made larger by increasing the gradiometer parameters N, A, and ℓ, and above all by increasing ω. Thus the sensitivity of a RILG can be made large by spacing its loops far apart, by giving them large areas and many turns, and by giving the sensor assembly a high rotation rate. It is of interest that the sensitivity can be varied continuously within wide limits by varying ω: this control could have many practical advantages. Note that the dependence of the sensitivity on ω and ℓ are perhaps more important than the dependence on N and A, because increasing the latter quantities will lead to an increase of thermal noise in the loops, whereas an increase in the former quantities will not lead to such an increase.

The second mode can similarly be considered to be a second-order gradiometer mode because of the dependence of its output on the inverse fifth power of distance to the source. Its sensitivity also depends on ω and can therefore be varied comparatively easily. It could be used where better discrimination against nearby sources of magnetic noise is required. Since there should be little difficulty switching the connections between the two loop sensors, a RILG is potentially two gradiometers in one: a first-order version for maximum range and a second-order version for better characterization of the sources at closer distances in the presence of noise.

Another dipole/RILG configuration that can be analyzed with little difficulty using basic principles is essentially the same as the one we have just studied but with the important

difference that the dipole moment lies in the plane of rotation of the loops. For this configuration the magnetic flux passing through the loops is zero, and thus the response of the RILG is also zero. This may appear to be a trivial example, but it indicates a potential weakness of the RILG: it will not always respond to a dipole field. To ensure a response under all circumstances it may be necessary to use two crossed RILGs. However, it should be obvious that the exact conditions for zero response of the RILG are likely to occur only rarely in practice, and if they do occur it is probable that they will only last for a short time.

As a partial generalization of the above results, I must now admit to excessive simplification in the use of the distance approximations in Equations 6.14. More accurate expressions for the distances are

$$\begin{aligned} r_1 &= r + \frac{\ell}{2}\cos(\phi-\varphi) - \frac{\ell}{8r}\sin^2(\phi-\varphi), \\ r_2 &= r - \frac{\ell}{2}\cos(\phi-\varphi) - \frac{\ell}{8r}\sin^2(\phi-\varphi), \end{aligned} \tag{6.19}$$

and when these distance expressions are used in the derivation of the RILG response for the vertically oriented dipole, it is found that

$$\begin{aligned} V_{g1} &= \frac{3NAK\ell\omega}{r^4}\left(\sin(\phi-\varphi) - \frac{\ell}{4r}\sin 2(\phi-\varphi)\right), \\ V_{g2} &= \frac{NAK\ell^2\omega}{r^5}\sin 2(\phi-\varphi). \end{aligned} \tag{6.20}$$

These more accurate expressions for the voltages produced by the rotating loop assembly in the RILG show that the response of the RILG connected in series opposition is actually a mixture of the first-order response derived previously with an additional second-order response. This appears to be a general feature of the series-opposition RILG response. However, it will be immediately apparent that the second-order response will be small and probably negligible compared with the first-order response under normal circumstances of use (*i.e.*, $r \gg \ell$) because of its additional ℓ/r factor. The response of the RILG connected in the series aiding mode remains essentially the same second-order response as before, with only a small numerical change in the magnitude of the voltage produced by the loop assembly. This purely second-order response of the series-aiding RILG also appears to be a general feature.

My colleague D. M. Bubenik has derived general expressions for the first- and second-order RILG responses. The first-order term has the form

$$C_1 NA\omega\ell((\hat{\boldsymbol{\omega}} \times \hat{\mathbf{g}}) \cdot \mathbf{grad}\,(\mathbf{B}.\hat{\mathbf{s}})),$$

where C_1 is a constant, and $\hat{\boldsymbol{\omega}}$, $\hat{\mathbf{g}}$, and $\hat{\mathbf{s}}$ are all unit vectors indicating the sense of rotation, the direction of the line joining the two sensors, and the direction of the sensitivity axes of the

loops. The second-order term has the form

$$C_2 N A \omega \ell^2 \hat{\mathbf{g}} . \mathbf{grad} ((\hat{\omega} \times \hat{\mathbf{g}}) . \mathbf{grad} (\mathbf{B}.\hat{\mathbf{s}})),$$

where C_2 is another constant and the same unit vectors are used as described above. These general terms can be used to investigate the response of the RILG under different conditions from those I have discussed above.

The response of the RILG differs intrinsically from the responses of the other gradiometers considered in this report. Unlike the other responses, it consists of a periodic variation with time (usually, but not always, a purely sinusoidal variation) and it is the amplitude of this variation that relates to the properties of the dipole. From the operational point of view this could have some advantage: when no dipole sources are in range the output of the RILG should be flat (assuming that the largely known gradient of the geomagnetic field has been removed by real time data processing—essentially a trivial procedure with modern microcomputers), and it is only when a source comes in range that any periodic variation will be seen. The distance from the source to the RILG and the dipole moment are both combined in the amplitude of the variation and they probably cannot be separated without additional information. Directional information is available, even though this may not be immediately obvious from the expressions I have given above. The directionality comes from the angle ϕ in Equations 6.17 and 6.18, for example, which implies that the direction to the source can be obtained from the times of the zeros or of the maximums/minimums in the periodic variation. There may be some ambiguity in the direction deduced from this information, but this problem, like the others I have pointed out, can probably be eliminated by further study and modifications to the measurement system.

§6.3 Conclusion

As I noted at the beginning of this chapter, the Rotating Component Gradiometer and the RILG are more speculative gradiometers than the others I have considered in this report. However, I should also note that they are speculative at this stage entirely because they are new and have not been studied to the same extent as other gradiometers. They are presented here partly to show that gradiometers departing from the conventional form are possible, and partly because they contrast with the conventional gradiometers, thus providing a fresh view of the properties of the conventional instruments. Above all, the rotating gradiometers are described to show that new ideas and concepts are possible in the field of gradiometer studies and to encourage further research on gradiometers.

Chapter 7

Discussion

This report cites many applications of magnetic field gradiometers in areas of particular importance to the United States: energy resources, defense, and health care. Despite these applications, there is a notable lack of articles in the recent scientific literature describing basic research relevant to magnetic field gradiometers. There are a few articles describing the results of basic research pertaining to superconducting gradiometers, but even in this case, where the opportunities are so great, the scientific literature suggests that basic research is not well supported. It is particularly disturbing to find so few measurements of the spatial uniformity of natural magnetic noise with magnetometer arrays and gradiometers, since such measurements are essential to the informed application of magnetic gradiometer and differential magnetometer techniques. It is surprising to find so few attempts to measure natural magnetic gradients, particularly gradients associated with ionospheric currents, either with high-sensitivity superconducting gradiometers or with long-baseline total field gradiometers. It was pointed out many years ago by *Chapman and Nelson* [1957] that measurements of these natural gradients could provide important information about the overhead electric current systems; the measurements would also help characterize a source of gradient noise. Despite the revolution currently taking place in the use of small computers for real-time computation, there is little evidence of this revolution having a significant impact on present gradiometer techniques. In the future I would expect to see small computers incorporated into the racks of electronic equipment at each gradiometer installation, or even included in the gradiometer sensor assemblies themselves, with the gradiometers being given greatly enhanced capability as a result. In short, there are many opportunities for innovative basic and applied research either specifically on gradiometers or in relation to them, and, instead of merely noting that fact and leaving it to the reader to work out what the opportunities really are, I will devote the remainder of this chapter to a listing of the areas where I perceive a need for further research, or where I believe research could provide new results and capabilities.

§7.1 Suggested Research Areas

7.1.1 Total Field Magnetometer Improvement

The first area where research appears to be needed is a broad one involving all aspects of total field magnetometers: their basic physics, improvements to their performance, and their use for measurements in the natural environment. I have deliberately given first listing to this area of needed research because of its particular relevance to energy resource development and defense, as I will now describe in greater detail. Although the total field instruments do not have the high nominal sensitivity of superconducting magnetometers and gradiometers at rest, they are still the most sensitive instruments of their kind to have been used routinely on aircraft, and they are likely to remain the most sensitive for some time to come, since the practicability of the airborne operation of superconducting magnetometers and gradiometers has yet to be demonstrated. I single out this airborne capability because of its pertinence to geophysical prospecting and to submarine localization. When considered within their wider contexts of energy resource development and, in particular, of antisubmarine warfare [*Wit*, 1981], these two activities have great strategic significance at the present time. Because of this significance, it would be expected that there would be a continued high level of research on total field magnetometers and gradiometers. Unfortunately, the level of research in the U. S. not only fails to meet this expectation, but it is at so low a level that a major failure of the research management process in the U.S. is indicated. Consider the following data:

The journal *Physics Abstracts* lists the abstracts of practically all scientific papers published in the world on what is very broadly classified as physics topics. In view of the pressure on scientists throughout the world to publish, the number of articles (and thus the number of abstracts) on a particular physics topic is likely to be a good measure of the level of research activity involving the topic. Let us now look at the number of abstracts of articles published during the four-year interval 1977 1980 that describe research either on or involving total field magnetometers. My source for this information is the issue of *Physics Abstracts* that specifically covers the indicated four-year interval, and I find that of the 232 magnetometer references listed there are 28, or 12% of the whole, that involve work either on or with total field instruments. Of these 28, 25 were references to articles by Soviet scientists (89% of the total field magnetometer articles), 2 by Japanese scientists, and 1 by scientists in the U. S. (4% of the articles on total field magnetometers; 0.4% of the total number of articles on magnetometers) The message of these data is unambiguous and it clearly supports my argument that more research is needed on total field magnetometers in the U. S.

It is interesting to list some of the titles of the Soviet articles: (1) "Enhanced accuracy of the helium M_Z magnetometer" [*Aleksandrov and Yakobson*, 1979], (2) "Alkali-helium magnetometer" [*Blinov et al.*, 1979], (3) "Selection of passband of a magnetometer when measuring

the induction of a moving magnetic body" [*Chechurina et al.*, 1976], (4) "High-accuracy T-MP field proton magnetometer" [*Maksimovskikh and Shapiro*, 1976], (5) "Evaluation of optimum conditions for towing a (proton) magnetometer" [*Shreyder*, 1977], (6) "Helium magnetometer with pulsed optical pumping" [*Yakobson and Aleksandrov*, 1978]. These examples illustrate the breadth of the Soviet research effort; the remaining 19 articles mostly describe either detailed studies of the basic processes involved in the operation of the total field magnetometers or specific improvements that have been achieved in their performance.

The Soviet work specifically on magnetic field gradiometers is much less comprehensive than the research on total field magnetometers that I have cited above (the few available Soviet articles on gradiometers mostly contain rather academic theoretical studies [*e.g.*, *Reznik*, 1967; *Roze*, 1973, 1978]), but sensor improvement is probably the foremost requirement for improved gradiometers and the Soviet program of total field magnetometer improvement could as well serve as a model for improved total field gradiometers.

7.1.2 Innovative Total Field Gradiometer Configurations

In addition to further research on the basic physics of total field magnetometers, as recommended above, it is also desirable that a fresh look be given to the better utilization of total field magnetometers in gradiometer configurations. It is well recognized that total field magnetometers are not as sensitive as the most recent superconducting models, and as a result it is commonly assumed that total field gradiometers must be much less sensitive than superconducting gradiometers. This assumption is not necessarily correct, however, since gradiometer sensitivity does not depend solely on the sensitivity of the individual sensors; the spacing between the sensors is also an important factor. Because of their need to be kept at liquid helium temperatures, superconducting gradiometer sensors are necessarily limited to sizes that can be inserted in a dewar this compactness is generally cited as an advantage, as indeed it is, but it limits the sensitivity that can be achieved. Total field gradiometers are not similarly limited and any baseline can be used that is consistent with gradiometer operation. When the combination of magnetometer sensitivity and baseline is considered, total field gradiometers are not inferior to the superconducting varieties in gradiometer sensitivity. To illustrate, suppose we have a superconducting magnetometer that is 1000 times more sensitive than the best available total field magnetometer, and that two of these superconducting magnetometers are combined to produce a gradiometer with a baseline of 30 cm, which is representative of the longest baselines that have been used up to the present time. To match the sensitivity of this superconducting gradiometer, a gradiometer constructed from the total field magnetometers would need to have a baseline of 1000×30 cm, or 300 m. Such baselines are quite feasible, and have already been used. In fact, there appears to be no reason why much longer baselines cannot be utilized, since natural geomagnetic field fluctuations are likely to be relatively uniform over

distances much greater than 300 m (but measurements of this uniformity are required, as detailed below).

For practical reasons, the total field gradiometers that have been developed for airborne use have typically had a vertical configuration, with the two magnetometers being towed one above the other on a single cable. Another possible configuration that could be developed is a synthesized horizontal gradiometer, which would require two separate total field magnetometers to be towed at approximately the same altitude by two separate aircraft. Large spacings would be possible with this configuration, giving it a high gradient sensitivity and making it more effective for surveying large areas than the vertical gradiometer. The important part of this suggestion is the requirement that the spacing, altitude, and responses of the magnetometers be monitored in real time and the gradiometer response of the combination be synthesized, using a small computer, either on one of the aircraft or on the ground. The spacing and altitude can be obtained by incorporating transceivers and altimeters in the magnetometer housings and the data fed, in real time, to the computer. Since one of the important results to be obtained during a survey is the identification and localization of sources of magnetic field, there is likely to be a transition from operation in the gradiometer mode (distance to the source large relative to the magnetometer spacing) to the differential magnetometer mode (distance to the source comparable to magnetometer spacing) during many surveys. The computer processing of the magnetometer data can take this transition into account, but it is a further topic that needs to be studied.

7.1.3 Computer Utilization

By using the techniques I have described in this report, it is possible to compute the response of any component or total field gradiometer to magnetic dipole sources. The computations are not extensive and there is no reason why a small computer could not be programmed to carry out the computations during a gradiometer survey and thus enable the operator to compare the actual measurements with theoretical predictions in real time. This is just one of many possible computer applications in gradiometer measurements. In the preceding subsection I introduced the idea of using a computer to synthesize a gradiometer response from the measurements made by two physically-separated total field magnetometers. Computers could also be used to remove a response to the geomagnetic field gradient or, more generally, to eliminate sources of gradient noise by adaptive techniques. In the use of multi-axis superconducting gradiometers, computers are essential for the processing of the different streams of data so that the gradiometers can perform in the "tracker-classifier" mode (Section 4.5), which may well be one of their most important applications. Clearly, the successful application of magnetic field gradiometers is likely to hinge on the efficient utilization of computers. Today, many small and easily portable computers are available that are ideal for gradiometer use and it is most desirable that they be incorporated into gradiometers. Modern computational

techniques, particularly adaptive techniques, also need to be studied with a view to improving gradiometer performance. Since there is little evidence in the recent scientific literature for the use of computers to analyze gradiometer data in real time, or to carry out the higher level procedures I have just described, I recommend computer utilization, and the accompanying use of modern computational techniques (including adaptive techniques), as another area for further gradiometer research.

7.1.4 Measurements with Superconducting Gradiometers

Despite their great promise for magnetic field gradient studies, few superconducting gradiometers have actually been used as scientific instruments for the measurement of natural gradients- either gradients of the geomagnetic field itself or the gradients produced in the geomagnetic field by other natural sources. One exception, which also indicates the kind of research that I would recommend, are the measurements made by *Gillespie et al.* [1977] and *Podney and Sager* [1979], first on the noise in a superconducting gradiometer at a remote location and then on the magnetic gradients produced by internal waves in the sea. Apart from the valuable contributions these measurements could make in a variety of geophysical disciplines, the measurements would help establish a foundation of expertise in the scientific community that, in the long run, is likely to be the most important factor in the successful application of superconducting gradiometers.

7.1.5 Superconducting Gradiometer Development

As I have mentioned many times in this report, one of the key requirements in a component gradiometer is accurate alignment of the component sensors. No matter what kind of component gradiometer is involved, there always appears to be some limit to the degree of alignment that can be achieved and continual research, and new ideas, are needed for further improvement. Superconducting gradiometers are most severely affected by this need for alignment, or balancing, because of the great sensitivity of the individual sensors: it is primarily the degree of imbalance that limits the gradiometer sensitivity. There is already a substantial level of research on the balancing of superconducting gradiometers [*e.g., Jaworski and Crum*, 1980], which I will assume will continue in the future. However, there is an important question concerning balancing that arises when the possible applications of superconducting gradiometers are considered: how well can such a gradiometer maintain its balance when airborne, or when used on a series of flights? There are other questions that arise when the airborne use of superconducting gradiometers is contemplated, all involving the motion of components of the gradiometer (*e.g.* the liquid helium in the dewar) or of the aircraft and the way these motions may degrade the gradiometer measurements. Research on the effects of motion on a superconducting gradiometer is therefore desirable, particularly the effects of aircraft motion.

7.1.6 Uniformity of Geomagnetic Noise

In several places in this report I have suggested that natural geomagnetic field fluctuations are likely to be uniform over distances ranging from hundreds of meters to hundreds of kilometers. This suggestion is in agreement with the few measurements that have been made [*e.g., Zelwer and Morrison*, 1972] and it is one of the basic reasons for the usefulness of magnetic gradiometers and differential magnetometers. However, there is an urgent need for better data on the spatial uniformity of the fluctuations. In particular, the variations of the uniformity with the frequency of the fluctuations and with location on the earth's surface are not well established. The mathematical quantities that provide a measure of the uniformity are the *coherence* and *phase angle*, where the coherence measures the similarity of the waveforms recorded by two sensors and the phase angle is a measure of the difference between the times of arrival of the waveforms at the sensors, and measurements of the coherence and phase angle need to be made at representative locations over the earth's surface for a variety of sensor spacings in the North-South and East-West directions and for a variety of frequencies. With some hesitation I will add that these measurements also need to be repeated at different times during the day (to detect diurnal variations), at different times during the year (to detect seasonal or annual variations), and at different times during a solar cycle (for solar cycle changes). I recommend the study by *Zelwer and Morrison* [1972] as a model for the more extended gradiometer-oriented study, and the report by *Banerjee et al.* [1982] also can be recommended for its particularly relevant discussion of the coherence of geomagnetic variations.

7.1.7 Rotating Gradiometers

As we saw in the preceding chapter, the rotating induction loop gradiometer, or RILG, has a response to magnetic dipole fields that varies either with the inverse fourth power of distance from the dipole or as the inverse fifth power of distance, depending on the way the two induction loops are connected. This variability of response is of some interest by itself; when it is also recognized that the response varies linearly with the frequency of rotation, the RILG begins to look as if it might have some potential for gradient measurements. It is unlikely that its sensitivity will approach that of superconducting gradiometers, but it is the RILG's other properties that are distinctive and which need to be studied further to see if it has any unique application.

7.1.8 Reexamination of the Source-Free Assumption

I have discussed the source-free assumption at some length in Appendix A. The problems that arise when the assumption is made for gradient measurements in sea water or other conducting media on the earth's surface need to be studied further in their appropriate context. For example, how do the problems affect the "tracking and classification" function of a five-axis superconducting gradiometer when it is immersed in sea water?

§7.2 Conclusion

To conclude this report, I would like to return briefly to my comments in the introduction about the great advances that have been made in magnetic field gradiometer technology over the last two decades. I hope I have clearly explained in the body of the report how these advances came about and how I believe the momentum can be maintained. Only a small number of scientists and engineers were involved in the advances and even today there is every reason to expect that the next improvements in gradiometer performance will come about as the result of the work of a single gifted student or professional researcher. Unfortunately, gradiometer research is difficult to conduct without gradiometers and the most sensitive gradiometers are costly to acquire (particularly multi-axis superconducting gradiometers). However, I have repeatedly emphasized how gradiometers and gradiometer research impact upon three areas of crucial importance to the U. S. and Western nations generally (energy resource development, defense, and health care) it is to be hoped that this fact will become recognized at what I have termed the "research management" level in the U. S. so that funds will be made available to our contract monitors and grant administrators to assist in gradiometer purchases. We can then proceed with our business as scientists and engineers: increasing mankind's knowledge and capability.

Chapter 8

References

A motley lot!

Unpublished marginalia
William Shakespeare

Ahonen, A. I., T. E. Katila, and O. V. Lounasmaa, Magnetogradiometry by means of a SQUID, *Commentat. Phys.-Math. (Finland), 42*, 301, 1972.

Aitken, M. J., and M. S. Tite, A gradient magnetometer using proton free-precession, *J. Sci. Instr., 39*, 625–629, 1962.

Aleksandrov, E. B., Optical magnetometry, *Soviet J. Opt. Technol., 45*, 759 765, 1978.

Aleksandrov, E. B., Enhanced accuracy of the helium M_Z magnetometer, *Soviet Phys.-Tech. Phys., 24*, 938–939, 1979.

Anderson, P. W., How Josephson discovered his effect, *Phys. Today, 23*, 23–29, November 1970.

Banerjee, B., D. Soller, and R. D. Brown, The utility of real-time monitoring and correction of temporal variations in magnetic surveys, Final Rept., ONR Contract N00014-80-C-0043, Phoenix Corp., McLean, Virginia, 15 March 1982.

Blinov, E. V., R. A. Zhitnikov, and P. P. Kuleshov, Alkali-helium magnetometer, *Soviet Phys. Tech. Phys., 24*, 336–341, 1979.

Boger, A. D., and F. X. Bostick, Jr., Gradiometer detection of magnetic dipole sources, Technical Rept., ONR Contract Nonr 375(14), Geomagnetics and Elec. Geosci. Res. Lab., Univ. of Texas at Austin, Austin, Texas, 1 October 1969.

Breiner, S., Gradiometers and gradient techniques, pp. 49 54 in *Applications Manual for Portable Magnetometers*, Geometrics, Sunnyvale, California, 1973.

Chapman, S., and J. Bartels, *Geomagnetism*, Oxford Univ. Press, London, 1940.

Chapman, S., and J. H. Nelson, Instrumental equipment for the recording of space gradients of the magnetic elements, *Annals IGY, 4*, 237–245, 1957.

Chechurina, E. N., R. G. Skrynnikov, A. F. Barabanshchikov, V. I. Tikhomirov, and V. V. Filippov, Selection of passband of a magnetometer when measuring the induction of a moving magnetic body, *Meas. Tech., 19*, 1769–1773, 1976.

Clarke, J., Josephson junction detectors, *Science, 184*, 1235–1242, 1974.

Cohen, D., Measurements of the magnetic fields produced by the human heart, brain, and lungs, *IEEE Trans. Magnetics, MAG-11*, 694–700, 1975.

Cohen, D., E. A. Edelsack, and J. E. Zimmerman, *Appl. Phys. Letts., 16*, 278–280, 1970.

Cornwell, J. D., and L. W. Hart, The effect of a shoreline on subsurface-to air propagation measurements with a submerged HED source, Tech. Rept. STD-R-214, Appl. Phys. Lab., The Johns Hopkins Univ., Laurel, Maryland, August 1979.

Dehmelt, H. G., Slow spin relaxation of optically polarized sodium atoms, *Phys. Rev., 105*, 1487–1489, 1957.

Dessler, A. J., Geomagnetism, in *Satellite Environment Handbook*, edited by F. S. Johnson, pp. 153–182, Stanford Univ. Press, Stanford, California, 1965.

Fowler, B. C., H. W. Smith, and F. X. Bostick, Jr., Magnetic anomaly detection utilizing component differencing techniques, Tech. Rept. No. 154, Electrical Geophys. Res. Lab., The Univ. of Texas at Austin, Austin, Texas, August 31, 1973.

Fraser-Smith, A. C., and J. L. Buxton, Superconducting magnetometer measurements of geomagnetic activity in the 0.1- to 14-Hz frequency range, *J. Geophys. Res., 80*, 3141–3147, 1975.

Fromm, W. E., The magnetic airborne detector, in *Advances in Electronics*, vol. 4, edited by L. Marton, pp. 257–299, Academic Press, N. Y., 1952.

Gillespie, G. H., W. N. Podney, and J. L. Buxton, Low-frequency noise spectra of a superconducting magnetic gradiometer, *J. Appl. Phys., 48*, 354–357, 1977.

Glicken, M., Uses and limitations of the airborne magnetic gradiometer, *Trans. AIME, 7*, 1054–1056, 1955.

Goodman, W. L., V. W. Hesterman, L. H. Rorden, and W. S. Goree, Superconducting instrument systems, *Proc. IEEE, 61*, 20–27, 1973.

Gordon, D. I., and R. E. Brown, Recent advances in fluxgate magnetometry, *IEEE Trans. Magnetics, MAG-8*, 76–82, 1972.

Goubau, W. M., T. D. Gamble, and J. Clarke, Magnetotellurics using lock-in signal detection, *Geophys. Res. Letts., 5*, 543–546, 1978.

Grice, C. F., Finding underwater objects, *Ocean Industry, 3*, 25–42, January 1968.

Grivet, P. A., and L. Malnar, Measurements of weak magnetic fields by magnetic resonance, *Adv. Electr. Electron Phys., 23*, 39–151, 1967.

Haalck, H., Der Erdinduktor als Lokalvariometer und seine praktische Verwendungsmöglichkeit, *Zeitschrift für techn. Physik, 6*, 377–380, 1925.

Hartmann, F., Resonance magnetometers, *IEEE Trans. Magnetics, MAG-8*, 66–75, 1972.

Hood, P., and D. J. McClure, Gradient measurements in ground magnetic prospecting, *Geophysics, 30*, 403–410, 1965.

Hood, P., Gradient measurements in aeromagnetic surveying, *Geophysics, 30*, 891–902, 1965.

Irons H. R., and L. J. Schwee, Magnetic thin-film magnetometers for magnetic-field measurement, *IEEE Trans. Magnetics, MAG-8*, 61–65, 1972.

Jaworski, F. B., and D. B. Crum, Sources of gradiometer imbalance and useful balancing techniques, paper presented at Squid Applications to Geophysics workshop, Los Alamos, June 1980.

Johnston, M. J. S., and F. D. Stacey, Magnetic disturbances caused by motor vehicles and similar ferrous bodies, *J. Geomagn. Geoelec., 20*, 1–6, 1968.

Joseph, R. I., M. E. Thomas, and K. R. Allen, Corrections for magnetic field and field gradient measurement in a conducting fluid limited to potential flow when the sensor enclosure is nonconducting, Tech. Rept. STD-R-549, Appl. Phys. Lab., The Johns Hopkins Univ., Laurel, Maryland, July 1981.

Joseph, R. I., and M. E. Thomas, Corrections for magnetic field and field gradient measurement in a conducting fluid when the sensor enclosure is non conducting—general formulation, Tech. Rept. STD-R-578, Appl. Phys. Lab., The Johns Hopkins Univ., Laurel, Maryland, December 1981.

Josephson, B. D., Possible new effects in superconductive tunnelling, *Phys. Letters, 1*, 251–253, 1962.

Karp, P., and D. Duret, Unidirectional magnetic gradiometers, *J. Appl. Phys., 51*, 1267–1272, 1980.

Ketchen, M. B., W. M. Goubau, J. Clarke, and G. B. Donaldson, Thin-film dc SQUID gradiometer, *IEEE Trans. Magnetics, MAG-13*, 372–374, 1977.

Ko, H. W., D. L. Thayer, and P. G. Fuechsel, ELFEX-I: Propagation phase final report, Tech. Rept. POR-3147A, Appl. Phys. Lab., The Johns Hopkins Univ., Laurel, Maryland, 16 July 1976.

Lewis, D. R., Experimental investigation of a fiber-optic magnetic field sensor model, M.S. thesis, Naval Postgraduate School, Monterey, California, June 1980.

Maksimovskikh, S. I., and V. A. Shapiro, High-accuracy T-MP field proton magnetometer, *Geomagn. Aeron.*, Engl. Transl., *16*, 231–232, 1976.

Morris, R. M., and B. O. Pedersen, Design of a second harmonic flux gate magnetic field gradiometer, *Rev. Sci. Instr., 32*, 444–448, 1961.

Nicol, J., Superconducting systems for magnetic anomaly detection, pp. 179–193 in *Proc. Workshop on Naval Applications of Superconductivity*, edited by J. E. Cox and E. A. Edelsack, Naval Res. Lab. Rept. No. 7302, 1 July 1971.

Otala, M., The theory and construction of a proposed superconducting aeromagnetic gradiometer, *Acta Polytech. Scandinavica*, Electr. Engin. Ser. No. 21, 56 pp., Helsinki, 1969.

Overweg, J. A., and M. J. Walter-Peters, The design of a system of adjustable superconducting plates for balancing a gradiometer, *Cryogenics, 18*, 529–534, 1978.

Packard, M., and R. Varian, Free nuclear induction in the earth's magnetic field, abstr., *Phys. Rev., 93*, 941, 1954.

Podney, W., and R. Sager, Measurement of fluctuating magnetic gradients originating from oceanic internal waves, *Science, 205*, 1381–1382, 1979.

Reznik, E. Ye., Value of a magnetic gradient meter, *Geomagn. Aeron.*, Engl. Transl., *7*, 764 765, 1967.

Roman, I., and T. C. Sermon, A magnetic gradiometer, Trans. AIME, 110, 373–390, 1934.

Roze, Ye. N., Information available from the gradient method of measuring the geomagnetic field, *Geomagn. Aeron.*, Engl. Transl., *13*, 647–649, 1973.

Roze, Ye. N., The integration of gradiometer data, *Geomagn. Aeron.*, Engl. Transl., *18*, 651 653, 1978.

Rubin, L. G., and H. H. Sample, Hall effect magnetometers for high magnetic fields and temperatures between 1.5° K and 300° K, pp. 463–479 in *The Hall Effect and its Applications*, edited by C. L. Chien and C. R. Westgate, Plenum, N. Y., 1980.

Serson, P. H., An electrical recording magnetometer, *Can. J. Phys., 35*, 1387–1394, 1957.

Shreyder, A. A., Evaluation of optimum conditions for towing a magnetometer, *Oceanology, 17*, 362-363, 1977.

Skilling, H. H., *Fundamentals of Electric Waves*, 248 pp., Krieger, Huntington, N. Y., 1974.

Slack, H. A., V. M. Lynch, and L. Langan, The geomagnetic gradiometer, *Geophysics, 32*, 877 892, 1967.

Smith, H. W., F. X. Bostick Jr., and J. E. Boehl, Preliminary report on submarine detection by a magnetic gradiometer, Tech. Rept., ONR Contract Nonr 375(14), Geomagnetics and Elec. Geosci. Res. Lab., Univ. of Texas at Austin, Austin, Texas, 1 October 1969.

Staff Rept., A new tool for mineral exploration, *Ocean Industry, 2*, 17–19, December 1967.

Staff Rept., Filter Center, *Aviation Wk. Space Techn., 116*, 81, 1 February 1982.

Stratton, J. A., *Electromagnetic Theory*, pp. 233–237, McGraw-Hill, N. Y., 1941.

Troitskaya, V. A., Pulsations of the earth's electromagnetic field with periods of 1 to 15 seconds and their connection with phenomena in the high atmosphere, *J. Geophys. Res., 66*, 5–18, 1961.

Usher, M. J., and W. F. Stuart, Stability and resolution of a rubidium magnetometer, *J. Phys. E: Sci. Instr., 3*, 203–205, 1970.

Vrba, J., A. A. Fife, M. B. Burbank, H. Weinberg, and P. A. Brickett, Spatial discrimination in SQUID gradiometers and 3rd order gradiometer performance, *Can. J. Phys., 60*, 1–12, 1982.

Ware, R. H., High-accuracy magnetic field difference measurements and improved noise reduction techniques for use in tectonomagnetic studies, *J. Geophys. Res., 84*, 6291–6295, 1979.

Waters, G. S., and P. D. Francis, A nuclear magnetometer, *J. Sci. Instr., 35*, 88–93, 1958.

Webb, W. W., Superconducting quantum magnetometers, *IEEE Trans. Magnetics, MAG-8*, 51–60, 1972.

West, F. S., W. J. Odom, J. A. Rice, and T. C. Penn, Detection of low-intensity magnetic fields by means of ferromagnetic films, *J. Appl. Phys., 34*, 1163–1164, 1963.

Wickerham, W. E., The Gulf airborne magnetic gradiometer, *Geophysics, 19*, 116–123, 1954.

Williamson, S. J., and L. Kaufman, Biomagnetism, *J. Magnetism Magn. Materials, 22*, 129–201, 1981.

Wit, J. S., Advances in antisubmarine warfare, *Sci. American, 244*, 31–41, February 1981.

Wurm, M., Beiträge zur Theorie und Praxis des Feldstärkedifferenzmessers für magnetische Felder nach Förster, *Z. angew. Phys., 2*, 210–219, 1950.

Wynn, W. M., C. P. Frahm, P. J. Carroll, R. H. Clark, J. Wellhoner, and M. J. Wynn, Advanced superconductive gradiometer/magnetometer arrays and a novel signal processing technique, *IEEE Trans. Magnetics, MAG-11*, 701–707, 1975.

Yakobson, N. N., and E. B. Aleksandrov, Helium magnetometer with pulsed optical pumping, *Soviet Phys.-Tech. Phys., 23*, 1089–1092, 1978.

Yariv, A., and H. V. Winsor, Proposal for detection of magnetic fields through magnetostrictive perturbation of optical fibers, *Optics Letts., 5*, 87–89, 1980.

Zelwer, R., and H. F. Morrison, Spatial characteristics of midlatitude geomagnetic micropulsations, *J. Geophys. Res., 77*, 674–694, 1972.

Zimmerman, J. E., and N. V. Frederick, Miniature ultrasensitive superconducting magnetic gradiometer and its use in cardiography and other applications, *Appl. Phys. Letts., 19*, 16–19, 1971.

Appendix A.
Validity of the Source-Free Assumption

The Maxwell equation linking the magnetic field at a point with the conduction current density $\mathbf{J}$ and displacement current density $\partial\mathbf{D}/\partial t$ at that same point is

$$\mathbf{curl}\,\mathbf{B} = \mu_0(\mathbf{J} + \frac{\partial \mathbf{D}}{\partial t}), \tag{A.1}$$

where it is assumed that the medium is non-magnetic ($\mu = \mu_0$). As discussed in Section 2.3, in a region where $\mathbf{J} = \partial\mathbf{D}/\partial t = 0$ (described as 'source free'), this equation can be written

$$\mathbf{curl}\,\mathbf{B} = 0, \tag{A.2}$$

and three terms in the gradient matrix become redundant. Under such circumstances only five measurements of spatial variations of magnetic field components need be made to determine the gradient of the magnetic field completely. This apparently purely academic result is important in magnetic field gradiometer studies because its assumption forms part of the theoretical basis for a method of measuring the position and moment vectors of a magnetic dipole source [*e.g.*, *Wynn et al.*, 1975].

Unfortunately, the source-free assumption (*i.e.*, the assumption that $\mathbf{J} = \partial\mathbf{D}/\partial t = 0$), involves an idealization that may fail in practice. Two specific conditions for this failure to occur are (1) use of a highly sensitive gradiometer, which has the capability of measuring very small spatial rates of change of the magnetic field components, and (2) operation of this gradiometer in a conducting medium (such as the sea) at large distances from the source of magnetic field, *i.e.*, at locations where the gradients of the magnetic field are small. These conditions are most likely to apply when a sensitive gradiometer is being used in the sea to measure the nearly undetectable gradient produced by a far distant source. Under less demanding conditions, the source-free assumption may not necessarily fail but it will be a poor assumption and measurements based on it will be inaccurate. The purpose of this appendix is to show how the problem with the source-free assumption arises and to indicate some general theoretical criteria for establishing its validity.

Before we examine the conditions under which a region can be considered to be source free, there is an important clarification that needs to be made concerning terminology. As I have stressed in the first two lines of this appendix, Equation A.1 links the magnetic field at a point with quantities at that point representing sources of magnetic fields. However, the source quantities should not be viewed as being the source of the magnetic field at the point, for otherwise we would undoubtedly have $\mathbf{B} = 0$, and not $\mathbf{curl}\,\mathbf{B} = 0$, whenever we specify $\mathbf{J} = \partial\mathbf{D}/\partial t = 0$. Thus we can have a region, described as source free, in which $\mathbf{J} = \partial\mathbf{D}/\partial t = 0$ at every point, but where electric and magnetic fields exist that are produced by sources outside the region. Note that no statement is made about the size of the region; it can be of any size. It is only in such a region that we can write $\mathbf{curl}\,\mathbf{B} = 0$ and, as we have seen, it is only for magnetic fields in such a region that the gradient matrix contains only five independent terms. The difficulty that arises with these source-free regions is a practical one. It is simply not feasible, except under the most exceptional circumstances, to monitor $\mathbf{J}$ and $\partial\mathbf{D}/\partial t$ with great accuracy throughout a nominally source-free region where gradient measurements are being made and to determine that the two source quantities are zero at all times. Whether it is because of this difficulty, or because of the perception that $\mathbf{J}$ and $\partial\mathbf{D}/\partial t$ are negligible under all conditions at low frequencies, it is not common practice for the source terms to be measured, and they are usually assumed to be zero. As I will now show, this source-free assumption may not be valid when small gradients are to be measured in such a region.

At low frequencies in a conducting medium such as sea water it is common practice to neglect the displacement current term in Equation A.1 in comparison with the conduction current term. This gives us a convenient point at which to start our review of the source-free assumption. If the time variations of the fields and source terms are all assumed to be harmonic with angular frequency ω, Equation A.1 can be written

$$\begin{aligned}\mathbf{curl}\,\mathbf{B} &= \mu_0(\mathbf{J} + i\omega\mathbf{D}) \\ &= \mu_0(\sigma\mathbf{E} + i\omega\epsilon\mathbf{E}),\end{aligned} \tag{A.3}$$

where ϵ is the permittivity of the medium and σ its conductivity. It follows that the displacement current term in Equation A.3 can be neglected if $\sigma/\omega\epsilon \gg 1$. For sea water, which has a conductivity close to 4 S/m and a permittivity of $80\epsilon_0$, this condition implies that the displacement current can be neglected in comparison with the conduction current for frequencies very much less than 890 MHz. For other common conducting media on the earth's surface, the conductivity is generally substantially smaller than the conductivity for sea water, but typically no less than 10^{-3} S/m, and the permittivities of these media will probably be 1 2 orders of magnitude smaller than the exceptionally high permittivity for sea water. The comparison frequency for these media is therefore likely to be 1 2 orders of magnitude smaller than 890 MHz. It is clear, however, that if the frequencies of interest are restricted to the ultra-low and extremely-low frequency bands (i.e., to frequencies less than about 3 KHz) the displacement current term will be negligible in comparison with the conduction current term.

The problem in obtaining a source-free region for the gradiometer measurements can now be discussed. Suppose we take a relevant situation and assume that magnetic field gradient measurements are to be made in the sea at frequencies less that 3 kHz. There is no doubt that the displacement current term can be neglected for this situation, but the conduction current term remains and it may be substantial, depending on the frequency. The currents included in **J** may be induced by acoustic or infrasonic waves propagating through the sea, by surface and internal waves or other sea motions, or by magnetic field fluctuations originating above the sea surface (e.g., by geomagnetic pulsations), to name just three general classes of possible sources. Recognizing the problem obtaining $\mathbf{J} = 0$ in the sea, or other conducting medium on the earth's surface, suppose we move our gradiometer up above the sea and proceed to make gradient measurements in the air, which is largely non-conducting. The conduction current term can now be neglected, but the displacement current term, although small, cannot be discarded automatically, since it is the only source term remaining. For this situation, Equation A.3 has to be reexamined to see when the displacement current can be neglected.

Expanding Equation A.3, with $\sigma = 0$, we have

$$\left(\frac{\partial B_z}{\partial y} - \frac{\partial B_y}{\partial z}\right)\mathbf{i} + \left(\frac{\partial B_x}{\partial z} - \frac{\partial B_z}{\partial x}\right)\mathbf{j} + \left(\frac{\partial B_y}{\partial x} - \frac{\partial B_x}{\partial y}\right)\mathbf{k} = \mu_0 i\omega\epsilon(E_x\,\mathbf{i} + E_y\,\mathbf{j} + E_z\,\mathbf{k}).$$

Thus, for the displacement current to be completely negligible, the following three conditions should all apply:

$$\begin{aligned} \frac{\partial B_y}{\partial z} &\gg \omega\mu_0\epsilon E_x, \\ \frac{\partial B_z}{\partial x} &\gg \omega\mu_0\epsilon E_y, \\ \frac{\partial B_x}{\partial y} &\gg \omega\mu_0\epsilon E_z. \end{aligned} \tag{A.4}$$

Note that simultaneous measurements of the electric field components and of three spatial rates of change of the magnetic field components are required to determine the applicability of these conditions.

How important are the above conditions? Few electric field data are available, but the limited measurements that have been made indicate that the displacement current conditions are easily satisfied, whereas the equivalent conduction current conditions are not as easily satisfied. For example, suppose the magnetic field gradient is to be measured in a 'source-free region' at a frequency in the Pc 1 pulsation frequency range (0.2–5 Hz). For convenience, I will assume that the frequency is 1 Hz. *Troitskaya*, [1961] quotes amplitudes of 0.01 0.1 mV/km for the horizontal electric fields induced in the earth by these pulsations during quiet days at middle latitudes, and amplitudes in the tens of mV/km on disturbed days. These electric fields are tangential to the earth/air boundary and they should therefore apply in the air just above

the earth's surface. If we suppose it is E_x that is being measured and that there is a mild Pc 1 disturbance in progress, the maximum value of E_x can be taken to be 10mV/km or 10 μV/m, giving $\partial B_y/\partial z = \omega\mu_0\epsilon E_x = \omega\mu_0\epsilon_0 E_x = 7.0 \times 10^{-10}$ pT/m. This spatial variation of magnetic field is much lower than the noise level of 0.1–0.3 pT/m (1 Hz bandwidth) that has been measured at 1 Hz with a sensitive single-axis superconducting gradiometer [*Gillespie et al.*, 1977]. This calculation suggests that the displacement current source term can certainly be ignored in the air. Since the conduction current term is also very small, we can conclude that the source-free approximation is valid in the air. The situation is quite different in the sea or in the earth.

For conducting media, the source-free criteria equivalent to those above for a non-conducting medium are

$$\frac{\partial B_y}{\partial z} \gg \mu_0\sigma E_x,$$

$$\frac{\partial B_z}{\partial x} \gg \mu_0\sigma E_y, \qquad (A.5)$$

$$\frac{\partial B_x}{\partial y} \gg \mu_0\sigma E_z,$$

where the displacement current density has been neglected. Once again using Troitskaya's electric field amplitude of 10 μV/m for the Pc 1 pulsations occurring during a day of mild activity, an amplitude that is likely to be equally applicable in the sea or in the earth, we obtain values for $\mu_0\sigma E_x$ of 50 pT/m for sea water ($\sigma = 4.0$ S/m) and 0.13 pT/m for moderately dry earth materials ($\sigma = 10^{-2}$ S/m). The former of these spatial variations would be easily measurable with a superconducting gradiometer, and the latter probably also could be measured at 1 Hz [*Gillespie et al.*, 1977]. The sea water spatial variation is quite large, and if the computation were to include the electric fields generated by motions of the water in the presence of the earth's steady magnetic field it could well be considerably larger. These computations are order-of-magnitude only, and they only apply over a limited frequency range, but similar results would probably be obtained for other frequencies in the ultra-low range (f < 5 Hz).

Up until this point we have been considering low-frequency magnetic (and electric) fields and sources. Let us now briefly consider the situation at dc. The displacement current term $\partial\mathbf{D}/\partial t$ is necessarily zero for $f = 0$ and it is probable that the conduction current term $\mathbf{J}$ will be close to zero, since there are no obvious mechanisms for maintaining steady currents in the conducting media encountered on the earth's surface. Under these circumstances, it might well be thought advantageous to use dc measurements of the various terms occurring in the magnetic field gradient; it certainly appears that these measurements could be made in regions satisfying the source-free assumption and that all five independent terms in the gradient matrix could be measured satisfactorily. There are some difficulties, however. The designation dc is

to some extent relative in practice, and there exist a variety of slowly varying electromagnetic phenomena in the geophysical environment that would appear to be dc during the course of a 'dc' measurement. In particular, there are well-known slowly varying ionospheric current systems that produce electromagnetic fields on the earth's surface and below (for example, the electric current system producing the quiet-day solar daily variation [*Chapman and Bartels*, 1940]), and these electromagnetic fields will appear to be dc over intervals of several minutes up to several tens of minutes. For measurements in the air, the fields can be ignored, but in the sea or other conducting media on the earth's surface there is likely to be a significant **J** and the source-free assumption will not be applicable.

Two new circumstances also arise at dc. First, some sources of interest are variable they are either rarely at rest or they have varying magnetic dipole moments. Unless these variations take place very slowly, a dc approach is not applicable. The second circumstance is likely to be more important: at dc the earth's own magnetic field becomes a significant factor. As shown in Appendix B, the earth's steady magnetic field has a gradient and the spatial variations included in the gradient are substantial. Whether these circumstances are relevant in practice or not will depend on the particular situation.

The limits on the applicability of the source-free assumption are now reasonably clear. There certainly seems little doubt that the assumption is valid in the air, or other non-conducting medium. However, in the sea, and other conducting media typically met on the earth's surface, it appears that the source-free assumption will not generally be valid, although there may be certain frequency ranges (yet to be determined) where the assumption is not a bad approximation. There is another problem with conducting media that should also be mentioned. It is obviously not good experimental practice to immerse a magnetometer or gradiometer directly in the sea, for example. Thus some form of container is required. Superconducting instruments already have their sensing assembly enclosed in a dewar, but the dewars are not usually designed for immersion in the sea and an additional container is necessary. These containers change the distribution of current density around the sensors and reduce it to zero in their immediate vicinity, thus distorting the measurements- a typical example of the measuring instrument altering the quantity it is supposed to measure during the measurement process. This problem pertains to any gradiometer immersed in the sea in a container; an additional problem arises if the container is in motion, for example, if it is being towed behind a vessel. In this latter case the turbulent flow of the sea around the container in the presence of the earth's magnetic field will generate electric currents that will produce spurious signals in the gradiometer. *Joseph et al.* [1981] and *Joseph and Thomas* [1981] have studied these container problems and proposed corrections for motion of the container through the sea. However, the distortions produced simply by the presence of the container, without motion, cannot be avoided and they must be taken into account when interpreting the gradiometer measurements.

In summary, it appears that the source-free assumption will be valid for gradiometers operating in the air at frequencies less than 3 kHz. However, for gradiometers operating in

such conducting media as the sea or the earth the source-free assumption is unlikely ever to be entirely valid in practice and under some circumstances it could be substantially incorrect. The containers necessary for operation in tha conducting media also introduce perturbations into the measurements. The implications of these problems for gradient measurements in the sea or earth are unfavorable, and it appears unlikely, in particular, that the technique proposed by *Wynn et al.* [1975] for deriving the location and strength of a magnetic dipole source will be effective in the sea except at very short ranges. I might conclude by observing that experimental data are badly lacking in this area, and the right experimental results could alter the negative picture I have drawn for measurements in conducting media.

Appendix B.
Gradient of the Geomagnetic Field

The earth's steady magnetic field approximates to a dipole field, with the dipole located at the earth's center and tilted at an angle of about 11.4° to the rotation axis. The moment of this dipole is about 0.815×10^{23} A m^2, and the field calculated from it is commonly referred to as the geomagnetic field. We can use this dipole field model to estimate the gradient of the earth's magnetic field, provided it is understood that is is an imperfect model on the earth's surface and that there will be regional and local anomalies where the gradient is likely to be larger than our estimates.

Using a spherical polar coordinate system based on the geomagnetic dipole, as shown in Figure B.1, the geomagnetic field $\mathbf{B}_E$ can be written

$$|\mathbf{B}_E| = \frac{\mu_0 M (3cos^2\theta + 1)^{\frac{1}{2}}}{4\pi r^3},$$

$$(B_E)_r = \frac{2\mu_0 M cos\theta}{4\pi r^3}, \qquad (B.1)$$

$$(B_E)_\theta = \frac{\mu_0 M sin\theta}{4\pi r^3},$$

where $M = 0.815 \times 10^{23}$ A m^2 is the dipole moment, $(B_E)_r$ is the radial component of the field, and $(B_E)_\theta$ is the angular component (there is no azimuthal component). Since MKS/SI units are used in this report, the units of the magnetic field quantities in Equation B.1 are Tesla. The orientation of the components relative to the dipole axis is shown in Figure B.1; the figure also shows how the geomagnetic dipole points toward the south.

As a check of the above expressions for the geomagnetic field and of the geomagnetic dipole moment, consider the magnitude of the geomagnetic field $\mathbf{B}_E$ at the poles ($\theta = 0°$, $180°$). Denoting the earth's radius by R_E, we have

$$|\mathbf{B}_E|_{pole} = \frac{2\mu_0 M}{4\pi {R_E}^3}, \qquad (B.2)$$

which gives $|\mathbf{B}_E|_{pole} = 6.3 \times 10^{-5}$ T (*i.e.*, 0.63 Gauss) if R_E is assumed to have a value of 6370 km. This value for the polar geomagnetic field is consistent with the total magnetic field amplitudes usually shown for the polar regions [*e.g., Dessler*, 1965].

Because the geomagnetic field is a vector field it would normally be expected to have three independent parts to its gradient. However, because the field is symmetric about the dipole axis, it only has two parts, **grad** $(B_E)_r$ and **grad** $(B_E)_\theta$, in our adopted spherical polar coordinate system. These gradients can be written

$$\begin{aligned} \mathbf{grad}\,(B_E)_r &= \frac{\partial (B_E)_r}{\partial r}\,\hat{\mathbf{r}} + \frac{1}{r}\frac{\partial (B_E)_r}{\partial \theta}\,\hat{\boldsymbol{\theta}}, \\ \mathbf{grad}\,(B_E)_\theta &= \frac{\partial (B_E)_\theta}{\partial r}\,\hat{\mathbf{r}} + \frac{1}{r}\frac{\partial (B_E)_\theta}{\partial \theta}\,\hat{\boldsymbol{\theta}}, \end{aligned} \tag{B.3}$$

where $\hat{\mathbf{r}}$ and $\hat{\boldsymbol{\theta}}$ are unit vectors in the direction of increasing r and θ. We therefore have four gradient terms to consider.

Using equations B.1, the four terms can be expressed in the following functional forms:

$$\begin{aligned} \frac{\partial (B_E)_r}{\partial r} &= \frac{-6\mu_0 M cos\theta}{4\pi r^4}, \\ \frac{1}{r}\frac{\partial (B_E)_r}{\partial \theta} &= \frac{-2\mu_0 M sin\theta}{4\pi r^4}, \\ \frac{\partial (B_E)_\theta}{\partial r} &= \frac{-3\mu_0 M sin\theta}{4\pi r^4}, \\ \frac{1}{r}\frac{\partial (B_E)_\theta}{\partial \theta} &= \frac{\mu_0 M cos\theta}{4\pi r^4}. \end{aligned} \tag{B.4}$$

Table B.1 gives representative values of these spatial variation terms on the earth's surface ($r = R_E = 6370$ km) for $\theta = 0^\circ$, 180° (polar), 45° and 135° (midlatitudes), and 90° (equatorial). These values show that the steady magnetic field has substantial gradients even in the absence of the regional and local anomalies that are known to exist.

First consider the *polar fields* at the earth's surface. Combining the previous equations and the data in Table B.1, these fields have the following properties:

$$\begin{aligned} (B_E)_r &= \frac{2\mu_0 M}{4\pi {R_E}^3} = 6.3 \times 10^{-5}\,T, \\ (B_E)_\theta &= 0, \\ \mathbf{grad}\,(B_E)_r &= \frac{\pm 6\mu_0 M}{4\pi {R_E}^4}\,\hat{\mathbf{r}} = \pm 29.7\,\hat{\mathbf{r}}\ \text{pT/m}, \\ \mathbf{grad}\,(B_E)_\theta &= \frac{\mp\,\mu_0 M}{4\pi {R_E}^4}\,\hat{\boldsymbol{\theta}} = \mp 5.0\,\hat{\boldsymbol{\theta}}\ \text{pT/m}, \end{aligned} \tag{B.5}$$

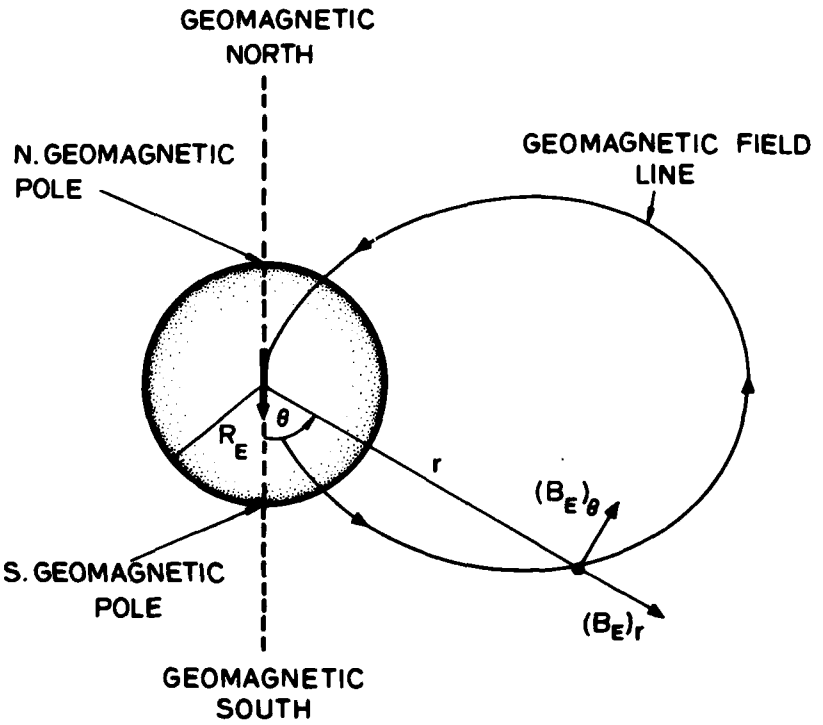

Figure B.1. Geometry of the geomagnetic field. Note the orientation of the geomagnetic dipole; the geomagnetic field is directed out of the earth at the south geomagnetic pole ($r = R_E$, $\theta = 0^\circ$) and into the earth at the north geomagnetic pole ($r = R_E$, $\theta = 180^\circ$).

where the upper and lower signs in the gradient terms apply to the north and south polar fields respectively. Because $(B_E)_\theta = 0$, the polar magnetic fields are entirely radial, or, equivalently, vertical to the earth's surface. The gradient of the vertical component of the geomagnetic field is also entirely radial at the poles, but its direction is antiparallel to the direction of the field. Thus, at the north geomagnetic pole the field is directed into the earth's surface, whereas the gradient of the vertical component (the only component of the field at the pole) is directed outwards. Note that the gradient of the horizontal component of the field is not zero at the poles, even though the component itself is zero. However, the magnitude of the gradient of the horizontal component (5 pT/m) is substantially smaller than the magnitude of the gradient of the vertical component (29.7 pT/m).

TABLE B.1. Some representative numerical values of the four terms comprising the gradient of the geomagnetic field in the geomagnetic-dipole-based spherical polar coordinate system (Figure B.1). The units are pT/m, and the values apply on the earth's surface ($r = 6370$ km) at the geomagnetic south pole ($\theta = 0°$), southern midlatitudes ($\theta = 45°$), the geomagnetic equator ($\theta = 90°$), northern midlatitudes ($\theta = 135°$), and the north geomagnetic pole ($\theta = 180°$).

θ	$\frac{\partial (B_E)_r}{\partial r}$	$\frac{1}{r}\frac{\partial (B_E)_r}{\partial \theta}$	$\frac{\partial (B_E)_\theta}{\partial r}$	$\frac{1}{r}\frac{\partial (B_E)_\theta}{\partial \theta}$
0°	−29.7	0	0	+5.0
45°	−21.1	−7.0	−10.5	+3.5
90°	0	−9.9	−14.8	0
135°	+21.1	+7.0	+10.5	−3.5
180°	+29.7	0	0	−5.0

The *equatorial field* at the earth's surface can also be obtained from the preceding equations and the data in Table B.1; it has the following properties:

$$
\begin{aligned}
(B_E)_r &= 0, \\
(B_E)_\theta &= \frac{\mu_0 M}{4\pi {R_E}^3} = 3.4 \times 10^{-5}\, T, \\
\mathbf{grad}\,(B_E)_r &= \frac{-2\mu_0 M}{4\pi {R_E}^4}\,\hat{\boldsymbol{\theta}} = -9.9\,\hat{\boldsymbol{\theta}}\ \text{pT/m}, \\
\mathbf{grad}\,(B_E)_\theta &= \frac{-3\mu_0 M}{4\pi {R_E}^4}\,\hat{\mathbf{r}} = -14.8\,\hat{\mathbf{r}}\ \text{pT/m}.
\end{aligned}
\tag{B.6}
$$

Because $(B_E)_r = 0$, the equatorial geomagnetic field is entirely horizontal. The gradient of the radial component of the field is also horizontal, even though the radial component itself is zero. The gradient of the angular component $(B_E)_\theta$ is radial (*i.e.*, vertical to the surface) and directed into the earth; its magnitude of 14.8 pT/m is larger than the magnitude of 9.9 pT/m for the gradient of the radial component, but the difference between the two magnitudes is much less than the corresponding difference for the polar gradients.

DISTRIBUTION LIST

ORGANIZATION	COPIES
DEPARTMENT OF DEFENSE	
OUSDRE (C3) ATTN: T. P. Quinn Pentagon, Room 3E160 Washington, DC 20301	1
OUSDRE (Cruise Missile Systems) ATTN: Col. S. F. Moore, USAF Pentagon, Room 3E139 Washington, DC 20301	1
OUSDRE (Defense Test & Evaluation) ATTN: Tactical Air & Land Warfare Sys	1
Test Facilities & Resources, W. A. Richardson	1
Pentagon Washington, DC 20301	
OUSDRE (Defensive Systems) ATTN: J. L. Gardner Pentagon, Room 3D136 Washington, DC 20301	1
OUSDRE (Naval Warfare & Mobility) ATTN: W. D. O'Neil	1
Cdr. Peter P. Buckley, USN Pentagon, Room 3D1048 Washington, DC 20301	1
OUSDRE (Offensive & Space Systems) ATTN: M. C. Atkins Pentagon, Room 3E129 Washington, DC 20301	1
OUSDRE (Research & Advanced Technology) Pentagon, Room 3E114 Washington, DC 20301	1
OUSDRE (Tactical Intelligence Systems) Pentagon, Room 3C200 Washington, DC 20301	1
OUSDRE (Tactical Warfare Programs) Pentagon, Room 3E1044 Washington, DC 20301	1
Defense Advanced Research Projects Agency ATTN: Deputy Director, V. L. Lynn	1
STO, A. J. Tether	1
TTO, A. E. Brandenstein	1
TTO, H. D. Fair	1
TTO, Cdr. D. L. Finch, USN	1
TTO, Col. J. O. Gobien, USAF	1
TTO, T. Kooij	1
TTO, Lt. Col. T. W. Swartz, USAF	1
TTO, E. C. Whitman	1
Technical Information Branch 1400 Wilson Boulevard Arlington, VA 22209	1
Director Defense Communications Agency ATTN: CCTC/C605, J. A. Hoff Washington, DC 20305	1
Director Defense Intelligence Agency ATTN: Code DC-7 Pentagon Washington, DC 20301	1
Director Defense Nuclear Agency ATTN: RAAE	2
DDST	1
RAEV Washington, DC 20305	1
Defense Technical Information Center Cameron Station Alexandria, VA 22314	12
Director National Security Agency ATTN: R06, J. Settles	1
Library Fort Geo. G. Meade, MD 20755	1
Director DOD-IDA Management Office ATTN: IDA, D. L. Randall 1801 N. Beauregard Street Alexandria, VA 22311	1
DEPARTMENT OF THE NAVY	
Office of the Asst. Secretary of the Navy (Research, Engineering & Systems) ATTN: F. Marshall Pentagon, Room 5E683 Washington, DC 20350	1
Office of the Chief of Naval Operations ATTN: OP-00K	1
OP-96C2, G. Haering	1
OP-961C	1
OP-094B	1
OP-943, Captain Larry Wilson, USN	1
OP-944	1
OP-951	1
OP-952	1
OP-098	1
OP-981	1
OP-982	1
OP-987	1
OP-009E	1
OP-22	1
OP-35	1
OP-50 Pentagon Washington, DC 20350	1
Center for Naval Analyses ATTN: G. Phillips 2000 North Beauregard Street Alexandria, VA 22311	1

ONR/Stanford University/June 1983

DISTRIBUTION LIST

ORGANIZATION	COPIES
Chief of Naval Development	
ATTN: Code 07C, L. L. Hill	1
Code 0724, Captain E. Young, USN	1
Code 073, Surveillance & C	1
800 North Quincy Street	
Arlington, VA 22217	
Chief of Naval Research	
ATTN: Code 102, J. A. Smith	1
Code 210	1
Code 222	1
Code 414, D. C. Lewis	1
Code 414, L. J. Griffiths	1
Code 414, R. Gracen Joiner	2
Code 422	1
Code 425	1
800 North Quincy Street	
Arlington, VA 22217	
Office of Naval Research Resident Representative	1
University of California, San Diego	
La Jolla, CA 92093	
Office of Naval Research Resident Representative	1
Stanford University	
Durand Building, Room 165	
Stanford, CA 94305	
Commander	
Naval Air Development Center	
ATTN: Code 3012	1
Library	1
Warminster, PA 18974	
Headquarters	
Naval Air Systems Command	
ATTN: NAIR-03A	1
B. L. Dillon	1
Jefferson Plaza #1	
Washington, DC 20361	
Commander	
Naval Electronic Systems Command	
ATTN: ELEX-06	1
ELEX-615, S. Arkin	1
PME 106-6, Capt. N. L. Wardle, USN	1
PME 107	1
PME 110-X1	1
PME 110-112	1
PME 120	1
PME 124	1
PME 154	1
National Center No. 1	
Washington, DC 20360	
Headquarters	
Naval Facilities Engineering Command	
ATTN: 04, Asst Commander for Engineering & Design	1
Hoffman II Building	
200 Stovall Street	
Alexandria, VA 22332	

ORGANIZATION	COPIES
Headquarters	
Naval Sea Systems Command	
ATTN: 003, Ofc of Research, Technology & Assessment	1
National Center #3	
Washington, DC 20360	
Commander	
Naval Underwater Systems Center	
ATTN: P. Bannister	1
E. Soderberg	1
Library	1
New London, CT 06320	
Commandant of the Marine Corps	
ATTN: Code RD-1, A. L. Slafkosky	1
Washington, DC 20380	
Project Manager	
Anti-Submarine Warfare Systems Project	
ATTN: ASW-01T	1
ASW-11	1
National Center #1	
Washington, DC 20360	
Commander	
Naval Coastal Systems Center	
ATTN: R. H. Clark	1
M. J. Wynn	1
Panama City, FL 32407	
Commander	1
Naval Intelligence Support Center	
4301 Suitland Road	
Washington, DC 20390	
Commander	
Naval Missile Center	
ATTN: Library	1
Point Mugu, CA 93041	
Commander	
Naval Ocean R&D Activity	
ATTN: D. L. Durham	1
D. W. Handschumacher	1
K. Smits	1
Library	1
NSTL Station, MS 39529	
Commander	
Naval Ocean Systems Center	
ATTN: Code 00, Capt. J. M. Patton, USN	1
Code 07, W. P. Mitchel	1
Code 16, C. Merrow	1
C. F. Ramstedt	1
Y. Richter	1
K. L. Grauer	1
Library	1
San Diego, CA 92152	
Commander	
Naval Oceanographic Office	
ATTN: O. E. Avery	1
T. Davis	1
G. R. Lorentzen	1
Library	1
NSTL Station, MS 39529	

DISTRIBUTION LIST

ORGANIZATION	COPIES
Superintendent	
Naval Postgraduate School	
ATTN: Dept. of Physics & Chemistry	
J. N. Dyer	1
O. Heinz	1
P. H. Moose	1
W. M. Tolles	1
Dept. of Electrical Engineering	
M. A. Morgan	1
J. M. Wozencraft	1
Library	1
Monterey, CA 93940	
Director	
Naval Research Laboratory	
ATTN: Code 4006, V. E. Noble	1
Code 5700, L. A. Cosby	1
Code 6605, G. T. Rado	1
Code 7500, J. R. Davis	1
Technical Information Division	2
Washington, DC 20375	
Commander	
Naval Security Group Headquarters	
ATTN: C3I Advisory Board, NRAC	1
Technical Director	1
G53, Ralph O'Dell	1
3801 Nebraska Ave, N.W.	
Washington, DC 20390	
Commander	
David W. Taylor Naval Ship Research & Development Center	
ATTN: W. Andahazy	1
F. E. Baker	1
Annapolis, MD 21402	
Commander	
David W. Taylor Naval Ship Research & Development Center	
ATTN: Library	1
Bethesda, MD 20034	
Commander	
Naval Surface Weapons Center	
Dahlgren Laboratory	
ATTN: Library	1
Dahlgren, VA 22448	
Commander	
Naval Surface Weapons Center	
White Oak Laboratory	
ATTN: J. J. Holmes	1
M. B. Kraichman	1
P. Wessel	1
Library	1
Silver Spring, MD 20910	
Commander	
Naval Underwater Systems Center	
New London Laboratory	
ATTN: P. Bannister	1
E. Soderberg	1
Library	1
New London, CT 06320	

ORGANIZATION	COPIES
Commander	
Naval Weapons Center	
ATTN: Code 013, Pierre St. Amand	1
Code 39D, J. A. Crawford	1
China Lake, CA 93555	
Commander-in-Chief, Pacific	
ATTN: J55, Research & Analysis Division, R. F. Linsenmeyer	1
Box 15	
Camp H. M. Smith, HI 96861	
Commander-in-Chief	1
U.S. Atlantic Fleet	
Norfolk, VA 23511	
Commander-in-Chief	1
U.S. Pacific Fleet	
Makalapa	
Pearl Harbor, HI 96860	
Commander	1
Oceanographic System Atlantic	
Box 100	
Norfolk, VA 23511	
Commander	1
Oceanographic System Pacific	
Pearl Harbor, HI 96860	
Commander Task Group 168.1/PACFAST	
Pacific Forward Area Support Team	
ATTN: R. Horton	1
Box 500	
Pearl Harbor, HI 96860	
Commander	
Patrol Wings	
U.S. Atlantic Fleet	
ATTN: Cdr. R. Johns, USN	1
NAS Brunswick, ME 04011	
Commander	
Patrol Wings	
U.S. Pacific Fleet	
ATTN: N53, Cdr. Tim Sullivan, USN	1
NAS Moffett Field, CA 94035	
DEPARTMENT OF THE AIR FORCE	
Office of the Assistant Secretary of the Air Force (R&D)	
ATTN: SAF/RD	1
Pentagon, Room 4D977	
Washington, DC 20330	
Headquarters	
U.S. Air Force	
ATTN: RDSD, Col. J. M. McCormack, USAF	1
Pentagon	
Washington, DC 20330	
Commander	
Air Force Systems Command	2
Andrews AFB, MD 20331	

DISTRIBUTION LIST

ORGANIZATION	COPIES
Headquarters Aeronautical Systems Division (AFSC) ATTN: ASD/EN, David Berrie Wright-Patterson AFB, OH 45433	1
Headquarters Air Force Geophysics Laboratory (AFSC) ATTN: PHY, J. Buchau Technical Library Hanscom AFB, MA 01731	1 1
Headquarters Air Force Office of Scientific Research (AFSC) ATTN: NE, Thomas E. Walsh Bolling AFB, DC 20332	1
Commander Air Force Technical Applications Center Patrick AFB, FL 32925	1
Headquarters Air Force Test and Evaluation Center ATTN: TEK Kirtland AFB, NM 87117	1
Headquarters Air Force Wright Aeronautical Laboratory ATTN: AFWAL/AAWA, Bill Lane Wright-Patterson AFB, OH 45433	1
Headquarters Armament Division ATTN: AD/YIMA Eglin AFB, FL 32542	1
Headquarters Electronic Security Command ATTN: ESC/XPZ San Antonio, TX 78243	1
Headquarters Electronic Systems Division (AFSC) ATTN: SCU-4, Col. A. L. Snyder, USAF XR Hanscom AFB, MA 01731	1 1
Headquarters Foreign Technology Division (AFSC) ATTN: Library Wright-Patterson AFB, OH 45433	1
Headquarters Rome Air Development Center ATTN: Library Griffiss AFB, NY 13442	1
Headquarters Rome Air Development Center ATTN: EEPS, P. Kossey Hanscom AFB, MA 01731	1

ORGANIZATION	COPIES
DEPARTMENT OF THE ARMY	
Office of the Asst. Secretary of the Army (Research, Development & Acquisition) ATTN: M. R. Epstein Pentagon, Room 2E673 Washington, DC 20310	1
Commander Ballistic Missile Defense Systems Command ATTN: BMDATC-R, Don Russ 106 Wynn Drive Huntsville, AL 35806	1
Commander U.S. Army Communications Command ATTN: CC-TD, L. J. Mabius CC-ATC Fort Huachuca, AZ 85613	1 1
Commander U.S. Army Electronics R&D Command ATTN: CS&TA, W. Vander Meer/ T. E. Daniels DELEW-DD, R. Giordiano Fort Monmouth, NJ 07703	1 1
Commander U.S. Army Electronics R&D Command ATTN: DELHD-D, W. W. Carter DRDEL-CT, R. Oswald 2800 Powder Mill Road Adelphi, MD 20783	1 1
Commander U.S. Army Foreign Science & Technology Center ATTN: DRXST-ES2, G. Hargis/ IS-1, C. Evans 220 Seventh Street, N.E. Charlottesville, VA 22901	1
Commanding General U.S. Army Intelligence & Security Command ATTN: MG A. N. Stubblebine III, USA Library Arlington Hall Station 4000 Arlington Boulevard Arlington, VA 22212	1 1
Commander U.S. Army Missile Command ATTN: DRSMI-RES, H. Buie/ DRSMI-RXE, Billy Tidwell Redstone Arsenal, AL 35898	1
Director U.S. Army Signals Warfare Laboratory ATTN: DELSW-D, H. S. Hovey, Jr. Vint Hill Farms Station Warrenton, VA 22186	1

DISTRIBUTION LIST

ORGANIZATION	COPIES
OTHER	
EG&G Incorporated ATTN: L. E. Pitts P.O. Box 398 Riverdale, MD 20840	1
Johns Hopkins University Applied Physics Laboratory ATTN: L. W. Hart Johns Hopkins Road Laurel, MD 20810	1
La Jolla Institute ATTN: K. Watson La Jolla, CA 92407	1
Lockheed Palo Alto Research Laboratory ATTN: W. Imhof J. B. Reagan M. Walt 3170 Porter Drive Palo Alto, CA 94304	1 1 1
M.I.T. Lincoln Laboratory ATTN: R. M. O'Donnell, Group 43 P.O. Box 73 Lexington, MA 02173	1
NOAA Laboratories ATTN: Library 325 Broadway Boulder, CO 80303	1
Pacific-Sierra Research Corporation ATTN: E. C. Field 12340 Santa Monica Boulevard Los Angeles, CA 90025	1
R&D Associates ATTN: C. Greifinger Robert E. LeLevier P.O. Box 9695 Marina Del Rey, CA 90291	1 1
RAND Corporation ATTN: Cullen Crain 1700 Main Street Santa Monica, CA 90406	1
Science Applications, Inc. ATTN: J. Czika, Jr. 1710 Goodridge Drive McLean, VA 22102	1
SRI International ATTN: D. M. Bubenik J. B. Chown/R. C. Honey C. A. Cole H. Guthart/R. Williams L. E. Sweeney, Jr. 333 Ravenswood Avenue Menlo Park, CA 94025	1 1 1 1 1
SRI International ATTN: E. Lyon/W. Vail/J. J. Kane 1611 N. Kent Street Arlington, VA 22209	2
University of California Scripps Institute of Oceanography ATTN: Code A030, C. S. Cox La Jolla, CA 92093	1
University of Texas, Austin Geomagnetics & Electrical Geoscience Lab. ATTN: F. X. Bostick, Jr. Austin, TX 78712	1